The Influence of Cavity Widths and Lateral Ventilation Conditions on the Fire Behaviour within a Non-Combustible Ventilated Façade System

By Daniel Fogerty

HOST UNIVERSITY: Lunds Universiteit

FACULTY: Lunds Tekniska Högskola

DEPARTMENT: Brandteknik

Academic Year 2019-2020

Promoter: Kingspan Group

Master thesis submitted in the Erasmus Mundus Study Programme

International Master of Science in Fire Safety Engineering

Disclaimer

This thesis is submitted in partial fulfilment of the requirements for the degree of *The International Master of Science in Fire Safety Engineering (IMFSE)*. This thesis has never been submitted for any degree or examination to any other University/programme. The author declares that this thesis is original work except where stated. This declaration constitutes an assertion that full and accurate references and citations have been included for all material, directly included and indirectly contributing to the thesis. The author gives permission to make this master thesis available for consultation and to copy parts of this master thesis for personal use. In the case of any other use, the limitations of the copyright have to be respected, in particular with regard to the obligation to state expressly the source when quoting results from this master thesis. The thesis supervisor must be informed when data or results are used.

Read and Approved, signed:

Abstract

Present uncertainties in key ventilation parameters, characterising the fire performance of facades, has necessitated clarification in the foundational understanding of the Fire Science Body of Knowledge. A test program conducted in collaboration between Lunds Universitet and the Kingspan Group, studied the influence of cavity widths and lateral ventilation conditions on the fire behaviour within Intermediate-scale ventilated façades following the ISO 13785-1 standards. Experimental works were performed in parallel to a Computational Fluid Dynamics analysis performed in the Fire Dynamics Simulator software. The thesis reports on the influence of domain discretization and complex geometric substitutions on the representativeness of simulated data. The experimental and simulated data were shown to hold reasonable correlation of information referring to the influence of lateral ventilation conditions on fire behaviour. Indicating the variable influence of obstructions and openings dependent on the point of interest and proximity within the sample. Data presented more critical conditions in near-field locations when closed ventilation conditions were applied, while far-field analysis indicated open conditions to be more critical. In the absence of a full experimental schedule, extension of studies was performed in the FDS software for later validation. Demonstrating the importance in selection of performance metrics in evaluating critical cavity widths. The data indicated more critical conditions present within the 50mm cavity sample, however greater flame heights were produced in the 25mm cavity.

IMFSE Master Thesis Declaration

This form has been developed in the context of the unforeseen circumstances due to Covid-19, necessitating a reduction of practical project work (whether it be laboratory based, computational, or fieldwork) during the master thesis semester. It acts as a record of the impact on the master thesis. The form has been completed by the student and verified by the supervisor.

Name: Daniel Fogerty

Work completed

All items of wholly, or partially completed work must be listed, indicating the percentage completion for each task.

Three intermediate-scale façade tests following the ISO 13785-1 methodology were completed incorporating a 50mm cavity and all ventilation conditions for analysis. However, Cavity Barriers were omitted from the design as they were unable to be shipped and installed in time for testing. Therefore 33% of practical works were able to be performed with a reduced level of detail.

All reasonable Fire Dynamics Simulator analyses was able to be completed on the LU Aurora Cluster which remained functional throughout the thesis period. Therefore 100% of computational works were able to be completed.

Work not commenced

Any items of outstanding work that have not been started should be listed here.

Six intermediate-scale façade tests following the ISO 13785-1 methodology were omitted from works including the 25mm and 100mm cases of all ventilation conditions. Therefore 67% of practical works had to be omitted from the thesis studies.

Declaration

To the best of our knowledge, this form is an accurate record of the project status on 28/04/20

Student: Daniel Fogerty

Supervisor: Patrick van Hees

Acknowledgements

There are so many people who have contributed to the completion of this thesis and who have supported me in the process of its works. I would first like to thank my supervisors Prof. Patrick van Hees of Lunds Universitet and Roy Weghorst of Kingspan Group. The financial, knowledgeable and emotional support that they provided over this rather cumbersome four months, made an otherwise insane experience seem quite manageable.

Secondly, I would like to thank Talal Fateh, Maurice McKee and the Efectis UK/Ireland Ltd. staff for hosting us at such short notice and managing a rather trying schedule, amidst global shutdowns, to produce and transmit the experimental data for our studies.

I would further like to mention the amazing support of Dr. Bjarne Husted, who took the time to act as a pseudo supervisor for the completion of the FDS analysis, through the LU Aurora cluster.

To my thesis partner Tanja Černoša, this process would not have been the same without you. Your support and friendship in times when the world was turned upside down was essential.

Professionally, I would like to demonstrate my gratitude for the contributions of Karlis Livkiss, Marc Janssens, Alan Macklin, Jonathon Wahlqvist, and Antonela Čolić.

And finally, on a personal note, I would like to show my appreciation for my fantastic family (both by blood and IMFSE alike) and my wonderful friends at home and abroad for all the love.

Table of contents

List of abbreviations

Abbreviation	Description	Equation No.	Page No.
$\boldsymbol{\rho}$	Density (kg/m³)	3.1	8
T	Temperature (K)	3.1 & 3.5	8 & 49
$\boldsymbol{\phi}$	Entrained air to stoichiometric air requirement ratio	3.2	9
m	Mass-entrainment rate of air	3.2	9
$\boldsymbol{\Delta H_c}$	Heat of Combustion (kJ/g)	3.2	9
$\boldsymbol{\dot{Q}}$	HRR - Heat Release Rate (kW)	3.2, 3.3 & 3.4	9 & 35
r	Stoichiometric mass ratio	3.2	9
L	Flame height (m)	3.3	9
B	Length of a line burner	3.3	9
$\boldsymbol{\delta_x}$	Length scale for grid cells (m)	-	35
$\boldsymbol{D^*}$	Characteristic Fire Diameter	3.4	35
$\boldsymbol{\rho_\infty}$	Ambient Density (kg/m³)	3.4	35
$\boldsymbol{c_p}$	Specific Heat Capacity $(J/kg \cdot K)$	3.4	35
$\boldsymbol{T_\infty}$	Ambient Temperature (K)	3.4	35
g	Gravitational Acceleration (m/s^2)	3.4	35
v	Velocity (m/s)	3.5	49
$\boldsymbol{\Delta P}$	Pressure differential (Pa)	3.5	49
$\boldsymbol{P_\infty}$	Atmospheric pressure (Pa)	3.5	49
$\boldsymbol{M_w}$	Molecular weight of air (kg/mol)	3.5	49
R	Ideal gas constant $(J/K \cdot mol)$	3.5	49

Table of Figures

1. Introduction

In modern construction practice ventilated façade systems have become the most prominent technique, utilized to achieve global sustainable development goals (Akadiri et al., 2012). The systems have built acclaim for their practicality, and effectiveness in implementation on both new and existing buildings (Bikas et al., 2017). Whilst reports indicate 40% reductions in building energy usage requirements when appropriate façade designs are implemented (Mahdavinejad & Mohammadi, 2018). However, several major fire incidences involving ventilated façades have impacted confidence in the design, raising questions as to the appropriateness of its application in modern construction and the fire safety of existing installations (Chen et al., 2019). Under consideration of the fire safety objectives, Professor David Rasbash of the University of Edinburgh, indicated in his 1977 lecture that "not only should we consider the nature of the risk but also the acceptability of the risk." Following this ideology when regarding ventilated facades, the nature of the risk posed involves the ignition and spread of fire within the façade's cavity, such that internal building compartmentation designs are breached (Rockwool International A/S, 2017). In the instance that fire safe compartmentation is not maintained, the life safety of building occupants and individuals in the immediate vicinity of the structure is severely impacted, as design tenability limits are exceeded by smoke and thermal loading. Ultimately, the sustainability benefits of ventilated facades are not worth the lives of building occupants, as well as the resulting property damage. However, the acceptability of the fire safety risk associated with ventilated facades relies upon the understanding of the behaviour of fire within the cavity and the likelihood for fire spread, in response to parameters such as material composition and ventilation. Presently, the fire science body of knowledge regarding this unique scenario is incomplete, necessitating expensive performance-based design measures to ensure safe design application (National Housing Federation Ltd., 2018). The following thesis work has been performed with the aim of adding to the fire science body of knowledge regarding facade systems, in order to improve logical reasoning for façade development and reduce industrial expenditure on in-appropriate testing methodologies. The parametric focus of this thesis being, a development in understanding of the influence of ventilation conditions on flame progression through a ventilated façade cavity. The investigation will be performed on adapted intermediate-scale façade cavity arrangements following the conditions of the ISO 13785-1 methodology, incorporating a variation of façade cavity widths.

1.1 Ventilated Façade Functionality

In order to understand the influence of ventilation conditions on the fire performance of façade designs, it is important first to investigate how these systems utilize cavities to maximize a building's sustainability performance. The principle behind ventilated façades, is the provision of a passive system for the management of internal building comfort. The façade primarily comprises; an insulation layer placed flush to the surface of the structural wall, with a layer of cladding fixed offset to the insulation, maintaining the required air cavity for ventilation (Innowood, 2016), see Figure 1. The insulation enables the stabilization of the building's internal air temperature from environmental fluctuations, while the exterior cladding panels (often referred to as rainscreen panels) act as protection for the insulation against extreme weather conditions. The reason for positioning the insulative layer on the exterior face of structural elements and thus necessitating weather protection and the all-important air cavity, is so that the whole structure maintains a stabilized humidity, temperature and pressure, limiting thermal deformation and cracking of structural elements (Choi & Taylor, 1984). By managing the thermal performance of the structure passively, ventilated facades reduce need for the activation of HVAC (Heating, Ventilation and Air Conditioning) systems and therefore minimize energy expenditure.

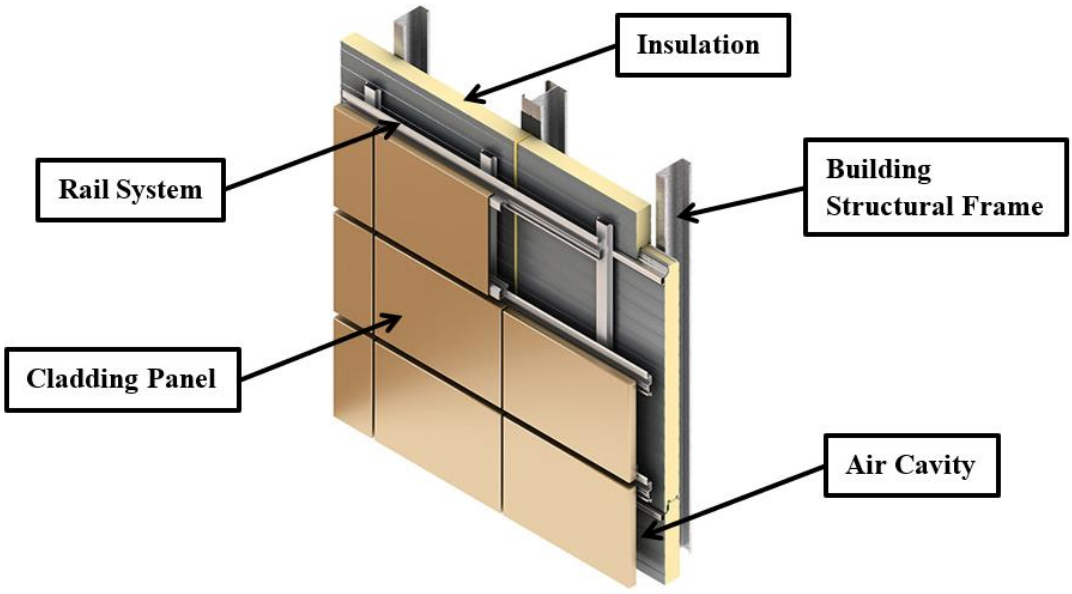

Figure 1: Ventilated Facade Schematic Diagram (Kinspan Group, 2019)

The function of the façade's air cavity is to provide a path for the escape of built-up structural condensation and intrusive moisture from the insulation, to protect against material degradation of the layer (Knaack et al., 2014). Naturally ventilated facades use the principle of the stack

effect to provide convective air flow, which assists in the drying of the insulation. The stack effect (aka the chimney effect) is a buoyancy driven flow that sources from differences in air density between the internal cavity environment and the ambient atmospheric conditions. Therefore, in cold climatic conditions, the hot, humid air of the cavity will have a reduced density in comparison to ambient air, causing it to rise-up the cavity through buoyancy. The flow results in a reduction of pressure at the base of the cavity, allowing the inflow of fresh, dry air for continued diffusive drying of the insulation (TLJ Engineering Consultants Ltd., 2016). This phenomenon, though extremely useful for its application, forms a large part of why these ventilated façade systems are under scrutiny regarding fire safety. As Colwell & Baker demonstrated in their 2013 BRE Trust publication, that through action of the chimney effect flames within an air cavity are drawn up to ten times higher than the external flaming portion of the plume. By providing a means for the lengthening of external flaming up the structure, the cavity is effectively laying a path for a concentrated, direct attack on the windows of the storeys above bypassing compartmentation (Rockwool International A/S, 2017). In order to combat this phenomenon in the interest of fire safety, it is first important to understand the fire dynamic principles at play.

1.2 Fire Dynamics of a Ventilated Cavity

The process of cataloguing and understanding the fire behaviour within a façade cavity, finds its origins in knowledge attained through investigation of fires within rack storage arrangements. The similarities in oxygenation pathways and burning behaviour, allow the primary principles of rack storage scenarios to be transferrable to façade cavity situations. Haukur Ingason detailed in his 1994 presentation to the Fourth International Symposium of Fire Safety Science, that “the flues created between adjacent pallets of stored goods tend to work as chimneys and subsequently they enhance acceleration of flames up to the ceiling.” This knowledge stands as a precursor to that expressed by Colwell for façade cavities, demonstrating the similarity in fire dynamic principles between the scenarios. When looking into the detail of the chimney effect, the function of the buoyant pull on the flame up the cavity is clear. When a flame is introduced into the enclosed region, the space is heated far beyond ambient temperatures. In turn the density of the region drastically reduces following equation 3.1, allowing the buoyant flows of the chimney effect to initiate. Notice too that the buoyant influences from the molecular weights of the gaseous products present within the plume are inconsequential in comparison to the impacts of temperature, and thus are omitted (Karlsson & Quintiere, 1999).

$$\rho = \frac{353}{T} \tag{3.1}$$

Throughout the analysis of the rack storage arrangement Ingason theoretically and experimentally explains the resulting entrained flows drawn into the induced low-pressure channel (flue) to sustain the diffusion flame present. Firstly, the cold velocity of the entrained ambient air at the base of the flue is shown to be independent of the flue width. Whilst the size of the horizontal openings accessing the flue within the rack have a negligible impact on the flow reported in the channel. Notice that the horizontal openings are presented normal to the line burner, with the sides of the rack at the short edges of the burner remaining closed. This indicates the dominance of the entrained flow at the base of the channel and therefore infers that the total entrained flow to the sample will be linearly proportional to the cavity width based on the cold velocity independence described. This knowledge is supported by the findings of Karlsson et al. (1995), in their similar preliminary investigations. Further, Ingason establishes that there is limited variation found in the entrained cold velocity when test values are plotted across the range of temperatures experienced within the vertical channel. The resulting plot shown below in Figure 2a) bears a strong resemblance with the plot for the variation in density factor in relation to temperature presented by Karlsson & Quintiere (1999) displayed in Figure 2b) below, confirming the density driven nature of the entrained flows to vertical flue arrangements. Noting that the 0 – 60kW scale of Figure 2a) equates to 20 – 800°C.

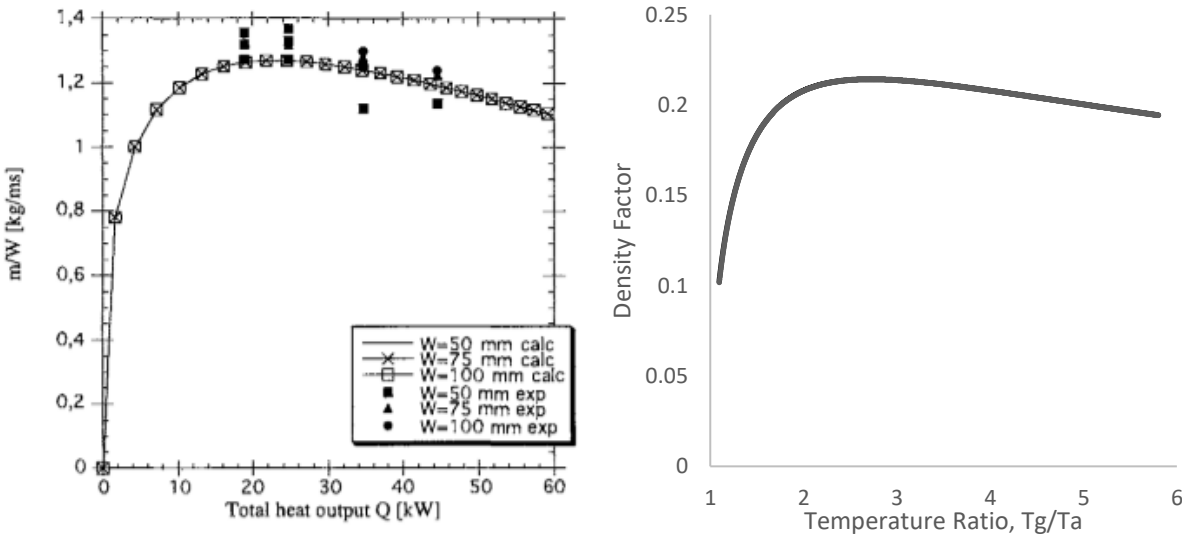

a) *b)*

Figure 2: a) Mass Flow Rate on Flue Width vs Heat Output plot for 2D Rack Storage Setups from Ingason (1994) with IAFSS permission, b) Density Factor vs Temperature Ratio plot for Mass Flows through Openings, Re-constructed from Karlsson & Quintiere (1999)

Despite the constrained nature of the entrained air to the sample, the paper demonstrates sufficiently oxygenated conditions for complete combustion within all cavity widths. With the ratio of entrained air to stoichiometric requirement of the burner approximating 6, 7.6 and 10 for channel widths of 50mm, 75mm and 100mm respectively, taking the calculation:

$$\phi = \frac{m \times \Delta H_c}{\dot{Q} \times r} \tag{3.2}$$

Even though the tests have been shown to be well oxygenated, the oxygen availability remained less than that of a free plume for the 50mm and 75mm channel widths. A free plume approximates an entrained air to stoichiometric ratio of 10 using the same calculation from Equation 3.2. Clearly, the 100mm case demonstrates the same oxygenation as a free plume, whilst indicating flame heights of around twice that of a free plume line burner. Notice that this ratio describes the entrainment from the fire source to the flame tip in each case. Therefore, based on the influence of the surrounding obstructions the fire can be seen to progress up the cavity to access free space for effective reaction with available oxygen. Hence demonstrating the flame height of a fire with a greater heat release rate than reality, correlating to the principles discussed for wall and corner flames by Karlsson & Quintiere (1999). Using the equation for the flame height of a line burner outlined by Karlsson and Quintiere (Equation 3.3), a flame height twice that of the free plume resembles a fire with 2.8 times the Heat Release Rate. Which upon reflection of the data provided by Ingason seems to be a reasonable approximation.

$$L = 0.035\left(\frac{\dot{Q}}{B}\right)^{\frac{2}{3}} \tag{3.3}$$

Notably, this equation was constructed from flame height data produced by burners with a long to short side ratio of 10. Given that Ingason's experiments held a ratio of approximately 30, the constant of the equation must be adjusted slightly to 0.025. However, this will not affect the HRR representative flame height multiplier calculated previously. Notice that this representative flame stands only for the 100mm case, as Ingason demonstrates that with the reduction of the vertical flue width, comes an increase in the flame height present. Algebraically, when the free plume flame height is increased by multiple x, the fire should represent a flame with HRR $x^{\frac{3}{2}}$ times its original value. This cannot be verified with the data provided in this test and should thus be investigated further. Further investigation into the variation of flame height has been performed by Hu et al. (2017) in determining the influence of the orientation of the line burner (flame) within an open cavity. By altering the configuration of the line burner in relation to two parallel fire-resistant boards, Hu et al. (2017) demonstrated

the dominance of air entrainment into the long edges of the fire plume. The tests presenting the burner perpendicular to the boards saw little change in flame height when the width of the cavity was shifted. Whilst the parallel configuration demonstrated flames extending up the cavity as in the Ingason tests. Indicating the impact of constraining the primary entrainment zone of the flame, in necessitating the extension of the flame up the cavity to provide space for effective oxidation. In both various cases cavity widths were taken up to free plume conditions.

The same trend for increasing flame height with reducing cavity width was depicted in the work of Livkiss (2018), however in this instance the sample incorporated two plain parallel calcium silicate panels. The primary detail of importance in this setup was the absence of side seals to the cavity, allowing substantial air entrainment into the sample throughout its height. As indicated in the Ingason paper, the ratio of entrained air to stoichiometric burner requirement was seen to decrease as the cavity width reduced and hence the smaller cavity widths presented by Livkiss should demonstrate low levels of entrainment, potentially close to parity with the stoichiometric requirement. However, with the sides presented open this influence will not be well represented. Rather, the tests reiterate that a flame with availability to oxygen in a confined space will be drawn upwards in search of space to effectively react with the available oxygen, indicating the potential danger of the chimney effect in confined oxygenated spaces. However, these conditions do not generally occur in realistic building façade designs as the applied rail systems for fixing the cladding panels to the structural wall, effectively seal the façade to heavily oxygenated conditions. Therefore, the primary focus of the tests to be performed herein, involves investigating the influence of this lateral oxygenation condition to fire behaviour within façade samples of varying cavity widths. To determine whether there is a limit to the extension of flames in the cavity, based on potential limits to the entrained air supply. In order to understand and direct the representative nature of the test data aimed to be produced, real fire incidences and the development of standardised testing measures should first be considered.

1.3 Ventilated Façade Fire Incidents

When addressing the current issues in fire safety of ventilated facades, the engineering community tends to focus on select fire incidents from the last decade that demonstrate priority issues endangering the global populous. Most notably, fires occurring in the Lacrosse Building (Australia, 2014), The Address, Dubai (United Arab Emirates, 2016) and the Grenfell Tower (United Kingdom, 2017) have highlighted the dangers in incorporating Aluminium Composite Material (ACM) cladding panels constructed with a Polyethylene (PE) core into a ventilated

façade design (Chen et al., 2019). Further, Guillaume et al. (2018) have expressed that for ACM façade systems, "the cladding is the most important parameter driving global fire behaviour," and thus is a primary focus of the industry at this stage. Before delving into the deeper understanding of the influence of this façade component on fire development, it is important first to build a fuller perspective of the fire incidents that brought this information to light.

1.3.1 Lacrosse Building

The fire which occurred on the morning of the 25th of November 2014, initiated on the balcony of a 6th floor apartment when a cigarette was improperly extinguished and disposed of, allowing ignition of a waste receptacle. The fire grew and spread to the wooden table, before progressing to the ACM cladding panels on the exterior wall of the structure, adjacent to the balcony and bedroom window (Chen et al., 2019). Within the façade, the fire spread up the side of the structure, impacting the 6th to 21st floors resulting in the evacuation of the entire structure (Genco, 2015). The fire reportedly damaged some of the alarm systems installed within the building, resulting in the required ingress of firefighting personnel to manually inform occupants of the evacuation proceedings (Chen et al., 2019). The evacuation saw all occupants egress the structure with only minor injuries reported. Genco (2015) detailed in the official Municipal Surveyor's report that amidst investigation of the incident, the Melbourne Metropolitan Fire Brigade indicated that the cladding panels applied on the affected face of the structure did not fit the prescription outlined in the Building Code of Australia. As the requirement for constructions of this nature (Type A – High rise, high occupancy) are indicated to require non-combustible cladding panels.

1.3.2 The Address, Dubai

The incident took place on the night of New Year's Eve 2015-16, when a malfunction in the circuitry of flood lights, perched on a ledge between the 14th and 15th floor, ignited a fire in the adjacent cladding panels (Chen et al., 2019). Strong winds reported on the night of the fire resulted in the reduction of fire growth rates on the structure, directing flames to the surrounding environment. Whilst falling cladding panels were said to have travelled a block before instigating secondary blazes on nearby roofs, drawing the focus of the fire department's aerial response teams (Spearpoint et al., 2019). Despite the wind, the fire was able to spread within the façade cavity up to the top of the panelised section of the tower, before beginning to decay. Noting that the fire was seen to be constrained to the face of the structure of fire origin (Torero, 2018). There is limited documentation that has been made available to the wider engineering community regarding the details of this event, as explained by Spearpoint et al.

(2019) and Torero (2018). However, it was confirmed that there were no fatalities, with 14 minor injuries and two moderate injuries reported, whether directly or indirectly related to the blaze. Further, the limited information suggests that the standards utilized for the fire performance of the cladding panels were insufficient to demonstrate the true in situ fire resistance of the façade element (Spearpoint et al., 2019).

1.3.3 Grenfell Tower

The events that transpired on the 14th of June 2017, began in the early hours of the morning when ignition of the blaze was reported from the back of a refrigeration unit, on the 4th floor of the apartment building, within Flat 16 (Torero, 2018). The fire was able to grow within the apartment to fully developed, under-ventilated conditions before fire-fighting teams were able to control the blaze (Chen et al., 2019). The under-ventilated conditions allowed the fire to breach the apartment windows and directly attack the building's façade, which had been installed amidst renovations just two years prior. Once the flames entered the façade cavity, fire was able to spread drastically over the structure. Uniquely however, the fire on the Grenfell Tower spread across the entirety of the structure, not only on the face of initial external ignition, as was the case in the Lacrosse and The Address, Dubai fires. Professor Jose Torero demonstrated in his Phase 1 Report, that the primary means of lateral flame spread, witnessed from video footage of the fire, was through the crown of the building. Torero explains that "the lateral spread of the flames through the architectural crown structure is faster than the lateral propagation through the façade system in the building" and that "as burning debris falls from burning areas, they will accumulate on window ledges or indeed on any available horizontal surface, igniting new localised fires" (Torero, 2018). These secondary individual fires will then progress up the structure and re-join the instigating blaze until the entire building is engulfed. Chen et al. (2019) further explains that the spreading fire was able to re-enter the structure, bypassing building fire compartmentation design and trapping residents. The falling debris also raised significant issues for the fire-fighting ground staff acting to extinguish the blaze and help occupants (Spearpoint et al., 2019). The disaster lead to 72 fatalities in total, with 70 occupants perishing within the structure and two later succumbing to injuries sustained (Torero, 2018). As part of the official Grenfell inquiry, the cladding material was subject to BS EN ISO 1716 calorific reaction to fire testing and was rated Category 3, indicating "no flame retardant properties" (BRE Global Ltd., 2017). Therefore, the cladding panels were unsuitable for the design, as "Categories 2 and 3 in the screening test would not meet the requirements for limited combustibility set out in Approved Document B guidance" (BRE Global Ltd., 2017).

1.4 Standardised Testing

Investigation of ventilated façade fire incidents have displayed the short comings of the present industrial approach to fire safety and have instigated shifts in building regulations to ensure appropriate routes to compliance are made. Due to the complexity and variety in building construction in the modern setting, buildings no longer fit to prescriptive regulations and thus require performance-based proceedings to demonstrate compliance with fire safety regulations (Hurley & Rosenbaum, 2015). The means to achieving compliance for façade constructions within the UK, pre-Grenfell incorporated; the application of a limited or non-combustible design, complete fire safety analysis certification, fire testing under the principles outlined in BS 8414 and BR 135, or a desktop assessment indicating that a new design poses equal or lesser risk than a previously approved design (National Housing Federation Ltd., 2018). As demonstrated previously by BRE Global Ltd., the cladding panels applied to the structure were neither limited nor non-combustible in nature and hence were not suitable for the construction. Whilst further investigations from the BRE Global team determined that, not only did the façade system installed on the structure not reach compliance from BS8414 testing, but a substitute panel with a fire-retardant core also failed testing (Guillaume et al., 2018). This information calls into question the first method of achieving compliance, of which was later rectified in the 2019 Edition of Her Majesty's Government's Approved Document B. The document now states that for buildings greater than 18m in height, all construction materials for external walls shall be rated class A2-s3, d2 or safer, indicating non-combustibility of the design, with exceptions for BS 8414 and BR 135 performance-based design approval dependent on structural occupancy.

Further, the post-Grenfell testing performed by BRE Global Ltd. questions the final compliance method for fire safe façade installation. By demonstrating the importance of the combined influence of façade components on fire behaviour, the BRE team highlight the danger of substituting components in a façade design. In the initial BS8414 tests conducted, the cladding panels incorporating a fire-resistant core, failed when paired with the PIR combustible insulation, that had been applied to the Grenfell tower (Guillaume et al., 2018). Whereas, additional trials with Mineral Wool insulation resulted in a passing grade. Reflecting on the material behaviour of façade components in interaction with one and other, Guillaume et al. (2018) discusses that "the fire behaviour of a building façade is dependent on the overall system's performance, rather than the performance of the individual components." For instance, McKenna et al. (2019) details the 'antagonistic' reaction between the ACM-PE

cladding and PIR insulation materials applied to the Grenfell façade. In that “a few burning drips of polyethylene from the panelling are enough to ignite the foam insulation, providing a novel explanation for rapid flame-spread within the façade” (McKenna et al., 2019). Amidst separate investigations Choi & Taylor (1984) explained this phenomenon based on material type, specifying that thermoplastic materials like polyethylene, will melt when exposed to heat resulting in secondary flame spread, whereas thermoset plastics will char and retard the growth of a fire. Choi & Taylor go on to discuss the important influence of the cavity width in accentuating or limiting the impacts of façade components on fire behaviour. This understanding indicates the value of the BS 8414 methodology and complete fire safety analyses approaches to compliance, in demonstrating façade performance as a whole in a performance-based manner. This is reflected on by Dame Judith Hackitt when she discusses that “The Government should significantly restrict the use of desktop studies to approve changes to cladding and other systems to ensure that they are only used where appropriate and with sufficient, relevant test evidence” (National Housing Federation Ltd., 2018).

Finally, in demonstrating the importance of performance-based fire testing, recent fire incidences have subsequently highlighted the disparity in testing methodologies within the European construction industry. Previously, EN 13501-1&2 standards were used to classify the reaction and resistance to fire of façade components across Europe, respectively. However, understanding of the complete system performance of façades discussed prior, and a European Inquiry detailing additional requirements outlined by member nations, demonstrates the need for a new unified methodology for testing and classification (Boström et al., 2018). It was outlined in the inquiry that 14 of the European national bodies held requirements that extend beyond the EN13501 standards, to address issues of; systems performance, flame spread, falling debris and smouldering. Accordingly, these new requirements each incorporate various unique testing methodologies for evaluation of façade fire performance, totalling 12 separate procedures present throughout Europe (Boström et al., 2018). With varying conditions applied to samples in each methodology, it is clear that products cannot be held to the same standards throughout Europe. It is therefore vital to decide upon a unified methodology, to ensure that a standardised level of fire safety is enforced throughout the European construction industry. The tender report published by the European Commission, outlines the intension of establishing a methodology based on the British BS 8414 and the German DIN 4102-20 testing standards.

The methodology selected for the purposes of this thesis, as previously mentioned, is the ISO 13785-1 arrangement. This Intermediate-scale test characterizes a one third scale representation of the BS 8414 methodology and is used widely in the industry for research and screening of designs for full-scale BS 8414 classification (Guillaume et al., 2018). The standard is a primary tool for reducing expenditure in the process of façade design development and is likely to remain so as European regulations unify. It is thus the standard of focus in this thesis, as the work aims to validate the methodology in its representation of realistic façade ventilation conditions, whilst adding to the presently incomplete body of knowledge of fire behaviour in ventilated facades, to assist in future complete fire science compliance analyses.

1.5 State of the Art

The present fire science body of knowledge documents a vast array of testing in the wake of the global fire incidents reported. The variety of testing methodologies, developed around the world for determining local standardised performance requirements, have resulted in the availability of a plethora of fire science data for ventilated façades. However, the ranging conditions upon which these tests are based results in arising questions as to the validity of conclusions made when addressing data comparison, and subsequently significant knowledge gaps within the field become apparent. The following information is collated to highlight the important fire dynamic principles investigated in existing façade fire investigations, whilst addressing the key characteristics of these methodologies that may have a distinct influence on conclusions made. With the aim of drawing attention to potential knowledge gaps which will shape the focus and manner of testing for this thesis within the ISO 13785-1 testing arrangement.

1.5.1 Guillaume et al. (2018)

Firstly, Guillaume et al. (2018) have utilized the standardised ISO 13785-1 methodology for material analysis of the façade system applied to Grenfell Tower. The conclusive argument produced from their investigation involves the dependency of fire behaviour on the combination of components within a façade system as a whole, as described in substitution

. The cladding panels were shown to act as the primary contributor to the performance of the façade, with the insulation layer demonstrating an impact primarily in the decay phase of burning. The reasoning behind the ACM-PE cladding panels' performance, is its combustibility and the manner with which the integrity of the underlying cavity degrades under the impact of fire loading. When an ACM-PE cladding panel is exposed to fire, the Aluminium layer will begin to melt and drip due to its low 660°C melting point (The Engineering ToolBox,

2005). As Professor Torero explains “Flames are typically between 600℃-800℃, thus are hotter than the melting temperature of aluminium” (Torero, 2018). With the degradation of the aluminium layer, the combustible Polyethylene insulant layer is exposed to direct attack from the flame, eventually resulting in the failure of the cladding panel, as demonstrated in the time lapse photos presented in the paper. With the integrity of the cavity breached, the protective function of the installed cavity barrier system is removed, allowing flames to bypass the barrier and progress up the structure, as witnessed in the three fire incidents reported.

The paper presents comprehensive evidence for the impact of the ACM-PE cladding panel in comparison to the ACM panels with Non-combustible and Fire-retardant insulant cores, in the presentation of time lapsed photo sequences, along with plots depicting the comparative heat release rate of the samples over time. The data demonstrating the near complete burn out of the ACM-PE samples within 10 minutes, with the alternate samples indicating the effective function of the cavity barrier in limiting fire spread due to the maintained integrity of the cladding panels. Notice that the tests were run with a 50mm cavity width, constrained to 24mm in the region of the un-activated intumescent barrier. The bottom of the sample was closed off by an ‘L’ profile constructed of Aluminium, simulating the façade construction over a window. Whilst the sides of the sample were closed off with additional cladding panel material. Therefore, the oxygenation of the sample is initially limited both horizontally and vertically. However, as discussed, the flames will melt the aluminium, allowing the entrainment of oxygen vertically into the sample. While the side closures will react in the same manner as the panels, indicating that there will be horizontal entrainment in the ACM-PE case, as the material degrades and fails. Further, the top of the sample remains open to allow the flow of oxygen anticipated in a ventilated façade. As discussed in Section 1.2 the influence of lateral entrainment on a test sample may be important regarding stoichiometric requirement ratios and will thus be a primary focus of this thesis, while the provision of side closures will influence heat losses due to the additional means of re-radiation.

1.5.2 Efectis UK/Ireland Ltd. (2018)

The Efectis team performed a similar study using the ISO 13785-1 methodology, as in the tests of Guillaume et al. (2018). Notice that both tests were performed in the same facility located at the Efectis Fire Laboratory in Jordanstown, Ireland, as Efectis was contracted for both studies. Thus, it can be deduced that the tests would be investigated under generally the same conditions, with the same equipment. However, in the Efectis UK/Ireland Ltd. (2018) study the top and sides of the samples were closed with non-combustible boards, while the bottom

was fitted with an aluminium profile to hold insulation but did not close the cavity. The test saw two samples analysed with the same façade components applied in both scenarios, but each incorporated a different cavity width (Test 1 – 40mm and Test 2 – 100mm). The façade incorporated stone cladding panels, phenolic foam insulation and a cavity barrier positioned just above the base of the upper cladding panel, as in Guillaume et al. (2018). The fire performance results of the tests were presented through time lapsed photo sequencing, thermocouple data and heat release rate plots.

Contrary to the logic presented by Ingason (1994) and Livkiss (2018), the time lapse comparison between the two tests indicates more adverse conditions in the larger 100mm cavity width. The images depict breakages in the cladding panels much earlier in the sequence for the 100mm case, while flames were seen to progress up to the horizontal joint below the cavity barrier faster than the 40mm case. Upon inspection of the heat release rate plot for each test case, the data can be seen to support the evidence provided in the time lapses. Given that the 40mm sample demonstrates a relatively constant heat release rate of 120kW throughout the length of the 30-minute test. Whereas the 100mm sample is initially stable at 120kW until it spikes at 5 minutes, leading to a maximum of almost 180kW, before settling at a relatively constant 150kW for the remainder of the test duration. This reduction in heat release rate of the 40mm sample may relate to the principle of constrained oxygen availability discussed in Section 1.2, given that Ingason (1994) did not report widths less than 50mm. Therefore, a higher entrained air availability is present in the 100mm cavity width, for more effective oxidation of gases produced in the pyrolysis of the insulation material, resulting in the heightened heat release. Professor Jose Torero further indicates in his Grenfell Phase 1 report that “thermal expansion of the gases block the flow” within a small cavity, meaning “flames cease to spread internally” (Torero, 2018). As discussed, these principles will be explored further in the tests of this thesis, noting however that the exploration will be entirely non-combustible. Parallel studies performed by Tanja Černoša, will incorporate combustible insulation for consideration, as well analysis of non-combustible insulation applied with and without a combustible water-resistant barrier.

The disparity between the Efectis data and the prior Ingason (1994) and Livkiss (2018) is understandable based on a few key principles. Firstly, the previous data incorporated only non-combustible materials and hence will maintain a steady state flame height. The Efectis data does initially demonstrate greater flame heights for the 40mm case, when flames were shown to reach the first horizontal joint faster in this case. However, once pyrolysis of the insulation

and combustion of the pyrolysis gases takes hold the flame heights of the 100mm case extend higher within the sample. This is seen to take place at around the test's 5-minute mark, indicated in the jump in the heat release rate plot. Notice that the oxidation of combustibles requires a much greater amount of oxygen than for a simple diffusion flame burner, therefore drastically changing the entrained to stoichiometric air ratio reported in Section 1.2. Further, the previous data was undertaken with the top of the sample open over the cavity width. Whereas the Efectis tests were closed at the top of the cavity, leaving only the 20mm panel joint for the escape of smoke gases. As such this may hold a significant limiting factor on the chimney effect following mass conservation laws. Where pressure progressively builds up within the cavity from the upper section, constraining the draw of the flames up the cavity. Thus, the effect is not nullified but will be less accentuated as in the prior cases. The tests to be performed within this thesis will be non-combustible and hence should rather follow the principles of Ingason (1994) and Livkiss (2018) however the impact of cavity closure on the chimney effect will be represented by use of a cavity barrier placed just above the upper horizontal joint. Čolić & Pečur (2020) demonstrate the effect of the cavity barrier in this function in their work, detailing that "the chimney effect is physically disabled with the horizontal barrier." Noting that in the thesis test case, the horizontal joint will provide 20mm for the escape of smoke gases, representative of the conditions of Efectis UK/Ireland Ltd.

Finally, the thermocouple data presented demonstrates the importance of cavity width in the progression of heat about corner sections of a façade. For instance, the data indicates that the 100mm case passes heat around the corner well, as there are more angles of radiation for the heat to be transported. Whereas the 40mm case shows lower heat transfer to the wing thermocouples as the heat is either re-radiated or absorbed by the panelling and insulation, keeping it within the domain of the main section of the sample. This principle will be explored further within this thesis with the varying cavity widths to be analysed.

1.5.3 Choi & Taylor (1984)

The experiments reported, were undertaken by W. Taylor on a fit for purpose rig demonstrating a façade spanning two storeys. The tests incorporated a 1.25m wide by 5m high sample of non-combustible material, closed at the sides and top of the cavity. While the base remained open by allocation of a hole 25mm in height presented along the full 1.25m sample width. Viewing ports were presented at 500mm intervals for visualisation of the flame heights up the façade structure. The sample was constructed such that combustible foamed plastic insulation (polyurethanes and polystyrenes) could be installed directly to the non-combustible structure,

with variable adjacent cavity widths. The test studied the influence of the cavity width on the flame behaviour within the façade air cavity for both combustible insulation types. Similarly, to the Efectis UK/Ireland Ltd. (2018) case the tests demonstrated more adverse conditions in the larger cavity spaces. However, in this case widths of 40mm and less were investigated, indicating that a continual reduction in width will result in further constraining of the air supply for oxidation of the sample. Again, however this test case has incorporated the closure to the top of the cavity, reducing the impact of the chimney effect and entrainment. Therefore, it is of high priority to investigate the impact of this blockage in the tests to ensue. Distinctly, Choi & Taylor (1984) report on a critical cavity width of 25mm, present with both material insulations tested. The results indicated the 25mm width as the optimal solution for the cavity, based on a balance of ventilation and limitation of flame spread within the façade. Initial tests demonstrated cavity widths of 13 and 19mm showing signs of very limited burning of the insulation layer, with flame heights of only approximately 1-2 metres witnessed. While in the 25mm case, despite additional burning reported in the post fire investigation of the insulation layer, the flames were also limited to only 2 metres in height. However, when the cavity width was extended to 40mm the burning was seen to be much more severe, with flames engulfing the full height of the façade cavity. In consideration of this information amongst other sources, this logic was accepted into the National Building Code of Canada in 1993, where it is presented that the cavity must contain "not more than one concealed air space and the horizontal thickness of that air space is not more than 25mm" (Building Code Commission, 1994). This standard is accepted as an industry norm to this day to limit external fire spread of a structure, though not openly specified in current standards (Canadian Commission on Building and Fire Codes, 2015). As Choi & Taylor discuss that "when the air space is large enough to allow an adequate supply of oxygen for the burning process, the likelihood of fire propagation from storey to storey within the wall cavities increases greatly." This principle is not followed in European norms however as a cavity width of 50mm is taken as standard practice. Despite once again not openly being specified in the current standards (HM Government, 2019). Hence, the cavity widths planned for investigation within this thesis will be primarily 25 and 50mm cases to provide further evidence for the discussion of an optimised cavity performance. Further, a 100mm case will be investigated to complete the analysis spreading data across the range of data provided by Choi & Taylor (1984) and Efectis UK/Ireland Ltd. (2018) to link the analyses and their conclusions.

1.5.4 Kolaitis, Asimakopoulou & Founti (2016)

The experimental analysis incorporated a purpose-built rig for the analysis of the flow conditions of externally venting flames in interaction with a façade's air cavity. The façade was constructed above a small compartment designed to create the required under-ventilated conditions for the fire. The fuel source utilised in this case was a pan of liquid n-hexane, which emitted approximately 2.76MW in the fully developed stages of burning. The façade was composed of non-combustible materials constructing an air cavity of width 25mm with the edges of the sample remaining closed. The lower edge was left partially open with the provision of a perforated steel sheet, while the top of the cavity remained open allowing the vertical flow of gases. The tests indicated that "though gaseous combustion products have managed to penetrate into the air cavity of the Ventilated Façade system, no consistent flaming conditions have been established" (Kolaitis et al., 2016). Inferring that there is insufficient oxidation of the pyrolysis gases once they have entered the cavity to sustain burning. This information appears contrary to the data presented by Choi & Taylor, as they were able to demonstrate sustained burning within a 25mm air cavity. However, the important difference in the two cases is the application of the perforated steel bracket at the base of the cavity and the absence of combustible insulation. Given that insulation will only serve to consume further oxygen in the pyrolysis process, the perforated steel appears to be the cause of the disruption to burning. This may refer to information relating to the quenching diameters of fuels presented by J. R. Grove amongst PhD research. Grove (1968) establishes that when a fire is present external to a container of fuel from which it is fed, a critical diameter hole exists that allows sufficient oxygenation of the fuel chamber to draw the flame into the container. Else the fire will quench on the outside of the container. The same principle can be expressed with the perforated steel sheeting, in that the cavity contains the fuel and an insufficient amount of oxygen for sustained burning while the fire is on the outside of the cavity at the base and unable to enter the cavity due to the lack of entrainment through the perforations. This may be a key concept for further exploration into façade design development in limiting vertical flame spread. Notice too that the perforated section is constructed of steel and thus has a much higher melting point than the prior aluminium sections used in other tests, allowing it to maintain integrity throughout the investigation (The Engineering ToolBox, 2005). Perforated steel sections will be included in the tests of this thesis to simulate a reduction in the entrained air supply from the sides of the set-up. These sections will not have the same impact as above, due to their orientation parallel to the flow of pyrolysis gases and the open condition at the bottom of the cavity.

1.5.5 Agarwal (2017)

The work of Agarwal has demonstrated a comparison between three ventilated façade testing methodologies; the ANSI/FM 4880 16-ft Parallel Panel Test, the British BS 8414 full scale test, and the American NFPA 285 rig. The primary point of comparison made between the procedures, is the crucial factor of the burner applied to the samples. There is a great disparity in the heat release rates and radiant heat fluxes provided by the burners onto the samples in each case, which will result in variable fire behaviour. The ANSI/FM 4880 and the NFPA 285 make use of a propane burner for a more controlled, regulated heat release of 360kW and 1.3MW, respectively. Whereas the BS 8414 method makes use of a standardised wood crib which will burn in a more natural, fluctuating manner releasing 3±0.5MW. The style and size of the burner and its proximity to the façade sample dictates the radiant heat flux applied to the panels, and thus also the type of fire that the test rig aims to represent. For instance, when commenting on the nature of the ANSI/FM 4880 test, Agarwal reports that the burner application onto the sample is effective in "simulating a realistic exterior and post-flashover fire" given that it demonstrates the highest heat flux attacking the panels(≈100kW/m²), despite its low heat release rate. The rig however demonstrates an atypical design, with two cladding systems facing one and other 500mm apart, with the burner positioned within the gap (Martinsson, 2018). In comparison to the BS 8414 rig which demonstrates a realistic externally venting flame from an under-ventilated compartment impacting a façade corner configuration, known to be the reasonable worst-case façade fire scenario. The text goes on to compare the results of the tests performed with Aluminium Composite Materials on all three rigs, showing that the ANSI/FM 4880 and BS 8414 actually demonstrate comparable characterisations of the façade arrangements. Whilst they are also considered more conservative than the NFPA 285 test, which produced passing grades for multiple samples of which the others demonstrated failure ratings. The NFPA 285 likewise represents an externally venting flame but by use of two-burners, a room burner and another applied directly to the bottom of the façade sample, which only provided a heat flux of 40kW/m² onto the panels. Further, an additional room is provided in the test set up above the burner room but does not incorporate any openings to the façade. It is clear therefore, that each particular test rig used for analysis of ventilated facades is set up with a unique fire incident in mind, which complicates regulatory proceedings. The comparative arguments presented by Agarwal between these testing methodologies, however, are based on data produced with inexact material components. As such, the validity of the comparison is called into question based on the principle of component substitution demonstrated in Section 1.4, hence further investigation is required to validate these findings.

Comparing the regulatory tests discussed above, to those for research purposes such as the ISO 13785-1 and the two-storey set-up reported by Choi & Taylor (1984), further indicates the importance of the burner applied to the samples. For instance, the research tests hold much lower heat release rates, but are applied directly to the base of a ventilated façade sample, with the ISO 13785-1 test applying 100kW from a propane burner and the Taylor setup utilizing 25kW from a Natural Gas burner (Taylor, 1983). The lower heat release rate allows for the reaction of materials to be more pronounced in the behaviour of the flame. While the rig remains constrained enough to demonstrate fluctuations in air entrainment using these smaller fires. Further, research cases however may also involve larger burners and test rigs for development in the understanding of alternate fire principles, as in Kolaitis et al. (2016). Similarly, Lee et al. (2007) demonstrated an analysis of the externally venting flames along with the length scales involved, to understand the impact of these flames on façade panels and surrounding obstructions. This research will influence prescriptive building regulations and the standardised performance-based testing used. For the purposes of this thesis, a parametric analysis of ventilation conditions within a non-combustible rig, it is concluded that the ISO 13785-1 rig is the most optimal set up for development in understanding. Resulting from its optimal heat release rate and test size for the representation of responses to entrainment conditions, along with its limited expenditure.

1.5.6 Principles of Ventilated Façade Development

Amidst further investigations, additional principles of façade construction have been realised and are presented for design consideration and system understanding. Firstly, it is important to consider the impact of decisions made, in the interests of fire performance, on the sustainability performance of ventilated façade designs. As a fire safe façade that negates sustainable functionality of a system is not a solution to the engineering problem. Upon inspection of the sustainability calculation guidelines presented by Anderson & Kosmina (2019), it is clear that a ventilated façade's sustainability or U-value is independent of the cavity width and the cladding panels applied. Given that the cavity is well-ventilated and the air temperature within is assumed to be equal to ambient. Therefore, the only major impact that a change in cavity width will play on the performance of a ventilated façade is in the strength of the chimney effect and the convective drying of the insulation within the cavity. As such, from the principles displayed in Section 1.1, it is clear that a smaller cavity width will indicate a more effective chimney effect, providing greater moisture protection for the insulation.

Further, the Phase 1 report for the Grenfell tower fire presented by Jose Torero, highlighted a key fire dynamics principle essential for understanding the development of a fire within a building's façade system. Torero (2018) expresses the reasoning behind the rapid vertical flame spread and the limited lateral flame spread based on the methods of heat transfer. Due to the action of the chimney effect, flame and hot gases drawn up the cavity pre-heat regions above the fire by convective and conductive means, which carry approximately 70% of the fire's heat. Whereas the lateral spread of flame must rely upon the small radiative portions of heat released from the fire, which in a free plume approximates around 5% of total heat from the fuel source in any one direction (Carvel, 2018). Therefore, the regions above the fire within the plume, will begin pyrolyzing and adding to fire development, while regions adjacent to the fire remain undisturbed. Fire spread down the structure is further restricted based on principles of counter-current airflow presented by Merci & Beji (2016). Due to the shape of the fire plume stretching up the structure, "the view factor for radiation heat transfer from the flame to the virgin material is much lower," (Merci & Beji, 2016) resulting in even less radiative heat transfer. However, as discussed in Section 1.3.3 the lateral and downward spread of flame in a façade is controlled not by direct influence of the fire source or plume, but by the secondary influence of falling, burning debris. As discussed in the Grenfell Tower case in Section 1.3.3, the fire began to spread rapidly about the structure when it reached the crown and was able to spread and drop burning debris. Hence, understanding of the dynamics of ventilated façade fire development will shape building and facade design to restrict these means of flame spread. Given, the non-combustible nature of the tests to be performed, the burning debris will not be a factor for analysis consideration. However, the principles of radiative heat transfer will assist in explaining thermocouple data of the ISO 13785-1 test wing, as discussed in Section 1.5.2.

2. Objectives

The primary objective of this thesis is to provide additional information to the Fire Science body of knowledge regarding fire behaviour within ventilated façade cavities. With the knowledge and understanding developed throughout the literature review, the ancillary objectives of this thesis were shaped to incorporate, the construction of intermediate scale testing rigs and a Fire Dynamics Simulator model following the standards outlined in ISO13785-1. In validating and assessing the influence of cavity widths, lateral ventilation conditions and cavity barriers on the behaviour of fire within a non-combustible ventilated façade. With respect to the impacts of the COVID-19 pandemic, the ancillary objectives were adjusted to involve; detailed analysis of FDS software assessing the representative nature of domain discretization and ventilation inputs. Experimental evaluation of the impact of lateral ventilation conditions on fire behaviour within a cavity. Validation of FDS files to the available 50mm experimental data. With an extension of FDS studies to develop an understanding of the potential influence of cavity widths and cavity barriers on fire behaviour.

3. Methodology

The experimental aspects of this thesis comprised two components; Intermediate-scale reaction-to-fire tests following the standards of the ISO 13785-1 methodology, and Fire Dynamics Simulator (FDS) solutions for model representation of the tests performed. The programme planned for experimentation involved a preparatory FDS analysis, followed by the conducting of the Intermediate-scale fire tests, in parallel with equivalent Fire Dynamics Simulations for model validation, finally concluding with extensions to the validated FDS models for additional data analysis output. The ISO 13785-1 methodology was harnessed for its representation of “flames impinging directly on the face of the façade” (International Organization for Standardization, 2002) for the demonstration of immediate fire behaviour within a cavity. Description of the specific testing apparatus of which the models will be based is presented in Section 3.2 and pictured in Figure 4.

3.1 Fire Dynamics Simulator

In anticipation of the laboratory experimentation designed to the ISO 13785-1 methodology, Fire Dynamics Simulator software was utilized as a preliminary means of data analysis. In collaboration with the fire science body of knowledge, the FDS analysis aimed to realise additional relevant fire dynamics principles, that would assist in the confirmation of exact detailing of the practical test arrangement. By demonstrating regions of critical importance

within the ventilated façade design, the practical testing is able to be optimised in its use of available devices for recording the fire dynamics phenomena present. Due to the size of the computational domain required to simulate the testing rig, along with the level of detail required for visualisation of key fire dynamics principles within the façade cavity, the simulations were deemed too computationally expensive for completion on a standard computer. Hence, the FDS files created for this thesis were run remotely, accessing the Lunarc Aurora cluster provided by Lunds Universitet. Discussion for the appropriate resolution applied to the FDS files in order to balance simulation time and output quality is demonstrated in Section 4.1. Noting that for this analysis FDS 6.7.3 was applied, as it was the most up to date version of the FDS software available when the thesis began. FDS 6.7.4 was released amidst testing but was not used to maintain the consistency of the analysis.

Initially, it was uncertain as to how a changing cavity width would be approached with regard to the ISO 13785-1 testing rig. As such, early FDS models demonstrate a consistent cladding arrangement across all cavity widths, to ensure that a constant oxygenation of the sample was maintained with regular cladding panel sizes. The front main cladding section was taken to hold the consistent 1200mm width determined by the ISO 13785-1 rig, while the wing cladding section held a width of 600mm. Hence the backing panels of the samples in these cases were extended to accommodate the provision of the ventilated cavities. Notice too that during the scripting of these initial cases, detailing of the structural supports holding the panels to the frame were not confirmed. Hence, all supports were omitted in these models due to the preliminary nature of the study and the primary focus on the impacts of the side ventilation conditions. Finally, to add additional value to these models beyond identifying regions for instrumentation, the vertical joints were provided with a greater width, to simulate the impact on sample oxygenation and the chimney effect. This was deemed an acceptable alteration given that these models would not be applicable for validation without relevant support detailing. One of the many iterations of trial FDS input files and its associated Smokeview (SMV) representation can be seen in Appendix A1 & A2, respectively. These preliminary files provided a wealth of knowledge regarding the requirements and use of the FDS software for this task, as well as information guiding design of the rig and its outputs. These adjustments will be reflected upon and demonstrated in changes made to later input files.

After inspection of the outputs of the first round of FDS files, presented in Section 5.1 & 5.2, input files for the purposes of model validation were created. Model adjustments were made in light of the understanding developed from the original files along with the provision of

additional information regarding the final detailing of the design test. These validation files saw the lowering of the cavity barrier into a similar position demonstrated in the papers of Guillaume et al. (2018) and Efectis UK/Ireland Ltd. (2018), such that the flow conditions within the cavity above the barrier could be represented. The top edge of the barrier was situated 200mm from the bottom edge of the upper cladding panel, allowing lateral escape of smoke gases through the horizontal joint below, for a continued function of the chimney effect as discussed in Sections 1.5.2 & 1.5.3. Further, with the movement of the cavity barrier it is clear that devices used in the centre of the cavity above the barrier, will be impacted by the permanent portion of the barrier even before the intumescent material activates. This is only applicable in the 50 and 100mm cases which incorporate these permanent portions of the barrier. Thus, the location of these devices should be shifted into the co-ordinates for the middle of the gap between cladding panels and the permanent cavity barrier. Such that data collected can be compared with the 25mm case, in showing the influence of intumescent activation. In all cases this location is 12.5mm from the cladding panel, due to the 25mm thick activated intumescent materials utilized for the investigation. Further, due to the importance of this region 12.5mm from the cladding panels, additional slice files were introduced in these areas. The slice files employed in these studies focus on temperature, gas velocity and oxygen mass fraction. Additional corrections to the model relate to the confirmed adjustment detailing of the ISO 13785-1 methodology to fit the study. Firstly, the backboards of the main and wing wall were adjusted to set lengths of 1200mm and 600mm, respectively. Thus, the panel dimensions were adjusted accordingly to maintain 20mm joint spacings, as demonstrated in Table 2. Further, the cladding panels were adjusted to finish flush with the backing boards, so that the sides of the rig could be completely closed by the steel ‘L’ profile. Finally, the adapted ‘Z’ profile and ‘U’ profile fixings (see Section 3.2) were applied to the model, but in a simplified manner. Such that only the sections of the profile normal to the cladding panels are modelled, due to their influence on ventilation. The only exception is the central span of the ‘U’ profile which is include as it obstructs the central vertical joint, all other portions are omitted. The basic Smokeview rendering of a validation file is presented in Figure 3, while the input file is provided in Appendix A3. For representation of the ventilation impacts of the perforated steel sheeting, the FDS ‘SCREEN’ surface input was initially utilized in the analysis, however this had to be replaced by a simplified block methodology, to be discussed in Section 4.1.

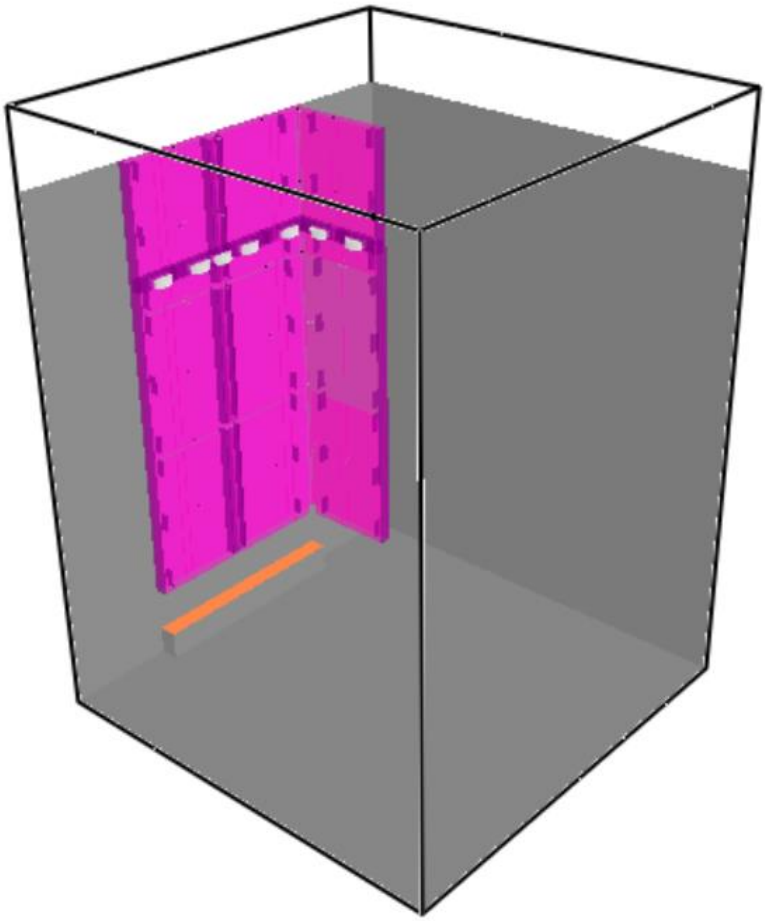

Figure 3: SMV Rendering of 50mm Closed-edged FDS file, Model Iteration 'a'

Unfortunately, during the completion of the fire testing, Cavity Barriers were not available for addition into the sample. Hence, the models initially designed for validation of the ISO 13785-1 rig, were no longer valid for that purpose. Thus, new models were created with the cavity barriers removed to match the tests. The function of the prior tests was therefore adjusted from tools for validation, to the models extended for the purpose of additional research and data collection, based off of validated models. It is important to note however that the cavity barriers employed in the model are highly simplified and formed to activate in blocks based on single point detectors. Hence, the function of the barrier will not reflect the correct activation process and closure of the cavity. Though, the resulting flow conditions will stabilize as the whole intumescent layer activates, demonstrating a reasonable estimate for the influence of a cavity barrier on the chimney effect. The new models for validation are the only models run with a heat flux detector positioned based on the ISO 13785-1 guidance. This is considered for validation purposes only, as the short simulation times should not represent the full severity of the heat flux, resulting in the production of misleading data, see Section 5.3. Finally, the devices above the anticipated cavity barrier were returned to the centre of the cavity.

3.2 ISO 13785-1

The Intermediate-scale ventilated façade fire tests were performed in the facilities of Efectis UK/Ireland Ltd. at the University of Ulster in Jordanstown, Northern Ireland. The tests were sponsored by the Kingspan Group and were planned to proceed in March and April of 2020. Initially nine tests were to be carried out, involving three different cavity widths (25, 50, and 100mm) in combination with three lateral ventilation conditions (open, closed and 50% perforated) as demonstrated in the test programme presented in Table 1.

Table 1: ISO 13785-1 Test Programme

		Cavity Width (mm)		
		25	50	100
Lateral Ventilation Conditions	Open	Sample Four	Sample One	Sample Seven
	Closed	Sample Five	Sample Two	Sample Eight
	Perforated (50%)	Sample Six	Sample Three	Sample Nine

The testing rig was constructed with; 12mm Calcium Silicate back boards attached to the steel Efectis ISO 13785-1 supporting structure, steel ‘Z’ and ‘U’-type flashings for securing the cladding panels to the backing boards, standardised steel fixings for securing the Calcium Silicate and steel flashings/profiles, steel ‘L’ profiles for changing the lateral ventilation conditions (2 sections 50% perforated and 2 closed section) and 9mm Calcium Silicate boards for the cladding panels. All other testing conditions remained consistent with the prescribed ISO 13785-1 methodology by use of the Efectis Laboratory equipment, with the addition of a bi-directional probe as indicated in the schematic diagram presented in Figure 4. The bi-directional probe, like the thermocouples, was installed into the sample by inserting the device through holes drilled into the calcium silicate backing board. The surrounding space of the hole around the device was filled with non-combustible mineral wool, closing the gap and avoiding influence on the test sample. This method of installing devices provides a distinct advantage in accessing required locations in the cavity, while providing protection to the non-flame resistant portions of the devices. For instance, the plastic tubing attached to the bi-directional probe and the wires attached to the thermocouples.

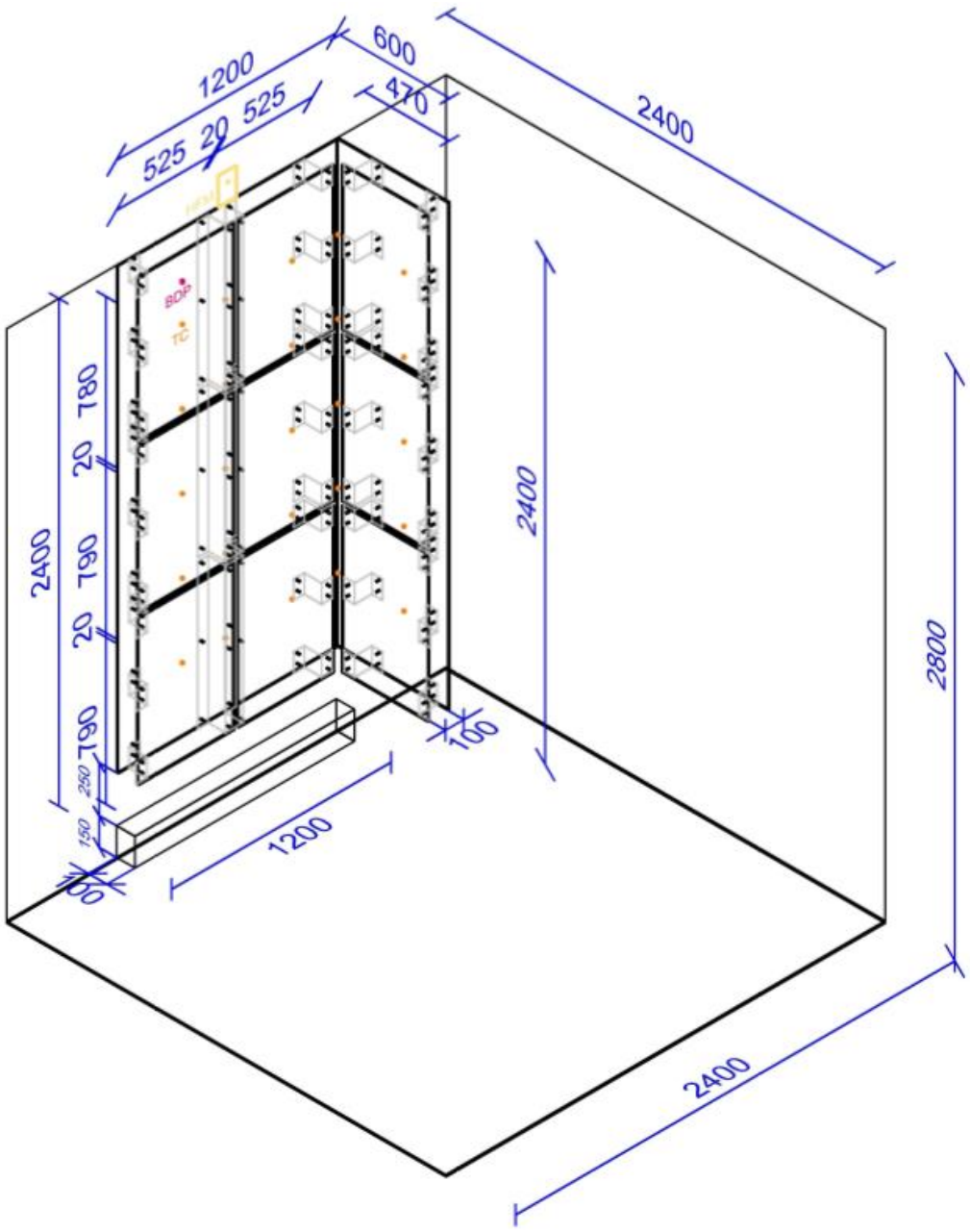

Figure 4: Schematic Diagram of the adapted ISO 13785-1 apparatus employed

Notice that the standard design of a façade has been slightly adjusted for the undertaking of this ventilation study. The general application rail system that is used to support the cladding panels, is replaced by the array of flashings as demonstrated in Figure 4 and detailed in Figure 5. The reasoning behind this substitution is to accentuate the influence of the lateral ventilation conditions applied between the various tests, else the rail systems would effectively close the sides of the cavities anyway. While the absence of insulation results in the reduction of the total cavity width to sizes that do not facilitate use of rail systems. The flashing details presented in Figure 5, illustrate the laterally open ventilation conditions provided by the flashing design, whilst the primary vertical joint remained sealed as in standard façade design.

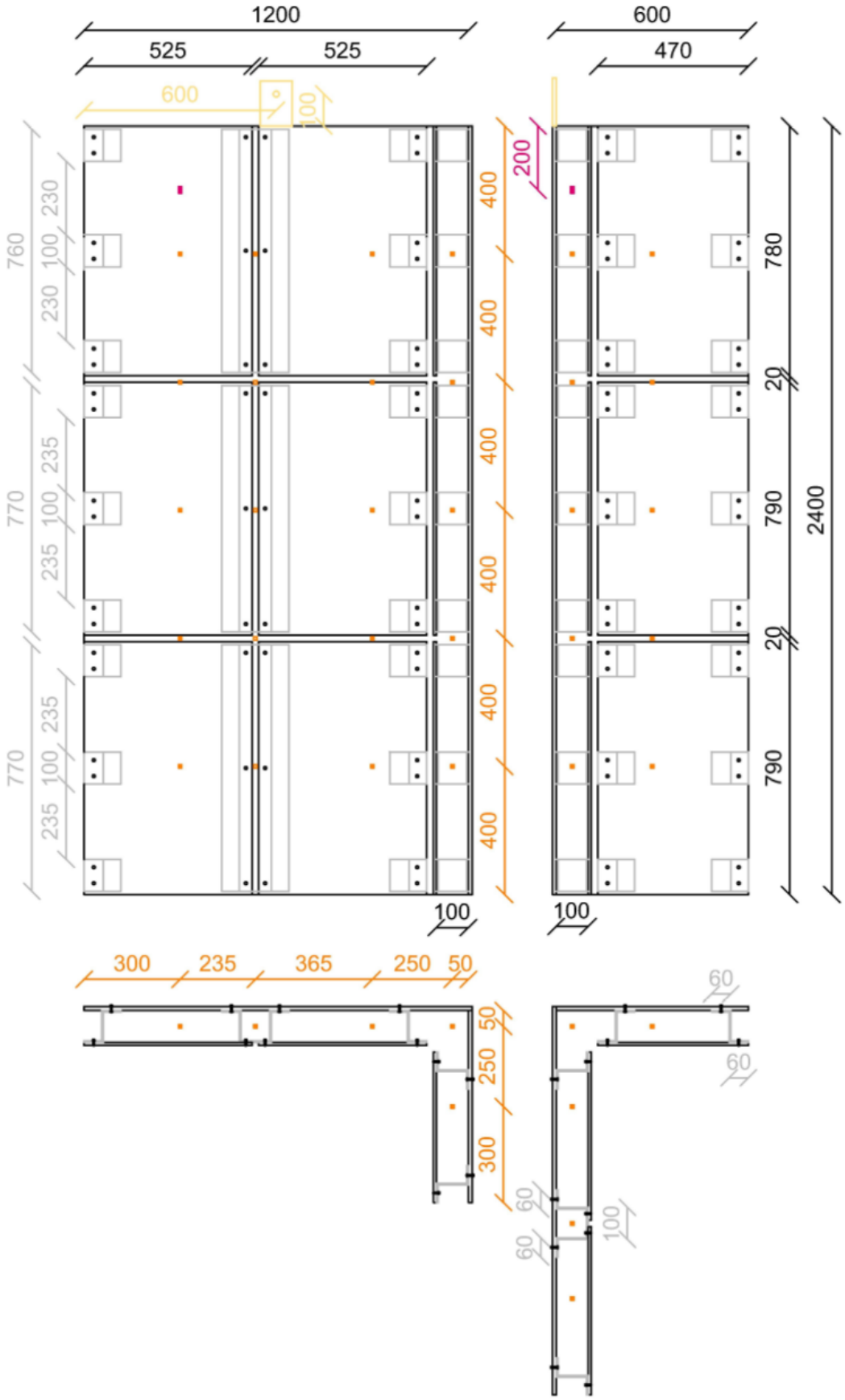

Figure 5: Adapted ISO 13785-1 Construction Detailing

Further, the detailing illustrates that the vertical joint in the corner of the rig remains open for oxygenation. This is unconventional compared to standardised façade design involving rail systems, as it allows heat to freely pass around the corner into the wing portion of the sample. The additional path for oxygenation, though minor, will also provide further insight into fire dynamic principles and flows within a cavity. Given that the left-hand portion of the rig will represent ventilation conditions with a closed opposing end of the cavity, with the U-type flashings limiting lateral drafts. While the wing ventilation conditions will be analysed with the opposing corner open, allowing additional lateral air flow. Another point of focus for the analysis is the influence of the cavity widths on a closed chimney effect, which will be demonstrated in the space provided at the centre of the U-type flashings.

Due to the standardisation of the backing boards of the ISO 13785-1 methodology it is clear that with a changing cavity width, variations in panel sizes must be provided to accommodate the cavity whilst maintaining joint sizes. As such flashings and thermocouples will also need to be adjusted to fit the new sample, with the interest of maintaining as much consistency with the other rigs as possible. Table 2 highlights the alterations made to fit the changing cavity widths, all other locations and dimensions remained constant. Therefore, it should be recognised, that some minor influences will be seen in the results of the thermocouple sets; H1, H3 and H5, the Bi-Directional Probe and the Heat Flux Meter, in comparing varying cavity widths. This is because these instruments remained in constant locations throughout all samples and thus their proximity to shifting joints and flashings may provide minor influences on the data produced. The reference system for the devices used in these tests is provided in Figure 6.

Table 2: Sample alterations dependant on Cavity Width

	Cavity Width (mm)		
	25	50	100
Main Face Panel Width (mm)	565	550	525
Wing Face Panel Width (mm)	545	520	470
H2 Thermocouple Set Location Distance from Outside Main Sample Edge (mm)	585	560	535

The particular devices utilized for the study were selected following industry standards and information provided by the ISO 13785-1 methodology. K type thermocouples were applied to the sample due to their accuracy over a wide range of temperatures, including the high temperatures anticipated in intermediate-scale tests (OMEGA Engineering, 2019). The bi-directional probe held an entry diameter of 16mm and was paired with a pressure transmitter

with an output voltage of 1-10V. The selection of probe diameter was made to suit the scale of the testing rig, while the pressure transmitter was selected to suit the Efectis data logging systems provided. The heat flux meter and propane burner incorporated into the analysis follow the guidelines portrayed in the ISO 13785-1 methodology. A standard camera was used in all test cases to observe and record the procedure from in front of the rig, while the test with open lateral ventilation conditions was able also to be filmed from the side to witness flame behaviour and height within the cavity. The camera and stand in this location were partially protected by additional calcium silicate board.

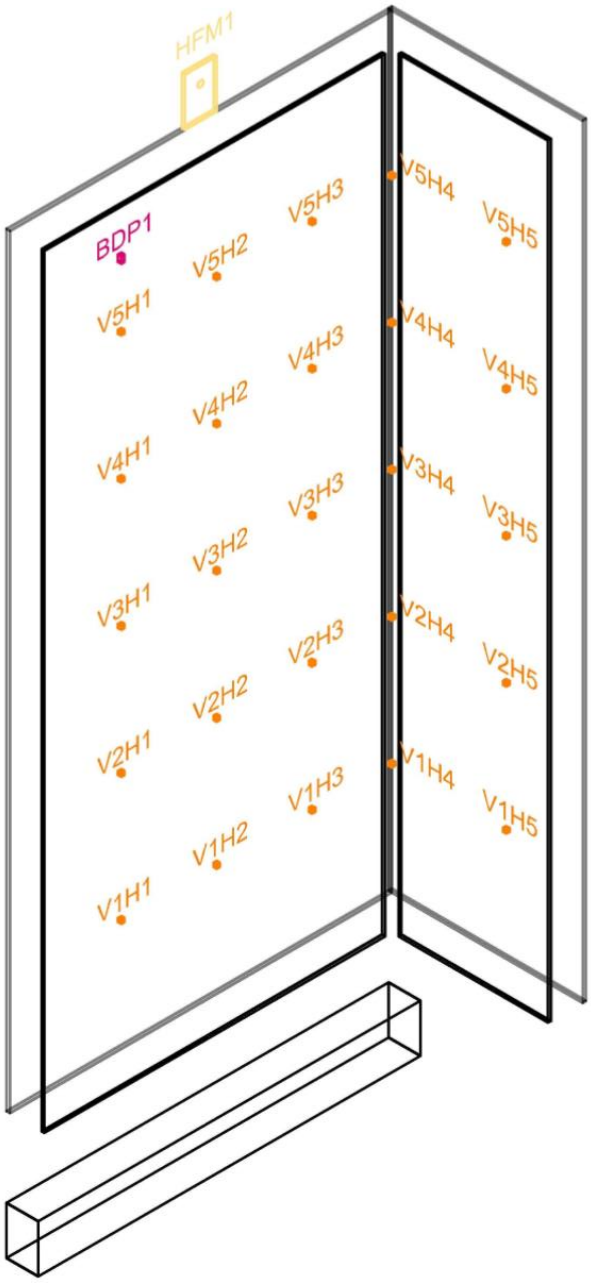

Figure 6: Device Reference System

Due to the impacts of COVID-19 and the time restrictions for the completion of the thesis work, only three of the nine tests were able to be performed, as discussed in Section 4.2. The tests selected for completion were the 50mm cavity cases (highlighted in Table 1) following European norms. The choice to select a single cavity width was made to allow a complete lateral ventilation influence study to take place, while the practicality of a single cavity width rig catered to the production of an accelerated testing schedule. The re-use of calcium silicate panels for all three studies was acceptable given that the boards were deemed to be in reasonable condition after each test. Noting that tests were performed on different days to ensure that the testing rig had been completely cooled. The assumption for the re-use of materials was that the calcium silicate boards utilized within the design did not significantly add to the fire load as a result of their non-combustible nature, and that re-use would not lead to significant impacts to the data produced. The absence of 25mm and 100mm Cavity Width samples infers that there will be no comparative data available for analysis of lateral ventilation incorporated with a variation in cavity width, apart from the preliminary information made available through Fire Dynamics Simulations.

Figure 7:Experimental Configuration for the 50mm Closed Lateral Ventilation Façade sample

4. Limitations

The primary restrictions faced in the undertaking of this thesis and the analysis of fire behaviour within both real and simulated ISO 13785-1 testing samples, incorporated a lack of access to required materials and available time for completion of all planned analyses. Organised research and deliveries of materials were delayed for a multitude of reasons throughout the allotted thesis time, with the final and most influential reason involving the COVID-19 pandemic which locked down the Efectis laboratory at the time of planned burn tests. The following sections depict the problems that were faced amidst completion of the studies and the methods by which these issues were managed to produce sufficient data for analysis.

4.1 Fire Dynamics Simulator

Despite being a highly functional and cost-effective tool for the simulation of fire behaviour within a system, FDS faces a number of limitations that restrict its capabilities. Firstly, and most importantly for this analysis is the computational time. FDS is a simulation tool that employs a Large Eddy Simulation (LES) model for solving turbulence, and as such to demonstrate a high level of detail within a simulation, a refined mesh must be employed. Discretization of the simulated domain will dictate the smallest turbulent eddy that can be witnessed by the solver, while all other smaller levels of turbulence will be approximated from the observable scales (Merci, 2019). Thus, an increase in the number of cells within a mesh will result in a significantly higher amount of calculations for the solver to perform to limit approximations and therefore lengthens compute times. Due to the large domain requirement for housing the ISO 13785-1 testing rig, and the high level of detail required for the analysis, the models studied contained over 2.32 million cells. As discussed earlier in Section 3.1, this simulation type is far too computationally expensive to be run on a standard computer. However, when the files were computed on the Aurora cluster a 60 second simulation would still take around 7 days to complete, dependent on the ventilation conditions and cavity widths applied. Therefore, it is entirely impractical to simulate a full 30-minute burn test as specified by the ISO 13785-1 methodology. However, upon inspection of the early informative simulations described in Section 3.1, it was found that in the absence of combustible materials, the fire generally reached steady state within the first 20 seconds of simulation, with exception of periodic oxygenation fluctuations. Hence, for the comparative assessment of cavity widths and ventilation conditions the 60 second simulation times were deemed sufficient for the analysis of general trends. Whilst the validation files were set to simulate 120 seconds to provide additional data for validation purposes, which took five and a half days to compute.

Due to the drastic changes made to the research setup and schedule the simulated analysis too had to display a reasonable degree of flexibility, hence simulation times had to be managed to allow quick access to reliable data. In managing computational requirements a few key principles within FDS can be addressed to optimise the output to computation time ratio. The level of refinement of the mesh selected is the most crucial aspect of optimising the FDS files, given that doubling the number of cells within a mesh will result in an increase in computation time by a factor of 16 (Merci, 2019). Hence, it is essential that the mesh selected is refined enough to present the required output data, without being overly refined resulting in diminishing returns on compute times. The FDS Technical Reference Guide for Validation provides a useable tool for approximating the required mesh size for a particular model, by use of the Plume Resolution Index (PRI). The index represents "the number of grid cells of length δx that span the characteristic diameter of the fire. The greater its value, the more resolved are the fire dynamics" (McGrattan et al., 2020). Realisation of the index requires calculation of the characteristic fire diameter (D^*) of the fuel source installed into the FDS model based on the equation:

$$D^* = \left(\frac{\dot{Q}}{\rho_\infty c_p T_\infty \sqrt{g}}\right)^{\frac{2}{5}} \tag{3.4}$$

Thus, the PRI is presented by dividing the Characteristic fire diameter (D^*) by the length scale for the grid cells (δx). The FDS Technical Reference Guide goes on to demonstrate prior FDS assessments for validation of the software and associated PRI values for each of these cases, for reference to appropriate mesh resolution (McGrattan et al., 2020). Using the heat release rate of the ISO 13785-1 methodology and standard atmospheric conditions, the characteristic fire diameter for the FDS models of this thesis is found to be $D^* = 0.38$. Hence, when a 10mm grid length scale is adopted, the PRI is found to be approximately 38. Upon inspection of the past validation research it appears that the resolution of this ISO model may be slightly too detailed, however the index is calculated with regard for free burning buoyant plumes and hence more complex turbulence will appear within the cavity, requiring greater refinement. While, the small cavity widths (25mm) of the model require smaller length scales for analysis, thus 10mm can be deemed as appropriately refined.

Additionally, simulation times can be reduced by playing with the number of meshes used to resolve the problem domain. By increasing the number of meshes used, the solver is able to calculate more regions of the domain simultaneously, however this may result in the formation

of numerical errors and instabilities. For example, the FDS User's Guide discusses that "FDS uses a low-Mach number formulation of the Navier-Stokes equations" (McGrattan et al., 2019), which results in the assumption of an infinitely fast speed of sound. Following this assumption, the pressure solver will become globally sensitive to changes throughout the domain. Thus, when the domain is divided into multiple meshes, pressure information will no longer be transmitted instantaneously throughout the domain. Rather, information will be transferred iteratively at the interface between meshes, resulting in numerical instability (McGrattan et al., 2019). It was deemed appropriate to attempt to split the domain into multiple meshes for this study to harness this additional saving to simulation times. Given that the discretisation of the domain was performed horizontally, while the majority of anticipated pressure differences of the chimney effect should be witnessed vertically, limiting errors. Hence, the original 6-mesh model run which took 7 days to run, was adjusted to incorporate 10 meshes as demonstrated in Figure 8. The 10-mesh solution was able to reduce simulation time to just two days, whilst sustaining a maximum percentage error between the models of 16.5%. Figure 8 demonstrates that the mesh was refined to cell sizes of 10mm near to the testing rig while, distant cells demonstrated cell sizes of 100mm. Notice that the figure demonstrates the experimental facade detailing for representative purposes, however the error analysis was performed with simpler models, shown in Section 5.1.

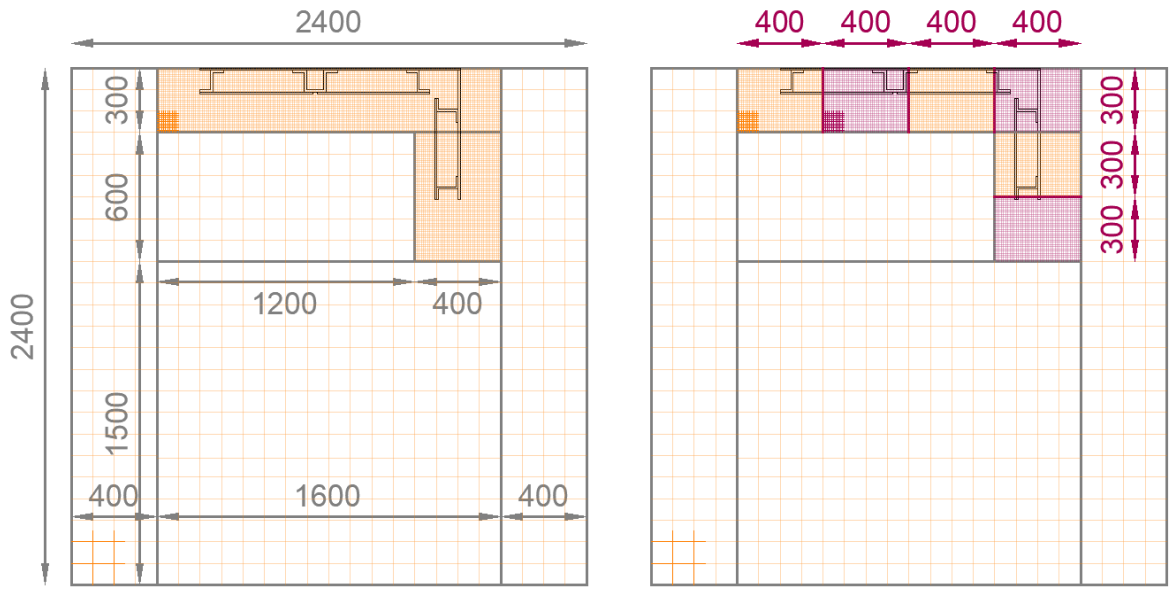

Figure 8: Comparative Discretisation of the Model Domain; 6 Mesh solution (left), and 10 mesh solution (right)

To further the investigation of the techniques used to reduce simulation times with regard for the resultant discrepancies in output data that they produce. A further simulation was run using the 6-mesh model, with adjustment to the resolved cell size from 10 to 20mm within the detailed façade analysis zone. The new model indicated a simulation time of just over 9 hours, whilst demonstrating a maximum error of 26.8% in comparison to the original model. Comparing the mesh resolution and the domain discretization methods, it was determined that the heightened accuracy of the 10-mesh domain discretization method was more important for the analysis than the increased flexibility provided by the available simulation times of the mesh resolution method. Hence, for the completion of the studies of this thesis, 10-mesh FDS solutions have been utilized for all analyses, keeping in mind the influence of these solutions on data output and discussions herein. Further, it is interesting to note that the error produced by the mesh discretization, results in an over-estimate of the influence of the chimney effect. While upon inspection of past validation data for fires in cavities, provided in the FDS technical reference guide. Files, such as the Bouchair Solar Chimney analysis, indicate an under-valuation of the influence of the chimney effect between FDS and real fire data, represented by comparative mass flow rates. This under-estimation is seen to become more prominent with decreasing cavity widths to a minimum width of 0.1m. Hence it is anticipated that in the smaller cavity widths of this thesis, a significant under-estimation of the chimney effect is anticipated and should be kept in mind amidst data analysis. Given that this valuation stems from mass flow rates, it may be that the pressure solver applied in FDS software is not suited to confined fire dynamic analysis and that the over-estimation of the mesh discretization may bring data closer to reality, which will be discussed further in Section 6.4.

Additional limitations of note within this thesis study, generally also stem from the need to limit computational time requirements of the simulation, thus resulting in simplifications to the model design. For instance, the cavity barriers employed within the later models, as discussed in Section 3.1, were simplified to block obstructions that appear based on the activation of a thermal detector. The code applied for a portion of the cavity barrier is demonstrated below:

```
&OBST XB=1.78,1.8,0.01,0.035,2.03,2.10, RGB=128,0,128, TRANSPARENCY=0.6,
DEVC_ID='thermal4'/

&PROP ID='Thermal Activation', QUANTITY='LINK TEMPERATURE', RTI=132.0,
ACTIVATION_TEMPERATURE=180.0/

&DEVC ID='thermal4', PROP_ID='Thermal Activation', XYZ=1.7,0.0225,2.03/
```

There are multiple points of limitation to the representation of an actual cavity barrier by use of this function. As demonstrated in Section 3.1, the barrier is broken up into several individual blocks to loosely represent the barrier activating at different locations at different times due to thermal exposure. Clearly, smaller the blocks will achieve a closer representation to realistic cavity barrier activation as the extents of the block are within a closer range to the detector and thus experiencing the same conditions. However, given that the focus of the thesis is on the fire behaviour within the cavity, the instantaneous effects of the cavity barrier are less important than the steady state achieved after activation. Further, the barrier is coded to appear abruptly in the simulation, which will result in numerical error and instabilities in representing the instantaneous chimney effect flow field. Again, this issue over the length of the study is of little concern as the conditions within the cavity will quickly return to steady state. The reason for the selection of this block activation, is because of the absence of a swelling function in FDS. The "swelling" presented in the User's guide is rather used in reference to thermal thickness and will not adjust the dimensions of an obstruction (McGrattan et al., 2019). Finally, limited information is given for the activation Response Time Index (RTI) of a cavity barrier, with product data sheets instead indicating a limiting temperature requirement of 180℃ in the protected region behind the barrier (Siderise Group, 2019). Again, the actual response time of the cavity barrier is of little concern in this case as these models will not be used for validation. As long as the tests are run with the same conditions employed between the varying simulations, general trends regarding the influence of ventilation conditions and cavity widths are still capable of being observed. Hence, the models applied a standard RTI for thermal detectors, as indicated in the FDS User's guide, with an activation temperature of 180℃. Clearly, this activation temperature is a conservative estimate for reaction of the barrier, as real barriers will react at lower temperatures in order to maintain conditions under 180℃. However, comparison to actual tests would need to be performed in order to determine the representative nature of the RTI.

The most complex and computationally expensive aspect of the trial FDS models, that had to be simplified in the interests of time saving, was the representation of the perforated steel sheets for the partial closure of the sample edges. Initially an adapted 'SCREEN' input was applied to the files, to simulate the oxygenation and drag effects provided by a perforated sheet, as detailed in the lines of input used:

```
&INIT N_PARTICLES_PER_CELL=1, CELL_CENTERED=.TRUE., PART_ID='SCREEN',
XB=0.59,0.6,0.0,0.045,0.4,2.8/
```

```
&PART ID='SCREEN', DRAG_LAW='SCREEN', FREE_AREA_FRACTION=0.5,
STATIC=.TRUE., SURF_ID='SCREEN', ORIENTATION(1:3,1)=1,0,0/

&SURF ID='SCREEN', THICKNESS=0.001, GEOMETRY='CYLINDRICAL', MATL_ID='STEEL'/

&MATL ID='STEEL', DENSITY=8000, CONDUCTIVITY=43, SPECIFIC_HEAT=0.47/
```

However, due to the complex fluid dynamic calculations required to solve such detailed oxygenation pathways, the calculation time for the models increased dramatically, with a 7-day simulation producing only 49 seconds worth of simulated data. As such, the representation of the perforated sheet had to be adjusted to investigate other potential solutions. The alternate solution attempted, incorporated a basic obstructions grid format, with 50% of the total area being open for aeration of the cavity. Appendix A4 demonstrates the input file for the alternate perforation design. This adapted solution was found to be far too simplified and will be discussed further in Section 6.2 of the results.

4.2 ISO 13785-1

The primary limitation faced in the practical testing of the ISO 13785-1 rigs, was the availability of time for the completion of testing. Due to the many setbacks faced, capped by the COVID-19 pandemic, only three of the nine testing samples were able to be analysed. Further, due to the impact of the pandemic on the industry, primary elements of the proposed test design were not available when testing was finally able to proceed close to the thesis deadline. As such concessions had to be made to ensure useable data was still available for analysis. For instance, the cavity barriers were not delivered in time for the completion of the 50mm cavity tests. As such, the analysis of the impact of these barriers on the influence of the chimney effect, will not be available for comparison with the data presented by Guillaume et al. (2018) and Efectis UK/Ireland Ltd. (2018). In the absence of experimental data, the simplified FDS models will provide an indication of the potential influence of the barriers to be discussed in Section 6.4. However, any information provided by these files must be considered to be incomplete until more complex model validation is able to be performed. Additionally, there was a limit to the involvement of bi-directional probes in the analysis of cavity pressures and flows, given that there was only one functioning pressure transmitter unit available for pairing with the available probes. As such each sample was only provided one probe location, which had to remain constant across all samples for comparative purposes. Hence, an appropriate test location had to be determined based on regions of greatest influence demonstrated in the initial trial FDS models. Figure 28 indicates that two primary regions of chimney effect activity occur in these initial models. The regions of chimney effect form behind

the cladding panels on the main face of the sample, separated by the entrained air through the vertical joint. Further, it is clear that devices positioned behind the left cladding panels on the main face of the sample should hold the greatest influence from the altered ventilation conditions. Whilst, in the interest of maintaining quality measurements and protecting equipment, the probe should be positioned high in the rig to avoid direct impact from the burner. Therefore, the location was selected as being 200mm from the top and 300mm from the edge of the sample as indicated in Figure 5. However, alternate device locations would have provided a wealth of information on the influence of ventilation conditions on cavity pressure throughout the sample, that will not be witnessed here. This too will become a focus of the outputs produced by the FDS files. In the instance that more devices were available, probes would be positioned at the same height as the original probe, in horizontal locations 3, 5, 4 & 2, indicating priority of device locations respectively. Additional probes would then be positioned at varying heights down horizontal location 1 from the original probe.

Additional limitations that were experienced amongst the completion of the tests, arose from inherent issues of practical experimentation. For instance, a key parameter for analysis in this investigation is the observation of the flame height within the samples. However due to the visual obstructions provided by the panels, flashings and ventilation closures, this visual method of analysis is not functional. Hence, analysis of flame height and subsequently, chimney effect, will be performed by use of the data presented by the thermocouples. Further, due to the safe practice procedure for lighting a burner, it is clear that discrepancies between simulated and real fire test data will result. In the case of the simulated data, the fire jumps almost immediately to the 100kW heat release rate requirement, as determined by the input code. However, in the practical case the burner must be originally set to 50kW for ignition, so that an excessive amount of propane gas is not expelled prior to ignition, signifying an explosion hazard. Once ignition occurs the experimental timer is initiated, and the propane flow is adjusted to the 100kW condition. As such a slightly delayed effect of the burner will be experienced in the cavity, as presented in the validation graphs presented in Section 6.3.3. Finally, as briefly mentioned in Section 3.2, the changes in sample geometries based on the adjustment of cavity widths, will result in variable conditions of devices between tests. The altered proximity of obstructions to the devices will change the levels of re-radiation and conditions of fluid flow experienced by detectors. These varying conditions should be considered in the analysis of output data and the resulting conclusions presented.

5. Results

Due to the resultant multi-faceted nature to this study, the data presented herein is broken down into sections defined by their intended purposes, demonstrating the progression of thesis works. Opening with introductory Fire Dynamic Simulator analyses for the selection of relevant model design inputs, followed by validation analysis of these model inputs in comparison to the real test data performed, and finalising with sections of extended research with the FDS software. Notice that experimental data is presented solely in the validation section, for parallel analysis of lateral ventilation conditions and comparative model validation of trends. Further, there will be two primary trends indicated for the legends of the graphical plots presented herein. Plots demonstrating a comparison within a single façade sample will present data at varying device locations following the reference system depicted in Figure 6. Plots comparing testing samples establish a three-part reference theme involving letters separated by numbers. The first set of letters refer to the test sample or model iteration applied, the numbers represent the cavity width of the sample, and the final letters indicate the sample's lateral ventilation condition, 'c' for closed, 'o' for open, 'ps' for perforated 'SCREEN', and 'p' for simplified perforated case. FDS model iterations demonstrate the progression of the FDS analysis within this thesis. Four main model configurations have been reported herein including; 'open75' for the computational time vs error analysis, 'iso' for initial perforated screen input studies, 'r' for validation of experimental data, and 'a' for the extended studies of cavity width and barriers. FDS input files for all configurations are presented in the Appendix.

5.1 Computational Time vs Error Analysis

At the very early stages of model development, FDS trial runs were performed with a very basic model set-up as presented in Section 3.1. Following the discussion in Section 4.1, three models were constructed for the determination of the influence of mesh resolution and domain discretisation on simulation times and data output error uncertainty. The models used incorporated a 75mm cavity width, demonstrating the time frame of completion of this analysis, before the scope of the analysis was narrowed to reduce the number of cavity widths analysed to the three indicated in Table 1. Notice too that in these models, there is an absence of cavity barriers, flashings and lateral obstructions, whilst thermal detection devices were used in place of thermocouples. Plus, an additional obstruction was present behind the façade in an attempt to centralise the burner to the cavity width, discussion of inputs selection is presented in Section 6.1. The 6-mesh 10mm domain was taken as the base data, from which the alternate solutions demonstrated differential percentage error values. Each domain is presented in Figure 9.

Upon inspection of the FDS device output files and the data presented for the maximum errors of each thermal detector, it is clear that the major discrepancies in both comparisons are experienced in the lowest row of detectors, signified by V1 for Vertical Elevation One. Hence, Figure 10 and Figure 13 are demonstrated as the primary plots in each case, indicating the percentage error between simulations, of each detector at this elevation over the full duration of studies. Alternate data plots are included for each case indicating important details for understanding the limitations of the simulation time saving methodology.

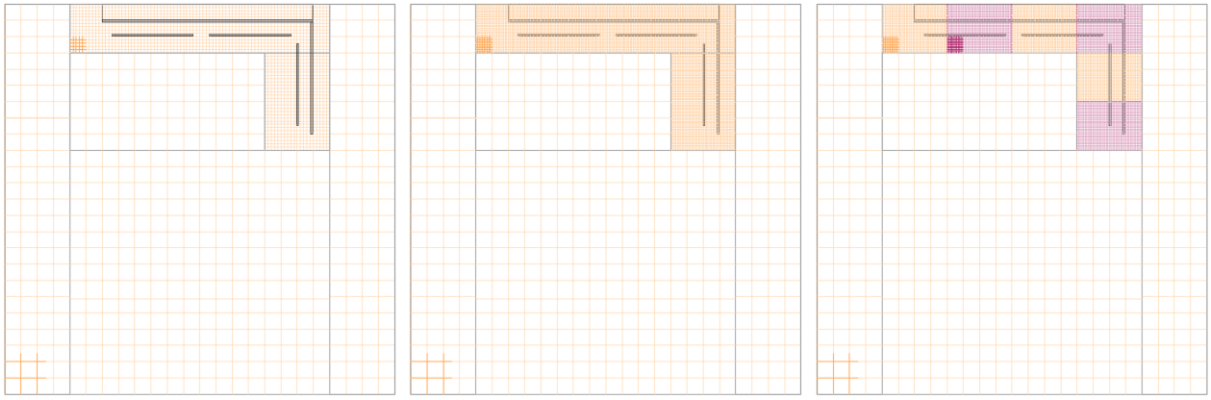

Figure 9: Computational Time and Error Analysis Domains; 6-mesh 20mm cell size (left), 6-mesh 10mm cell size (middle), and 10-mesh 10mm cell size (right)

5.1.1 6-mesh 10 & 20mm Cell Size Comparison

From the data presented in Figure 10 it is clear that the most critical (maximum) errors are experienced in thermal detectors V1H2 and V1H4. These detectors are presented in the vertical joints at the centre and corner of the rig. While the detectors present behind the cladding panels (V1H1 and V1H3) show more manageable errors, especially toward the back end of the simulation times. This information alludes to the importance of turbulence within these regions and the impact of the mesh resolution in solving turbulent flows, to be discussed in Section 6.1.1. Finally, the thermal detector positioned at V1H5 shows very minimal error because it is outside the fire plume in near ambient conditions.

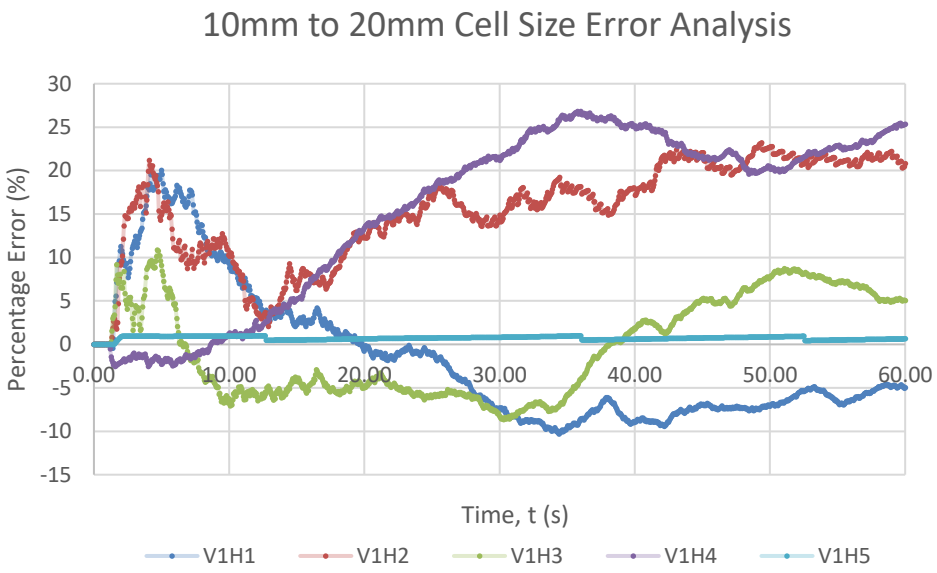

Figure 10: Error Analysis plot for V1 elevation thermal detectors between the 6-mesh, 10mm and 20mm cell length cases

These same trends are witnessed in the elevations denoted V2 and V3, however higher up in the sample the data presented for the thermal detectors in elevations V4 and V5 sees a shift toward all locations holding a positive error between 5 and 10%. This denotes an over-valuation of the temperatures higher in the rig, indicating greater flame heights and a miss representation of the combustion chemistry. This trend is also clearly presented in the plot of the Horizontal Position H3. Notice however the lowest detector in this data set V1H3 breaks from the trend, indicating the balance between the impacts of mesh resolution on turbulence and combustion representation, for discussion in Section 6.1.1. Elevations V4 and V5 plots are presented in Appendix A5.

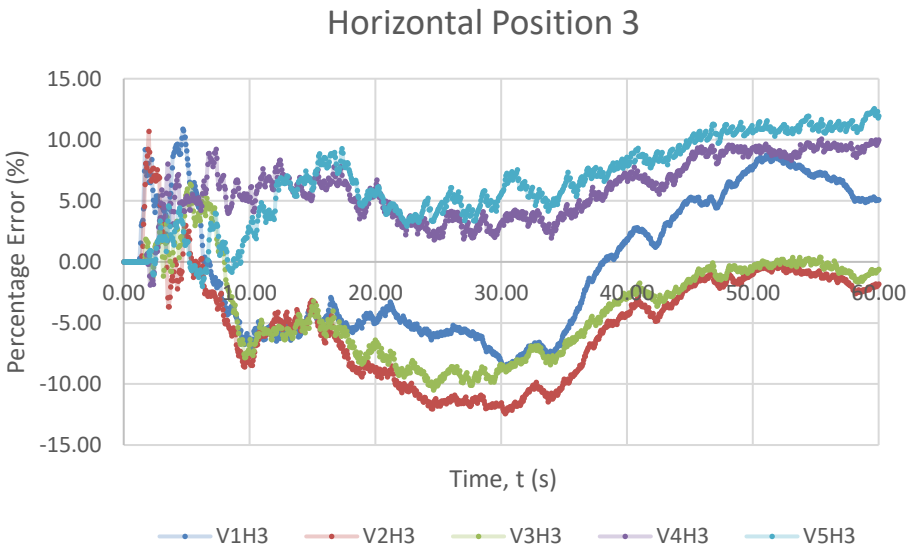

Figure 11: Error Analysis plot for H3 thermal detectors between the 6-mesh, 10mm and 20mm cell length cases

Finally, the plots for the horizontal locations for detectors in the corner and wing of the sample shed further light on the influence of mesh resolution on turbulence. In these particular locations the temperatures remain low given that the detectors are out of the immediate impact of the flames. Noting that the early FDS files were written so that the burner was positioned under the main face only, and not under the corner or the wing. Hence the detectors in these locations are interacting with the smoke plume, reflected upon further in Section 6.1.1.

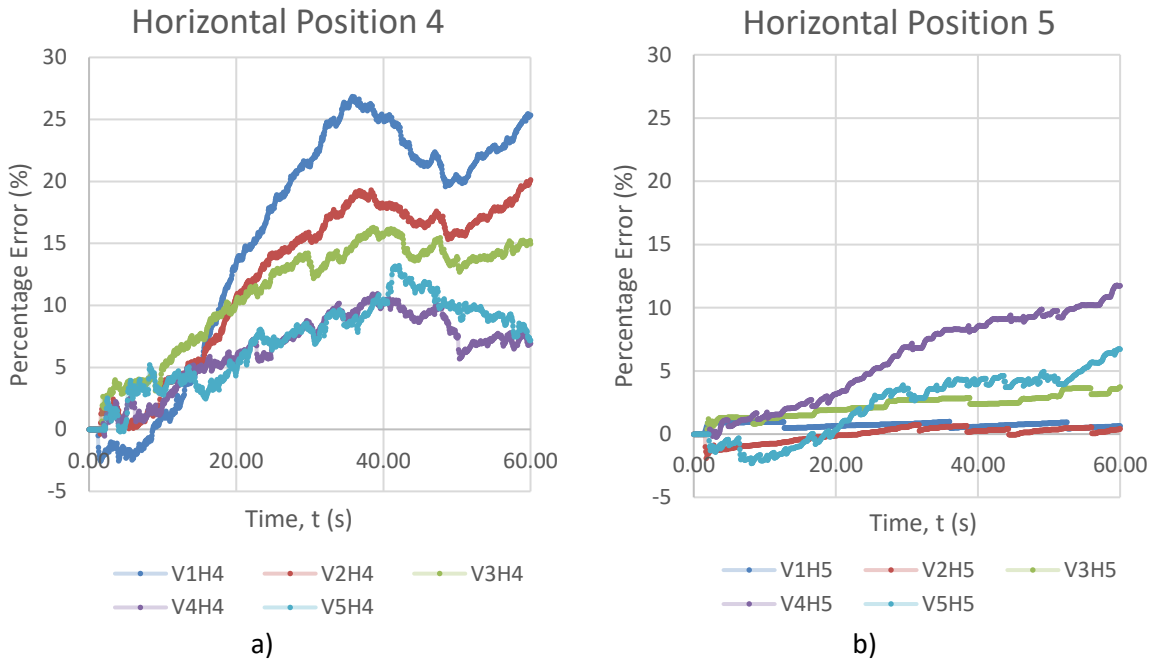

Figure 12: a) H4 Error Analysis plot, b) H5 Error Analysis plot (6-mesh, 10mm and 20mm cell length cases)

5.1.2 6- & 10-mesh 10mm Cell Size Comparison

When viewing Figure 13, trends are less clearly depicted than in the 10 to 20mm mesh comparison. However, key information can be discerned in indicating some limitations to the use of this technique. Clearly, the graph presents early spikes in data both positive and negative related to the drastic changes in pressure from the thermal loading provided by the burner. The detectors on the left most side of the sample (H1 and H2) are seen to produce positive error initially, while the detectors to the right (H3 and H4) show negative error. However, as the test progresses the situation seemingly reverses, as the H2 data turns negative and both the H3 and H4 data become positive. Interestingly H1 reduces but does not turn negative until much later in the test, rather sustaining about parity for the majority of the duration. This information alludes to the difference in the models' representations of lateral diffusion of pressure considered further in Section 6.1.2.

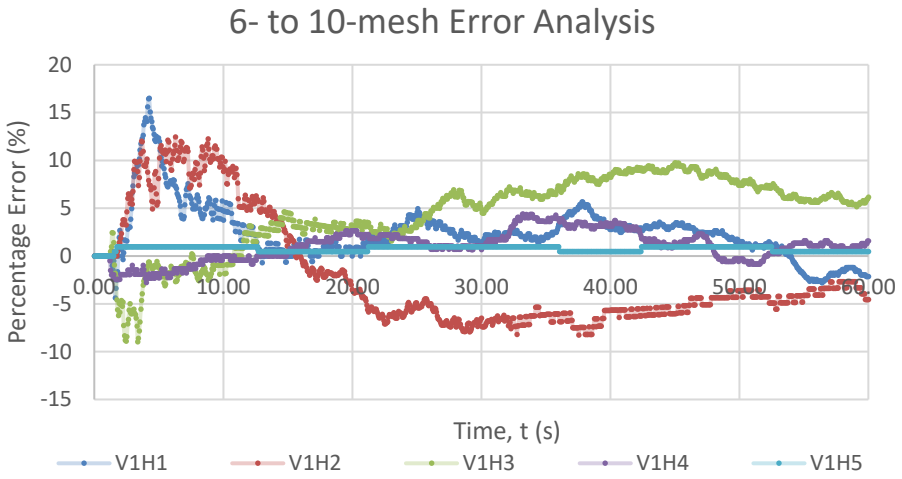

Figure 13: Error Analysis plot for V1 elevation thermal detectors between the 10mm, 6- and 10-mesh cases

The data presented in Figure 14, for the columns of thermal detectors located in horizontal positions H3 and H4, indicates similarity in the patterns of errors present at changing elevations. For instance, Figure 14a) demonstrates data following a similar pattern in time, however with low error percentages reported in the upper two elevations, and high errors in the bottom three elevations near to the burner. This touches on the logic of heightened pressure differentials experienced close to a burner based on the high temperatures within this region, resulting in greater errors due to model representation of pressure distribution, explained further in Section 6.1.2. While the data of Figure 14b) indicates limited differences between the elevations of detectors, due to the low temperatures experienced in this region as mentioned in Section 5.1.1. Interestingly in this case the middle elevations show the highest error and will be investigated further in Section 6.1.2.

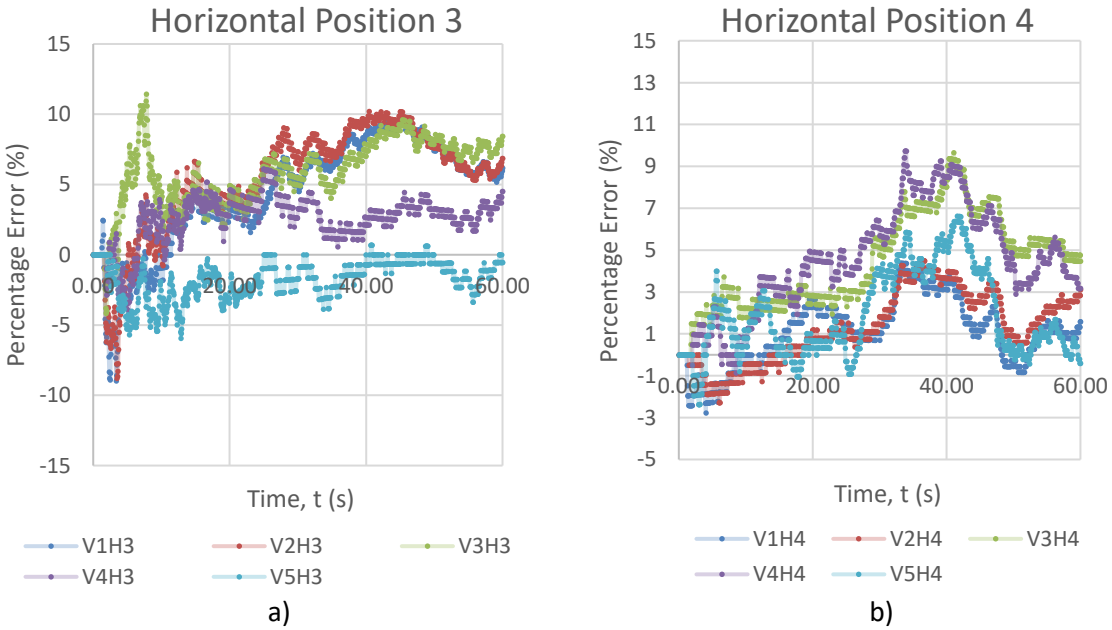

Figure 14: a) H3 Error Analysis plot, b) H4 Error Analysis plot (6- and 10-mesh cases)

5.2 Perforated Sheet Input Analysis

During the early stages of model development, a 25mm cavity width sample was run investigating open and closed ventilation conditions, as well as two types of 50% perforated inputs. As described in Section 4.1, the two perforated designs incorporated the complex and computationally expensive 'SCREEN' input and the simplified grid obstruction pattern. The results indicate an analysis of a thermocouple located near to the lateral obstructions, noting that the V6 elevation of thermocouple was added in some earlier models at a location in line with the top of the cavity. Figure 15 demonstrates that the simplified representation of the perforated obstruction holds little similarity to the complex 'SCREEN' obstruction, rather resembling the open sided condition. While the 'SCREEN' output unexpectantly indicates the most critical scenario within the cavity, which will be discussed in detail in Section 6.2. Therefore, it was determined that further perforated conditions should be investigated to ascertain an appropriate representation of reality in a computationally sustainable manner. However, upon inspection of the FDS User Guide, no suitable solutions for this representation were found during the studies of this thesis and were deemed outside the scope of works.

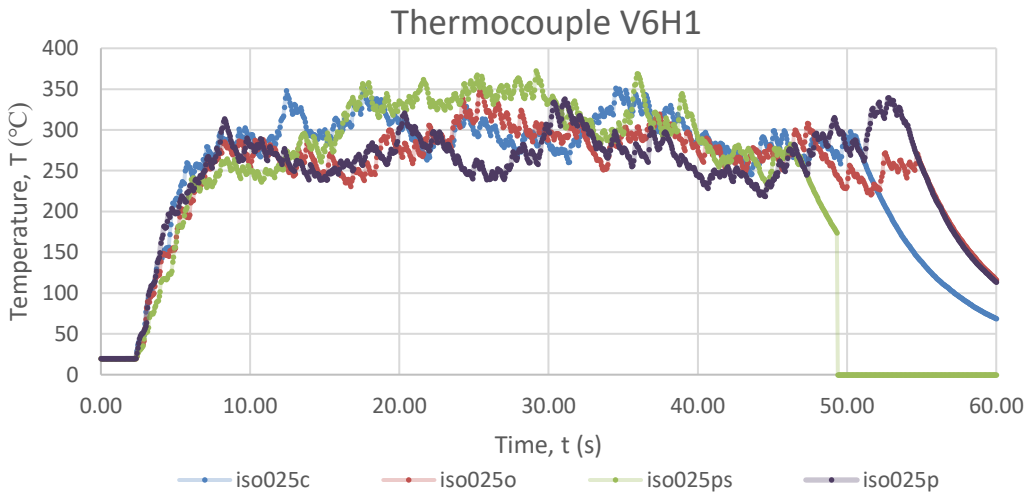

Figure 15: Temperature vs Time plot for Ventilation Inputs analysis within a 25mm cavity width, Model Iteration 'iso'

Further investigations into the perforated lateral ventilation inputs were run using the 'r' FDS models for validation against the experimental data. It is clear from the data presented in Figure 21, that once again the simplified perforation case demonstrates little resemblance to the 'SCREEN' perforation case, in place of the open ventilation case. However, in this instance the 'SCREEN' data depicts values between the open and closed ventilation cases as anticipated, although it is seen not to match the trends demonstrated in the experimental case, to be discussed in Section 6.3.3.

5.3 Model Validation

The process of validating the FDS models to the ISO 13785-1 experimental work incorporates three distinct sets of data based on the devices present in the samples. Firstly, the heat flux is compared based on the location set in the standards of the ISO 13785-1 methodology. The temperature and flame heights present are analysed based on the presence of thermocouples at the locations indicated in Figure 5. Whilst the pressure and resultant velocity in the sample at a given point is assessed via data from the bi-directional probe and SMV slice files. Notice that only the Open and Closed Ventilation conditions were presented for FDS validation, as a suitable representation for the influence of the perforated screen was not able to be modelled, discussed further in Section 6.3. However, the data for the experimental perforated screen test is presented for the analysis of varying ventilation conditions.

5.3.1 Heat Flux Analysis

In Section 3.1, a hypothesis for the functional use of the heat flux meter within the investigations of this thesis was presented. This hypothesis detailed that due to the slow growth of heat flux in practical experimentation, the 60 second simulation time of the FDS files would not be sufficient to identify the maximum heat flux experienced and therefore must be omitted from studies to avoid misrepresentative data. However, upon investigation of the data presented in Figure 16, it is clear that the heat flux meters in both the open and closed ventilation cases reach heat fluxes equivalent or within range of the maximum of the experimentation, almost immediately. Thus, the meter may in fact be a useable tool for future short simulation analyses to determine potential maximum heat fluxes experienced, however there still remains the issue of representation to actual heat flux development. Further the FDS analysis would need to be extended, to ensure that the heat flux values remain within this representative range and do not exceed beyond realistic conditions. Interestingly the experimental perforated data demonstrates unexpectedly high values while the comparative FDS data remains similar to the other cases. Once again, the simplified case was shown to resemble data closer to that expected in the open ventilation case. While the ‘SCREEN’ case actually reports lower values than all other ventilation conditions, noting that this file was only able to be run for half the simulated time, due to the computational expense of the model.

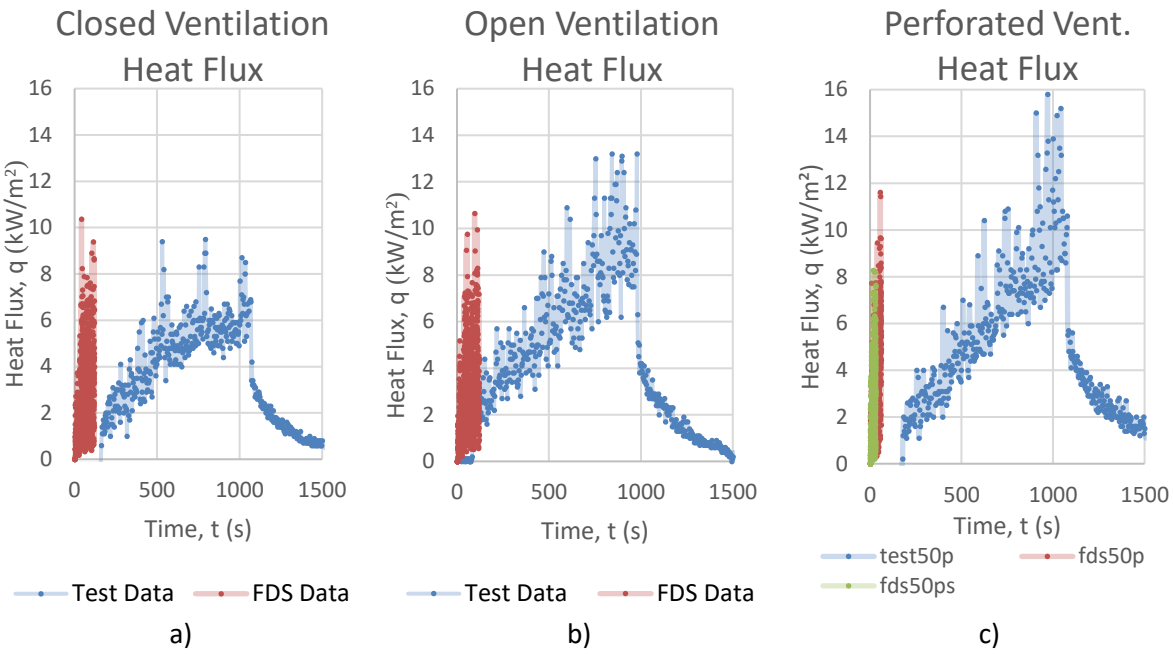

Figure 16: a) Closed Vent. FDS vs ISO 13785-1 Heat Flux plot, b) Open Vent. FDS vs ISO 13785-1 Heat Flux plot c) Perforated Vent. FDS vs ISO 13785-1 Heat Flux plot

5.3.2 Bi-directional Analysis

The data provided by the bi-directional probe resembles a pressure value experienced at the device location based on velocity. The logging system connected to the probe measures voltage differentials compared to ambient conditions recorded before initiation of the experiment, calibrating the base voltage of the device for comparison with the instantaneous conditions. Figure 17 demonstrates the experimental pressure recorded for all 50mm tests samples, in the location of the bi-directional probe as indicated in Figure 5. The data indicates that pressure is maintained generally constant, increasing only slightly over the duration of the test for all ventilation cases. The data is seen to generally fluctuate within a range of around 2-3Pa, whilst presenting the closed ventilation case as holding a slightly higher pressure than the perforated sample, with the open case demonstrating the lowest pressure of all samples.

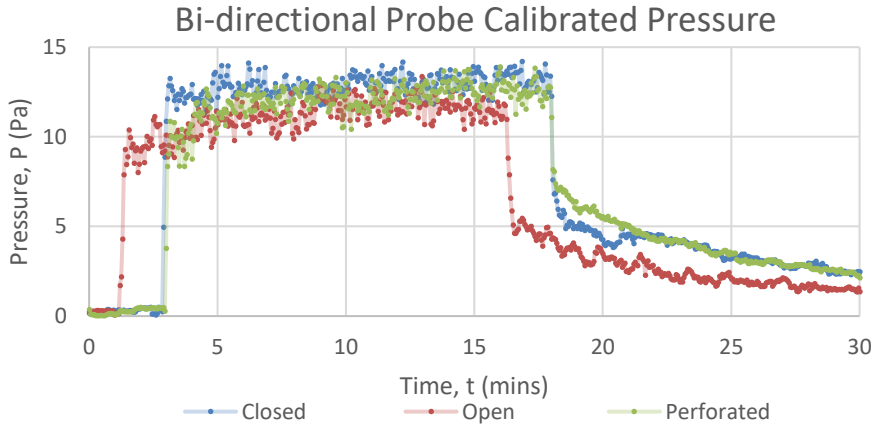

Figure 17: Comparative Pressure plot for Experimental Ventilation Conditions within the 50mm Cavity Width

The importance in tracking the pressure output of the probe within a façade sample, is for the calculation of the causal gas velocity, providing an indication of the activity of the chimney effect within the cavity. As such, the gas velocity within the cavity is calculated by use of the bi-directional probe data in collaboration with the formula for vent flow velocities presented in Karlsson & Quintiere's Enclosure Fire Dynamics book. Further, data for the calculation of gas density was incorporated into the calculations using information presented in Drysdale's Introduction to Fire Dynamics book, while a probe uniform calibration constant of 1.08 is applied to stabilise data as indicated in McCaffrey & Heskestad (1976). The resulting calculation is presented below in Equation 3.5 below.

$$v = \frac{\sqrt{\frac{2\Delta P}{\left(\frac{P_\infty M_w}{RT}\right)}}}{1.08} \tag{3.5}$$

Where v is the gas velocity, ΔP is the instantaneous pressure data, P_∞ is the atmospheric pressure 101325Pa, M_w is the molecular weight of air 0.02895kg/mol, R is the ideal gas constant $8.314 J/K \cdot mol$, and T is the temperature at the probe, which was assumed to be that of the nearest thermocouple V5H1.

From the calculations described the following velocity plot is demonstrated in Figure 18. The plot illustrates the same point as in the pressure diagram above, that the closed lateral ventilation condition shows the greatest activity of the chimney effect. However, the new velocity data provides the opportunity for validation, with the SMV slice files for the velocity experienced in the equivalent FDS simulations, presented in Figure 19.

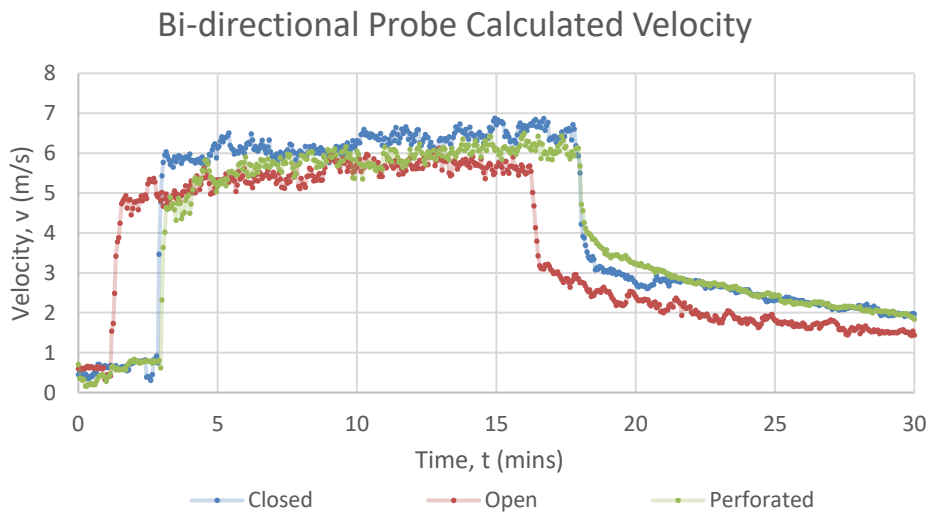

Figure 18: Comparative Velocity plot for Experimental Ventilation Conditions within the 50mm Cavity Width

Viewing the SMV velocity slice files of Figure 19, in comparison to the data presented from the bi-directional probes in Figure 18, it is clear that the FDS files indicate much higher maximum values for the velocity within the cavity. However, this data is presented across the whole cavity and is not necessarily present in the location of the bi-directional probe, marked by the purple dot. Notice that the data presented in the SMV file is an instantaneous screen capture of the vertical velocity, taken ≈50 seconds through run time of the FDS model and is thus not representative of the full range of fluctuations in velocity at the device location. When viewing the total simulation run however, it is clear that at the device location, the FDS files indicate greater fluctuations than the experimental data. However, the data remains centred approximately around the same average velocity values presented in Figure 18. Notice that the closed and 'SCREEN' perforated cases depict the probe as deeply embedded in the chimney effect flow, while the open and simplified perforation cases show that the probe resides closer to the edge of the flow where entrainment takes place, further discussed in Section 6.2.2

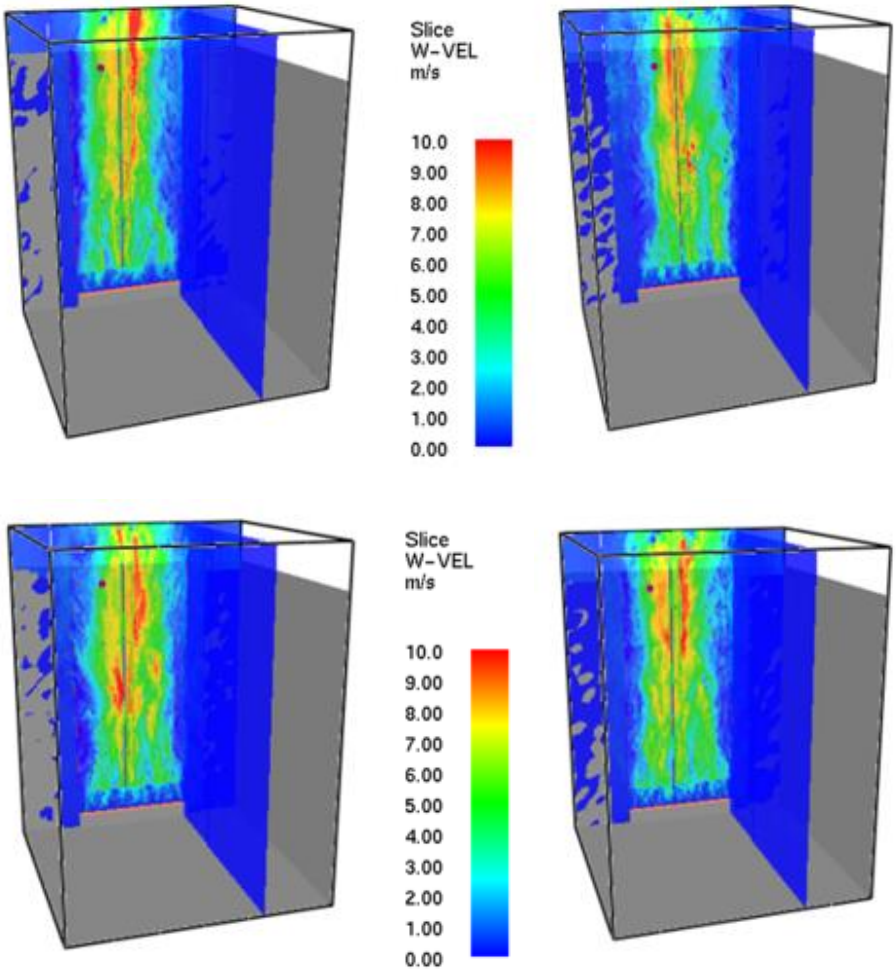

Figure 19: SMV Slice file data for the W- velocity profiles of the FDS closed (top left), open (top right), simplified perforated (bottom left), and 'SCREEN' perforated (bottom right) ventilation cases, Model Iteration 'r'

5.3.3 Thermocouple Analysis

Comparative data for model validation demonstrated in Figure 20, 21 & 22 all highlight the delay in activation of the burner in the real fire test case as discussed in Section 4.2. However, once the test progresses and reaches steady state conditions it is clear to see that in the lower portion of the sample the FDS data provides a reasonable estimate for real fire conditions with the addition of higher fluctuations in the FDS output. Further, in the higher portions of the sample, presented in Figure 21, it can be seen that FDS slightly over values the temperature, which may infer influence of domain discretization based as in Section 5.1.1, to be reflected upon further in Section 6.2.3.

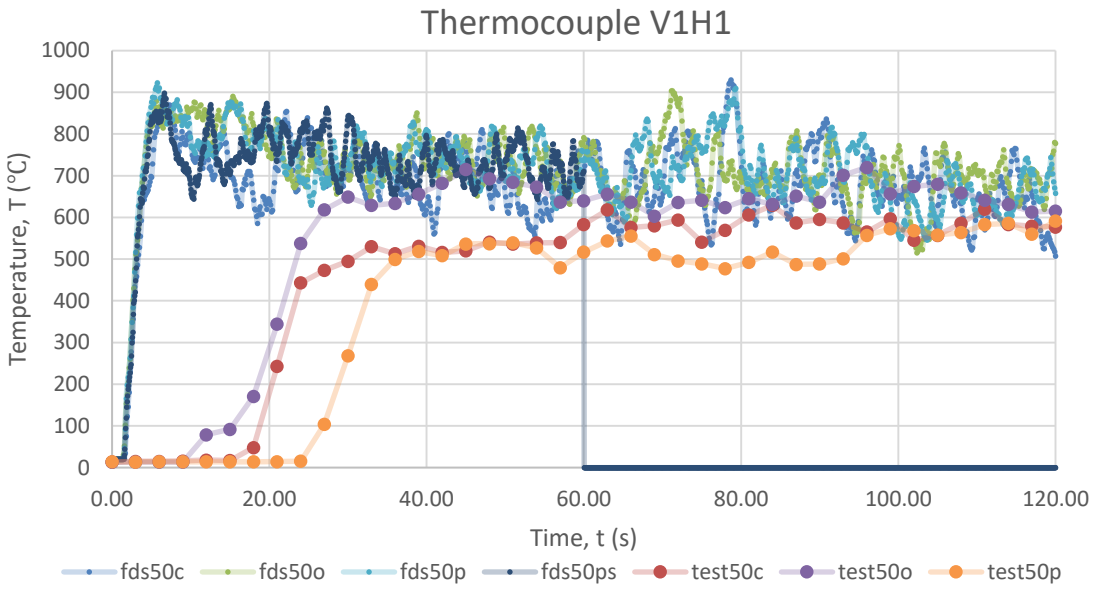

Figure 20: Temperature vs Time plot for comparison of Experimental and FDS data at Thermocouple Location V1H1

In comparing the ventilation conditions between the analyses, it is shown that in the lower portions of the samples, the open ventilation case is considered the worst case with higher temperatures presented in Figure 20, however in the upper regions the closed case takes over as the worst case scenario presented in Figure 21. The data hints toward the importance of the region of oxidation of the fuel, and the influence on the flame height, to be discussed in Section 6.2.3. Interestingly in both lower and upper regions of the sample, the experimental perforated data signifies the least critical case. This data seems to appear in contrast to logical reasoning which suggests that the additional oxygenation and re-radiation provided by the screen should result in conditions balanced between the open and closed cases, as depicted in the 'SCREEN' perforation case in Figure 21. Notice, this balance is much less discernible in Figure 20, in the lower regions of the FDS sample where high fluctuations are experienced near to the burner.

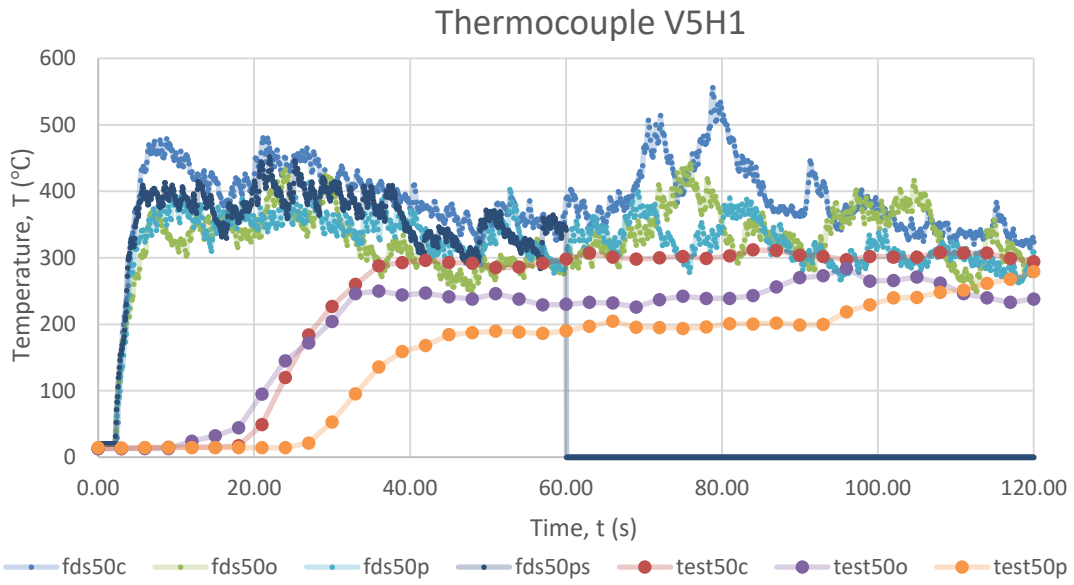

Figure 21: Temperature vs Time plot for comparison of Experimental and FDS data at Thermocouple Location V5H1

The data presented for the thermocouples in the corner of the sample slightly above mid-height (V4H4) in Figure 22, demonstrates the under-estimate of temperatures produced in the FDS files. This may indicate a disparity in the conductivity of calcium silicate boards applied between the FDS models and experimental samples to be discussed in Section 6.3.3. Further, the data indicates a change in the influence of the ventilation conditions in a far-field manner, demonstrating the importance of sample oxygenation over the effects of re-radiation. As Figure 22 depicts more severe conditions in the open ventilation case, while the information for the perforated screen seemingly divides the open and closed data, discussed in Section 6.3.3.

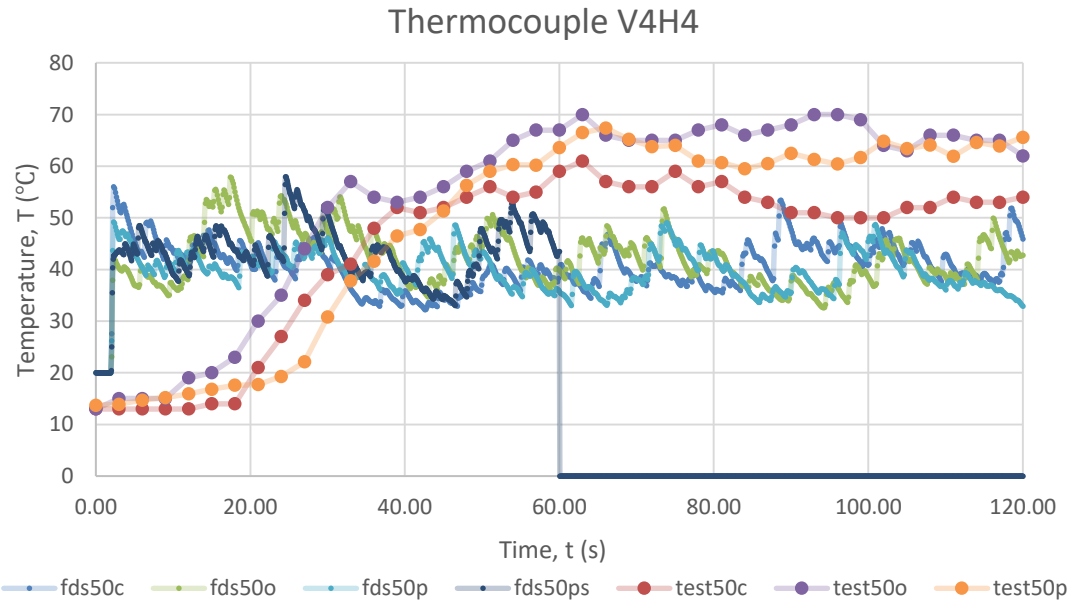

Figure 22: Temperature vs Time plot for comparison of Experimental and FDS data at Thermocouple Location V4H4

5.4 Extension of studies in FDS software

In light of the reduced experimental capacity of this thesis, studies using the FDS software have been performed in order to develop an understanding of the potential influences of cavity barriers and widths on the behaviour of fire within a façade. Notice, that in this adjusted design, the corner joint is sealed which is anticipated in industrial façade applications. However, in this case the seal does not incorporate rails, allowing heat to flow around the corner joint within the cavity. Seemingly contrary to the data presented by Livkiss (2018), Figures 22 & 24 indicate that more critical conditions and greater flame heights occur in the 50mm case, rather than the thinner 25mm cavity width. Interestingly, Figure 23 demonstrates that for these two cavity widths, the difference in lateral ventilation conditions causes no discernible impact to the temperatures experienced. But, cross-referencing this information with the data presented in Section 5.3.3, it can be seen that these are simply areas of limited influence of lateral ventilation. However, when viewing the much lower temperature 100mm samples, it is clear that the closed ventilation condition produces a more critical atmosphere within the cavity toward the latter stages of the test. This result follows principles of recycled heat within a cavity but provides questions as to why this phenomenon does not take effect on the results in the smaller cavity width cases, to be discussed further in Section 6.4. Further, display of greater severity in conditions of the closed case illustrates the plentiful supply of oxygen within the 100mm sample for facilitation of combustion processes.

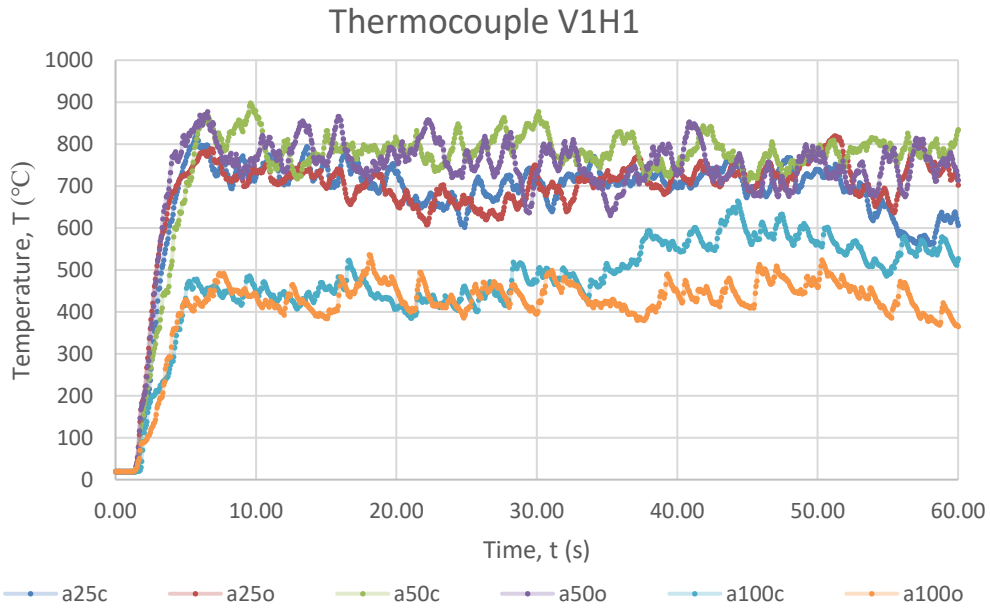

Figure 23: Temperature vs Time plot for the comparison of Cavity Widths and Ventilation conditions at V1H1

In keeping with the line of reasoning regarding radiative heat transport, the thermocouples positioned in the wing section of the façade indicate that the highest temperatures occur in the 100mm cavity model. Demonstrating that the corner of the 100mm sample is much more open, offering a much broader angle of incidence for radiative energy to travel to the wing section of the facade. Further, due to the low amounts of heat in the wing, the closed case demonstrates much higher temperatures, as it allows the build-up of heat in the region. Notice too that the 50mm case shows almost no deviation from ambient conditions, likewise to the 25mm case. Indicating that the critical cavity width for thermal transport to the wing lies between 50 and 100mm.

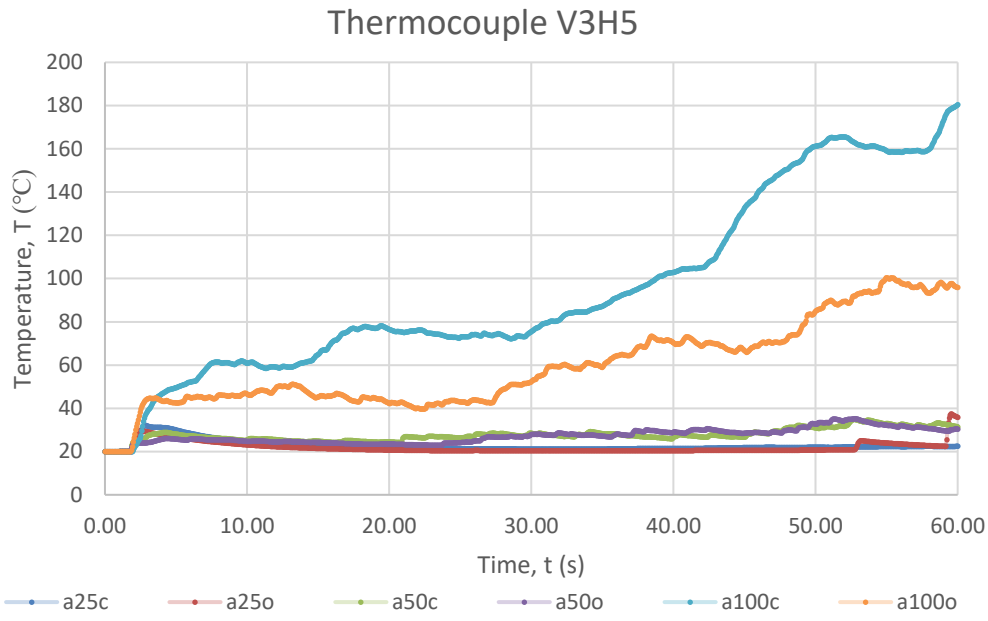

Figure 24: Temperature vs Time plot for the comparison of Cavity Widths and Ventilation conditions at V3H5

For the analysis of the influence of the cavity barrier, both temperatures and velocities are considered in Figure 25 & Figure 26, respectively. The temperature data is demonstrated by the detectors above and below the active barrier in locations V4H3 and V5H3. The data indicates that for both the 25 and 100mm cases the action of the cavity barrier sees an increase in the temperature beneath. While the 50mm case holds a steady temperature before and after barrier activation. Another note from the figures is the similar temperatures in the 25mm and 100mm cases at V5H3, however it is clear that the conditions are more adverse in the 25mm sample, as the cavity barrier is seen to activate slightly earlier in this case.

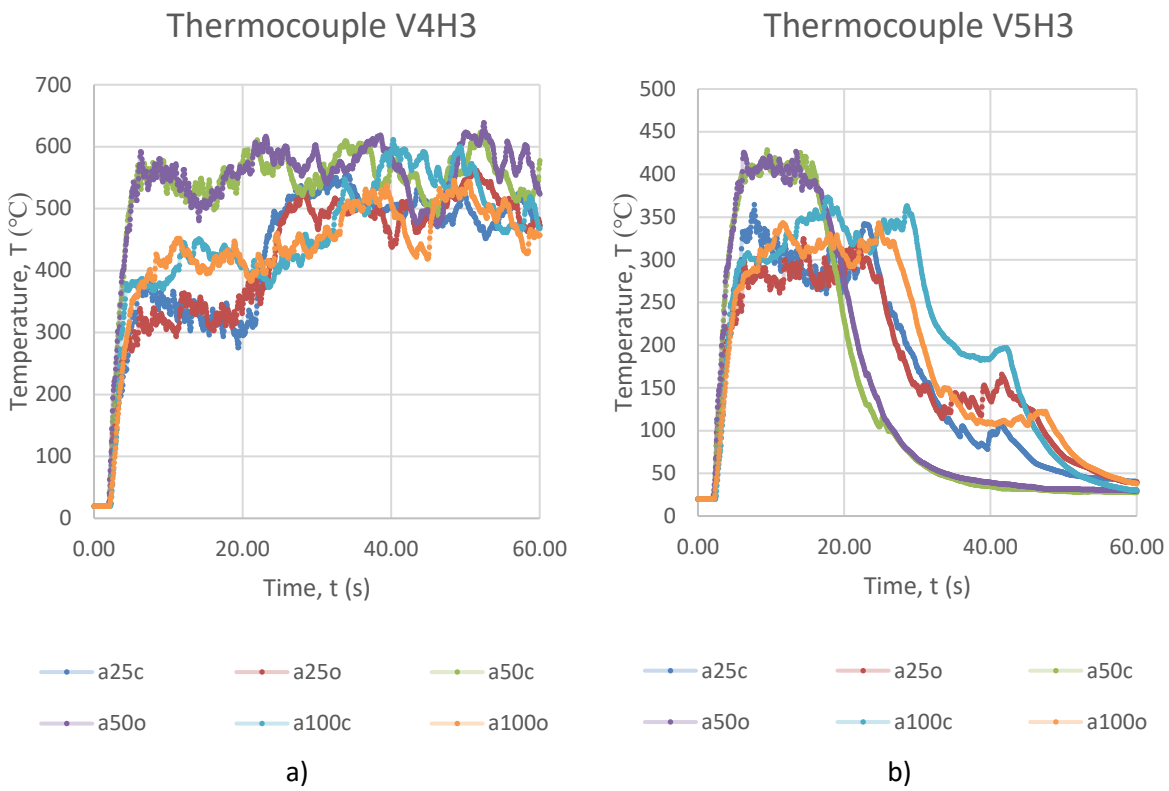

Figure 25: Temperature vs Time plot at locations below V4H3 (a, left) and above V5H3 (b, right) the cavity barrier

With regard for the impact of the cavity barrier on the chimney effect introduced in Section 1.5.3, velocity slice files were viewed in Smokeview. It was assumed that the most impact on the flow would occur in the closed cases as the open samples would allow continued flow out the sides of the sample. It is clear from Figure 26 that the activation of the barrier creates a high impact on the velocity, however it does not stem the flow of gases all together, as significant velocity is seen to persist. Notably the 50mm case was found to hold the highest velocity and most consistently high velocity flow. While the 25mm sample showed high velocities in areas such as next to the flashings. The 100mm case however showed limited influence of the cavity barrier on the velocity within the sample for the open case. Given that the lower velocity flows in this case were able to be re-directed out the joints of the sample more readily. However, notice that the 100mm closed case reported interesting turbulence to be discussed in Section 6.4. The SMV slice files for the 25mm & 100mm cases are provided in Appendix A7, demonstrating both ventilation conditions, along with the 50mm Open sample.

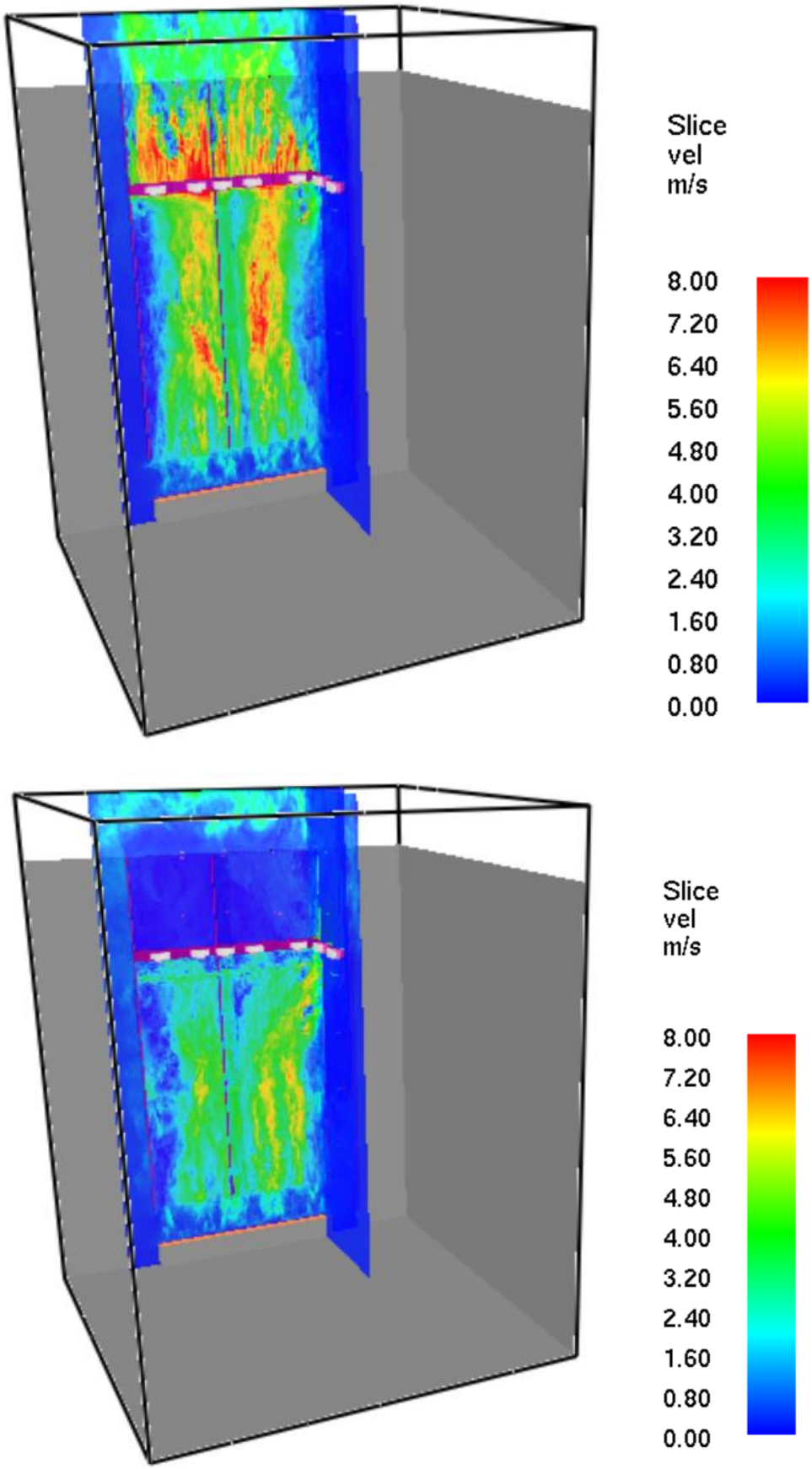

Figure 26: SMV Velocity slice files depicting the Cavity Barrier influence on the Chimney Effect for the 50mm Closed Sample, Screen-capture recorded at 10s (top) and 30s (bottom), Model Iteration 'a'

6. Discussion

6.1 Computational Time vs Error Analysis

In addressing the results of this analysis a few key inputs must be highlighted to understand the format of the output data. For instance, thermal detectors were used in this error analysis, due to their nature in the FDS program in comparison to thermocouples. Thermocouples have very limited mass and are sensitive to radiation, resulting in the approximation of the true gas temperature and fluctuations within the cavity, incorporating a slight delay for conductivity. Whereas the thermal detectors hold significant mass and a higher response time index, indicating that a slower and more consistent heat input response is produced. Hence, for the analysis of errors, a time averaged representation of thermal influence is a far more representative and reliable measure for model input comparison. Else the high amount of fluctuations in the thermocouple data will result in accentuated error margins and graphical noise which will act as a barrier to the representation of trends involved within the comparison. Another important input which can be seen in all models throughout this thesis, is the extent of the domain utilized for analysis. It is clearly seen in Figure 9, that the domain extends significantly from the front of the façade, resulting in a heightened simulation requirement. However, the selection of the bounds of the domain was made to align with and represent the draft screens established in the ISO 13785-1 methodology. The inclusion of the screens aimed to maintain consistency in the ventilation conditions of the samples analysed, in relation to standard testing conditions. Finally, an additional obstruction was applied to the model behind the façade in this case during investigation of potential model inputs and benefits. The idea of the obstruction was to centralise the flame to the façade cavity creating consistency in thermal loading between cavity widths. However, it was seen to produce additional flaming under the rig and was not incorporated in later models.

6.1.1 6-mesh 10 & 20mm Cell Size Comparison

The data presented in Section 5.1, indicating higher error percentages in the lower portions of the façade samples, can be rationalised based on the proximity of the detectors in this section to the burner and the impact of variations in mesh resolution between models. Firstly, it is clear that near to the burner, more complex fire dynamics will be present in the early stages of a diffusion flame, as large amounts of ambient air are entrained to oxidise the fuel. While, the principles of LES modelling demonstrated in Section 4.1, indicate that a lower resolution mesh will result in higher amounts of approximations for modelling turbulence. This is based on the fact that a larger portion of the turbulence length scales will be outside the solvable capacity of

the model. Therefore, the less refined 20mm cell sized model will not appropriately capture the complex turbulence and combustion chemistry, as a greater amount of turbulent information is estimated rather than simulated. Resulting in a reduction in dissipative energy of the model at the Kolmogorov scales, and an over estimation of temperature in the region of study (Merci, 2019). Further, the highest percentage differentials in this elevation of detectors is witnessed in the joints of the samples where ambient air is entrained into the fire plume. This entrainment is more significant than in other models of this thesis, due to the accentuated widths incorporated into these models. The entrainment results in the creation of significant turbulence at the interface between the slow laterally moving ambient air and the fast, buoyant fire plume gases. Following this understanding of turbulence, it is therefore clear why limited errors are observed behind the cladding panels. Once the chimney effect begins at the ignition of the flame, flows within the cavity protected by the cladding panels move to near laminar conditions. As such, reduction in the turbulence experienced in the region will therefore see limited errors resulting from mesh resolution. The fairly large early errors experienced in these thermal detectors, is caused by the turbulence created when the buoyant driving force of the burner interacts with the previously stagnant ambient air within the cavity before flows stabilize and become laminar.

Further, the combustion chemistry and oxidation processes within the models will be impacted in the same manner as the turbulent energy. Due to the lack of visualisation of combustion lower in the sample, un-combusted fuels will rise in the buoyant plume, resulting in an under-estimation of temperatures in the lower portion of the sample, parallel to the turbulence estimate. The remaining fuel is thus combusted higher in the rig when the combustion process can be witnessed resulting in overestimation of temperatures in higher regions of the sample. This influence of combustion chemistry on errors is indicated in the results of the Horizontal Position 3 in Figure 11. In this instance the data at the bottom detector demonstrated competition between the turbulent and combustion misrepresentations, fluctuating back and forth between positive and negative error. However, once the flame progresses into the sample and reaches more laminar conditions the effect of the combustion misrepresentation is more profound. Clearly demonstrating the underestimation of temperature in elevations two and three and overestimation in elevations four and five.

Finally, Figure 12 further illustrates the importance of turbulent representation, however in this case with regard to the lateral interface of the smoke plume. Notice that the data presented for the detectors in horizontal position four do not follow the trend previously described regarding

the influence of combustion chemistry. This is because the detectors in this location are not positioned above the burner, rather at the edge of the smoke plume. Hence limited combustion is found within this region, but there remains a high degree of turbulence at the interface of the smoke plume. Importantly, the lower detectors demonstrate higher percentages of errors due to their location at the edge of the plume. However, as the plume expands with elevation, as indicated in Figure 27, the detectors in the upper elevations end up deeper in the plume. Progression deeper into the plume results in the production of less turbulence, as buoyancy driven flows dominate. Demonstrated in the reduction of errors in the detectors progressing up the sample. Conversely, in the case of the detectors in horizontal position five. The detectors progressively become involved with the interface of the fire plume with greater elevation. Resulting in an increase in the levels of turbulence experienced, as demonstrated in Figure 12b). Especially noting that the plume extends to the point that the upper elevation detector of this location is engulfed by the plume, demonstrating a lower error than the detector at V4.

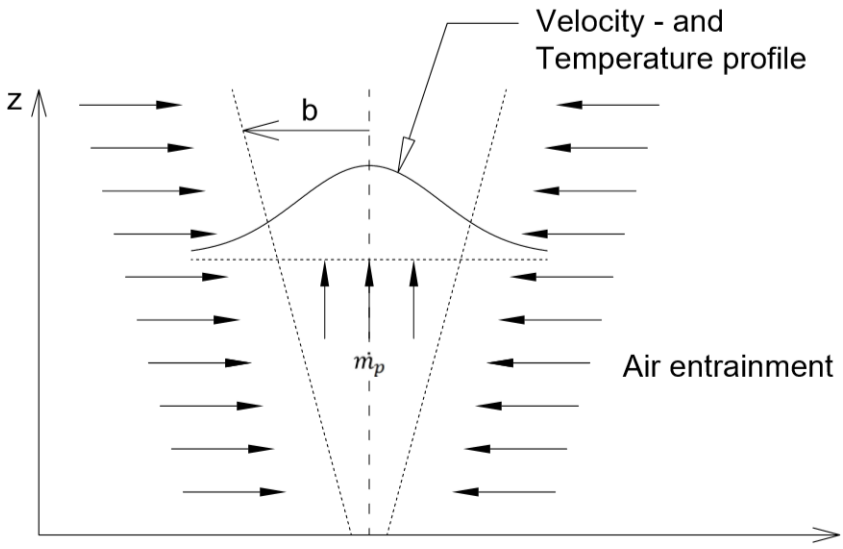

Figure 27:Smoke Plume Characteristics Diagram, Re-constructed from Karlsson & Quintiere (1999)

6.1.2 6- & 10-mesh 10mm Cell Size Comparison

The initial early spikes in data, in both the positive and negative sense, presented in Figure 13 demonstrates the changed conditions of the domain discretization. In comparing the 6-mesh and 10-mesh solutions, it is clear that the only variations occur within the façade. As the mesh interfaces adjusting from 10mm cells to 100mm cells remain the same in both cases. Hence, the only difference for the distribution of pressure between the models is the transport of pressure across the façade from the area of high pressure above the burner, to the regions of low pressure in the wing of the sample. Hence, the over-estimation of the temperature and subsequent pressure in the left side of the sample in the 10-mesh solution. As the mesh

interfaces block the instantaneous pressure transport, trapping pressure within the mesh of origin. Further, the areas toward the right wing will under-estimate pressure and temperature, because the pressure was unable to transport from the left side of the sample. This takes place primarily at the start of the test when the buoyant plume interacts with the stagnant air within the cavity resulting in this drastic pressure difference. As the chimney effect begins to act without resistance of stagnant air however, the buoyant plume produces low pressure regions at the base of the cavity for the entrainment of fresh oxygen, as described in Section 1.1. This results in the reverse draw of pressure from the right of the sample now to the left. As described in the latter stages of Figure 13. This pressure change has a reduced impact however as the majority of pressure transport now functions vertically due to the chimney effect. The reasoning behind the reduced influence of H1 in this instance is due to the dominance of the entrainment from the bottom and left side of the cavity to this section, which resembles the same mesh boundary condition for both models.

Further, the similarity in data at changing elevations presented in Figure 14 illustrates the importance of high- and low-pressure regions in the creation of error between the models. Areas of high pressure need to dissipate that potential energy more fervently than in regions of low pressure, thus if the pressure is able to be transported instantaneously then more pressure will be shifted in the high-pressure scenario. If then this pressure transport was suspended, there is a much greater excess of pressure remaining in the region of high pressure that it was not able to dissipated, resulting in the over-estimation presented in Figure 14. The reason behind the general similarity in percentage error up the sample, is due to the consistent shape of the enclosure. If the enclosure were to change in shape at the top a different capacity for pressure dissipation would be available, which would demonstrate a different pattern on the error plot. The corner detectors can again be seen not to be positioned over the burner, hence there is less temperature and pressure, and thus also error in these detectors. Demonstrated in the similarity of the plots in Figure 14. Interestingly the values for the corner detectors indicate greater error and thus a higher-pressure mid height within the façade. The reason for this deviation from the norm can be witnessed in the SMV files illustrated in Figure 28, it can be seen that the flame appears to bulge slightly midway up the sample, in combination with the presence of a rift in the buoyant flow caused by the entrainment of ambient air through the central vertical joint. The turbulence caused within the joint may act to push the fire plume outward at this height, while the plume restores higher up, due to the more powerful influence of lateral entrainment above the rig.

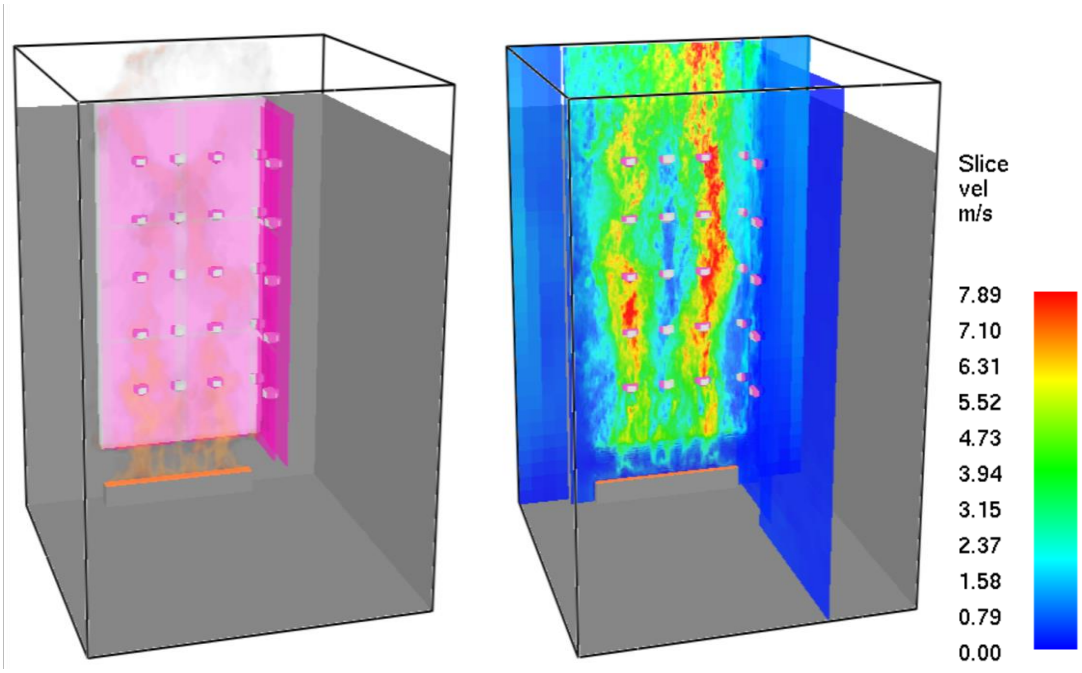

Figure 28:SMV 3D Temperature profile (left) and Velocity slice file (right) for the 6-mesh 10mm FDS input file, Model Iteration 'open75'

6.2 Perforated Sheet Input Analysis

From the results of Figure 15, it is clear that the two input files do not create similar results in representing the perforated sheeting applied to the ISO 13785-1 sample. Hence, the simplified solution cannot be used in place of the 'SCREEN' case in the remainder of the analysis, in the interest of reducing computational processing time. However, this does not mean that the 'SCREEN' case is the correct solution. The 'SCREEN' input is a substitute, used in an attempt to resemble the real-life perforated sheet scenario, but it too requires experimental data for its validation. The premise of the 'SCREEN' input is the representation of perforations, in a manner resembling the wire screens applied to windows. Hence this data would appear to be overly complex for the situation of representing a perforated steel sheet section. As such it is clear that both simplified and 'SCREEN' inputs will present flow conditions markedly different to that of a perforated steel sheet, resulting in variable oxygenation conditions of the sample. While varying obstruction detailing will also have an impact on the re-radiation of heat provided by the perforated representations. Interestingly, the real fire data produced for the 50mm case, pictured in Figures 19 & 20, indicates a less critical environment near to the sample edge when a perforated screen is used. While the 'SCREEN' FDS data is seen to create conditions between that of the Open and Closed cases as anticipated. The reasoning behind this present anomaly in experimental data is uncertain at this stage, however it highlights the issues in reliability of the experimental data presented. Because of the reduced testing schedule and financial cost of experimental analyses, only one test was performed for each sample case,

resulting in the potential for output uncertainties to develop. One primary reason that the perforated case may develop reduced thermocouple readings, may relate to the re-use and potential degradation of calcium silicate panels over the course of experimental analysis. Degradation of calcium silicate board material properties would see the increase in material conductivity, which would act to reduce thermal conditions within the cavity. Hence, repeat tests utilising fresh calcium silicate would be suggested for the course of future studies to determine the influence of material re-use on scientific analyses.

Comparing the data between the preliminary 25mm perforation tests and the 50mm validation tests, it is clear that the data does not discern the true influence of the 'SCREEN' input, given that against expectations the 25mm 'SCREEN' sample reported the most critical conditions at the device location. However, this discrepancy may relate to the simplified nature of these early FDS models. Which presented a gap between cladding panels and lateral obstructions, allowing additional oxidation of the sample, uncharacteristic of the obstructions applied. Both data sets generally agree on the similarity between the simplified case and the open ventilation case, with the preliminary tests demonstrating this more clearly based on the additional air gap mentioned. This model discrepancy alludes to an important point about appropriate installation and application of facades, in that slight variations to approved designs may lead to fire performance uncharacteristic of the investigated design. Hence, care must be taken to ensure that façade designs are applied in the manner presented throughout approval and compliance proceedings.

6.3 Model Validation

For the presentation of understanding developed amidst validation of the FDS models of this thesis, it is important to understand the capacity of the studies presented as a result of experimental restrictions. Due to the absence of 25mm and 100mm experimental data and the absence of cavity barriers provided in the 50mm samples tested, it is clear that the primary goal of this analysis is in the validation of the model inputs and trends produced regarding the influence of lateral ventilation conditions. Further, as stated in the limitations it is important to consider the influence of the slow and delayed activation time of the experimental burner in comparison to the near instantaneous activation of the burner within the FDS analyses.

6.3.1 Heat Flux Analysis

Reflecting upon the proceedings and results of the heat flux validation analysis, it is clear that the data produced by the FDS files are not representative of the experimental data. Given that the experimental data takes up to 15 minutes to reach its maximum value, while the FDS data which reaches its maximum within a minute. This information questions the similarity of devices used in each case for the analysis of heat flux. Noting that heat flux is recorded based on the temperature differential experienced on a target receiver to a reference base temperature. As such it would appear that the conductivity of the FDS receiver results in a fast indication of heat flux, while the experimental case holds a much lower conductivity. Hence, to improve the representative nature of the FDS software, the heat flux meter needs to be adjusted to suit the experimental scenario. The present device used the standard FDS input:

```
&DEVC ID='hf', QUANTITY='RADIATIVE HEAT FLUX GAS', XYZ=1.2,0.01,2.9, ORIENTATION=0,1,0/
```

However, this FDS heat flux meter may remain beneficial in the interests of saving time on computational processing. Given that, the maximum heat flux is an important output for analysis of a façade fire scenario, in determining the impact of the fire on the floors above. Hence, provided there are no combustibles in the design, a short simulation may be performed for the retrieval of maximum heat flux data for design development. However, that opportunity is available only under the assumption that the heat flux experienced by the FDS detector does not increase further when granted additional simulation time. Hence additional studies should be performed to check that the heat flux is limited to these general values. Further, the comparative maximums produced in both the experimental and simulated data highlight a disparity in the open and perforated ventilation condition cases. For the open case, the FDS data reaches just over 10kW/m², while the experimental data extends up to around 14kW/m². Despite the fact that in this region a high similarity in temperatures seems to be recorded for all samples as demonstrated in Appendix A8a). However, this temperature data details only the first two minutes in study, and as such the closed ventilation condition FDS test should support the open FDS case reaching a maximum of just over 10kW/m². But when regarding the experimental data, slight variations are witnessed in temperature throughout the 15-minute experimentation time as demonstrated in Appendix A8b). As such the heightened 14kW/m² in the open case is understandable in comparison to the 10kW/m² in the closed case due to a disparity in temperature caused by additional oxygenation of the sample. However, interestingly the perforated ventilation condition demonstrates a maximum heat flux of up to 16kW/m², against the logic of sample oxygenation, as temperatures were seen to slightly

increase past the open case in the latter stages of testing. This issue may relate to the re-use of calcium silicate for analyses described in Section 3.2, where the perforated case was the last to be run. Degradation of the board throughout multiple experiments may have resulted in un-representative temperatures in the latter stages of data recording. With degradation seeing the development of fissures in the calcium silicate board for greater oxidation of the cavity. Notice that this late temperature differential does not affect other subjects of data presented in this thesis as early steady state conditions are reported upon. Notice, that the perforated FDS files, both simplified and 'SCREEN' report heat fluxes similar to the open and closed conditions. With the 'SCREEN' input demonstrating the lowest value of approximately 8kW/m², which was only able to be simulated for 60 seconds, half that of the other files. Hence, further studies should focus on extending FDS simulation times, to investigate the manner with which the heat flux behaves beyond that simulated here.

6.3.2 Bi-directional Analysis

It is difficult to directly compare the data between the FDS slice files and the bi-directional probe outputs presented in Section 5.3.2. However, it can be seen that a reasonable correlation of data is produced, with FDS files slightly over-estimating the velocities in the region of interest. The presence of more consistent patches of yellow in the closed FDS case, presented in the top left of Figure 19, indicates values in excess of 7m/s, which was seen to be the maximum in the experimental case. The open ventilated scenario is harder to discern however, with fewer fluctuations of higher velocities being witnessed in the slice files. Comparing this information to the thermocouple data provided in Figure 21, provides a reasonable indication for the kind of comparison between the velocities in the region. Which is understandable based on the correlation between temperature and the action of the chimney effect demonstrated in Section 3.1. The over-valuation of the velocity and temperature for that matter, to be discussed in Section 6.3.3, may relate to the mesh resolution principle discussed in Section 6.1. By improperly resolving turbulence and combustion, heat losses in small scale eddies are missed, while combustion processes are stretched to the top of the sample as full combustion is not witnessed at the bottom of the sample. Hence, higher temperatures and higher activity of the chimney effect occur, in the presence of higher velocities. Interestingly this contradicts the conclusions of the Bouchair Solar Chimney analysis, presented in the FDS technical reference guide for validation (McGrattan et al., 2020). Where FDS is seen to undervalue the influence of the chimney effect in small cavity widths. Notice, the experimental data will also be slightly over valued, increasing the validation disparity. Given that the temperature data applied to the

calculations of Equation 3.5 were taken from a detector 200mm lower than the actual bi-directional probe. Hence, temperatures will be slightly over-valued resulting in higher velocities. For future studies it is thus recommended to position a thermocouple in the immediate vicinity of the bi-directional probe. Further, the presence of fluctuations in the FDS case and notable absence in the experimental outputs is determined by the requirements of each analysis. FDS requires in-depth calculation to ensure numerical stability of simulations, resulting in the display of all relevant data. While it is described in the ISO 13785-1 methodology, that time averaged data shall be taken to "eliminate momentary fluctuations in the values" (International Organization for Standardization, 2002).

Regarding the influence of the lateral ventilation condition on cavity velocities, it can be seen that out of all cases the closed samples produce the largest velocities, while the open cases result in the lowest velocities. This resolution makes sense given that, in the region of the bi-directional probe, a closure to the edge of the sample will create a chimney with the façade walls and the U-type flashing to its right. The elimination of lateral entrainment reduces the production of turbulence in the section and allows for high velocities to be attained. As expected, the perforated case provides small eddies of turbulence, from entrainment streams through the small holes, reducing velocity. But the influence of entrainment from the perforation is less than that of the open case which allows larger pockets of turbulence. Witnessed at the edges of the sample in the top right-hand side of Figure 19. Notice, that once again the FDS simplified perforation case closely resembles the open ventilation case in its presentation of large turbulent structures due to the large holes for entrainment at the edge of the sample in Figure 19 (bottom left), while the 'SCREEN' case demonstrates lesser turbulent entrainment in Figure 19 (bottom right), in its presentation of the greater flow field thickness produced, resulting in the greater embedded depth of the bi-directional probe within the flow. Therefore, the level of detail applied for the perforation sizes of the sheet obstruction holds a great influence on the representative nature of the fire behaviour within the cavity, through the size of turbulent structures able to pass through the obstruction. Hence, for appropriate representation in FDS true conditions must be input rather than substitute components. Notice however, that the perforated sheet in itself, is a substitute material used for representation of reduced oxygen conditions in façade sample analyses, and hence will also alter fire behaviour from conditions in reality. This logic touches on the concept of the near and far field sample representative nature of façade sample methodologies to be discussed further in Section 6.3.3.

6.3.3 Thermocouple Analysis

When referring to thermocouple data, the ignition of the experimental burner provides a significant delay to the heating of the cavity, as discussed in the limitations of the text. However, for future reference and analyses, the burner applied in the FDS model should be adjusted and should rather be ramped up progressively to resemble the experimental conditions anticipated in the fire laboratory. However, due to the delayed testing schedule of this thesis, FDS models were performed prior to the experimental analysis and thus this input was not known during creation of the models. However, this analysis does not incorporate any combustible materials resulting in the production of steady state conditions during testing. Hence, the delay in burner application does not cause any issues in the comparisons of data. When comparing the experimental data to the simulated information, it is clear from Section 6.3.2 that FDS over-estimates the temperature within the upper portion of the sample, following the principles of misrepresentation of turbulence and combustion outlined prior. In the lower portion however, the balance of unresolved turbulence losses and combustion processes result in a reasonable estimate of data as discussed in Section 6.1.1. However, when regarding the influence of ventilation conditions on thermocouple data within the façade sample it is clear that region specific data conclusions of worst-case conditions can be formed. For instance, in the data of Figure 20, it is clear that open ventilation conditions demonstrate the most critical conditions in the lower portion of the sample. However, Figure 21 illustrates closed conditions worse at the top of the sample. This demonstrates the presence of oxidation limits within the 50mm cavity width. As open conditions will allow for additional early oxidation of the propane fuel for combustion resulting in higher temperatures toward the samples base. While a closed sample will result in the restriction of oxidation and lengthening of the combustion region, and therefore flame height. Thus, causing higher temperatures in the upper portions of the sample, while re-radiation from the obstruction stems heat losses from the cavity. This implies that there will be an additional influence of oxidation restrictions in the 25mm samples to be analysed.

The low temperatures demonstrated in the experimental perforated case in the region of detectors H1, is not easily understandable. Following the logic of oxidation demonstrated above, it would seem that the data should present intermediate values between those of the open and closed cases as presented in the ‘SCREEN’ FDS data. However, the near-field complex impact of the perforations is not well understood and thus must be researched further, along with the influence of calcium silicate board degradation discussed in Section 6.2 . This

knowledge questions the use of the perforated sheet in façade analyses, given that its use was developed for the understanding and representation of reduced oxygen conditions present within a cavity. Which otherwise cannot be simulated in a reduced scale façade test rig. However, when the influence of the perforated sheet is analysed in a far-field manner, the expected conditions are reached. As Figure 22 highlights a balance between the open and closed data for thermocouples positioned in the corner of the rig. Indicating that medium levels of oxidation are presented as intended, along with reduction in heat losses due to re-radiation without the complexities experienced close to the sheet. Hence, for future applications if perforated sheeting is wished to be used, the testing rig should be extended such that the areas of interest and study are far enough from the sheeting to avoid this phenomenon. Comparing the experimental and simulated data at Thermocouple V4H4, highlights the potential disparity in the conductivity of calcium silicate panels employed between the two data sets. An over-valuation of the conductivity will result in greater removal of heat from the cavity, and thus also a reduction in the temperature of the flame experienced by the thermocouples. This factor is more pronounced and understandable in the corner of the sample, due to the lower temperatures present within the region, where errors from modelling turbulence and combustion chemistry are minimised. The conductivity applied to the FDS model was set to 0.17 W/mK based on initial sources of material supply (Promat International N.V., 2015). However, the limitations set on the testing schedule resulted in alternate sourcing of calcium silicate materials with a specified conductivity of 0.12 W/mK (RCM Roofing and Cladding Materials Ltd., 2014). Due to the schedule of works, the FDS models were run before this decision was made and hence was not able to be rectified in the thesis time frame and hence should be the focus of further analysis. This once again signifies the importance of ensuring that as-built products and components match the specified design, given the potential variation in fire performance, resulting from substitution methodologies, as introduced in Section 1.4. Notice too, that a set conductivity was input into FDS analyses to limit computational processing, however it is understood that the conductivity will increase under thermal loading. Hence, further iterations of model development should take this factor into account.

6.4 Extension of studies in FDS software

As demonstrated in Section 5.4, it is clear that the FDS analysis estimates that the most critical cavity width displayed in the ISO 13785-1 setup is the 50mm cavity. Again, in understanding the limitations of the conclusions that can be drawn from this data without validation. A few points of interest with reference to the fire science body of knowledge are raised. Firstly, despite the earlier data contradicting the conclusions of the Bouchair Solar Chimney analysis presented in the FDS technical reference guide (McGrattan et al., 2020). The reduced impact of the chimney effect in the 25mm cavity width presented in Section 5.4, may occur based on the principles discussed in the Bouchair case, with the critical point of undervaluation lying between 25 and 50mm widths. This must therefore be validated before conclusions are drawn. With that in mind, in the instance that the output data presented in Section 5.4 is shown to be valid, inferring a contradiction to the conclusions of Livkiss (2018), an important question arises as to what the cause of this contradiction is. Primarily, the studies differ in the heat release rate applied by the burner to the sample, and in the lateral ventilation conditions provided. However, the lateral conditions have been shown to cause a limited impact in the small 25 and 50mm cavity widths. Hence, the heat release rate must be the cause of the issue. Upon reflection of the FDS 3D Temperature outputs in Figure 29, it can be determined there is actually no contradiction with the fire science presented by Livkiss (2018) but a contradiction in the metric used to compare the data. For instance, Livkiss (2018) directly studies flame height whereas, due to the anticipated visibility restrictions of the experimental data, the metric of study for this thesis was taken to be flame heights by use of thermocouple data. The use of 100kW heat release rates in the ISO 13785-1 test resulted in excessive fuel supply to the 25mm cavity, resulting in flames extending above the rig, as pictured in Figure 29. This phenomenon resulted in combustion outside the range of the detectors and thus a seemingly less critical cavity performance, based on the lesser combustion occurring within that region. This understanding provides great insight into the decision of metrics for future studies, in the selection of heat release rates and device locations to ensure all relevant information is captured. Further, this information questions what the more critical case for a façade is, provision of longer but lower temperature flames or a more intense compact flame. This data infers that the reduction in cavity widths in the Ingason (1994) report would result in the same extension of flames, due to the non-combustible nature of the test arrangement. The SMV 3D Temperature output for the 100mm open sample is provided in Appendix A9.

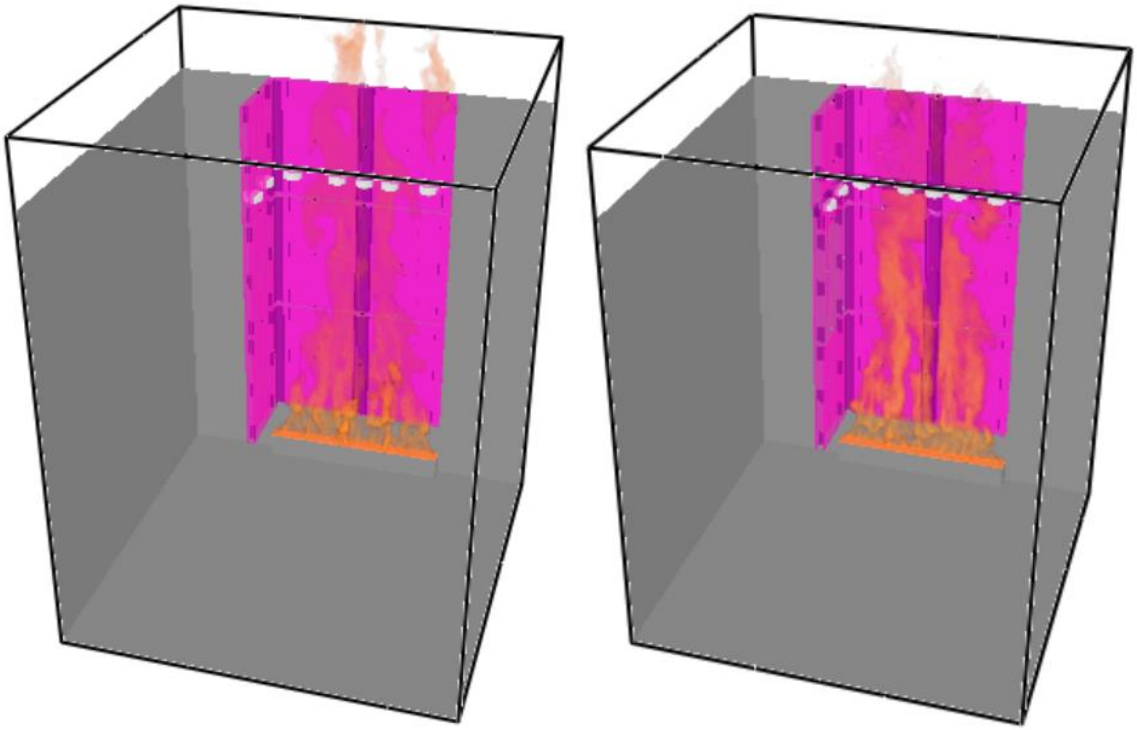

Figure 29: SMV 3D Temperature outputs for comparison of flame heights for 25mm (left) and 50mm (right) Open cavities, Model Iteration 'a'

Further, reflection of the FDS extension study indicates a limited influence of the lateral ventilation conditions on the 25 and 50mm samples in the locations presented, while holding a defining impact on the 100mm sample in the latter stages of testing. Upon witnessing the SMV 3D temperature output for the 100mm closed case in Figure 30, it is clear that once the cavity barriers have activated, large turbulent eddies form when cavity flows contact the cavity barrier and the edge closure. This large eddy cycles the heat back down into the cavity, impacting the V1H1 detector. The reason that this only takes place in the 100mm sample is due to the slow vertical flow of gases from the reduced chimney effect that does not force the gases bouncing off the obstructions through the nearest available opening. Further, the understanding of sufficient oxygen supply in the 100mm case quoted in Section 5.4, alludes to a useful fire dynamic principle presented by Foley & Drysdale (1995), where a wide cavity with an open base produces a flame that acts like a sheet in the centre of the cavity. This behaviour allows the flow of oxygen into the sample for oxidation of the whole flame, rather than purely the sides. Due to the large width of the burner in this study, this phenomenon is experienced as a thicker section of flame pushed to the back panel allowing the effect of the entrained flows described, into the front of the cavity.

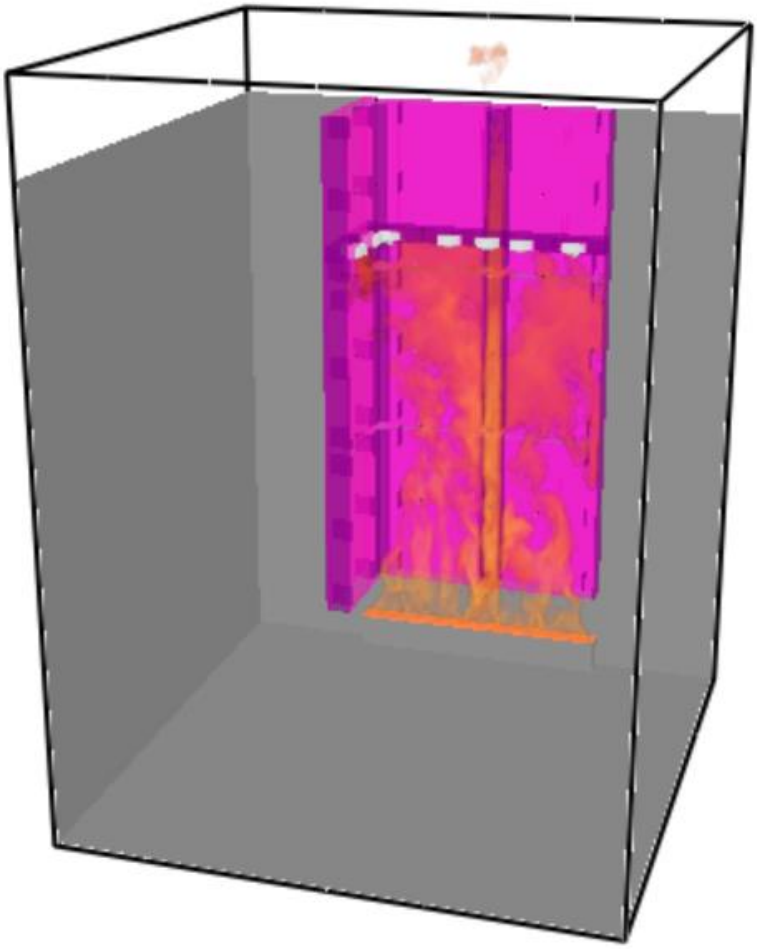

Figure 30: SMV 3D Temperature output for the 100mm Closed case, post-Cavity Barrier activation, Model Iteration 'a'

An additional point of influence of the cavity barrier, seen in the early stages of the 50 and 100mm sample tests, is the influence of the permanent barrier fixture. Provision of the permanent barrier, to bridge the gap for the intumescent strip to fill the cavity, results in a region of constrained flow in the upper portion of the cavity. Which can be seen to increase the velocity of the outgoing gases past the obstruction following the Bernoulli's principle of fluid dynamics, as presented in Figure 26. Finally, upon reflection of Figure 30, another important piece of information regarding the façade support detailing is demonstrated. As fire is shown to progress up the façade within the confines of the U-Type flashing, following the principles of closed channel chimney effects presented in Section 6.3.3 above. Therefore, the avoidance of closed channel detailing is an important point of consideration in the construction of fire safe ventilated façade design, in limiting vertical flame spread.

7. Conclusions

The primary objective of this research was to contribute to the fire science body of knowledge regarding fire behaviour in ventilated façade cavities. Through the parallel analysis of Fire Dynamics Simulator models and laboratory fire experimentation standardised to the ISO 13785-1 methodology, the thesis has highlighted important parameters governing the behaviour of fire within non-combustible facades, and critically analysed the representative nature of the FDS software.

At this stage of computational development, the Fire Dynamics Simulator software provides a valuable tool for the analysis of non-combustible facades, with consideration for the implications of inputs and solvers applied. The thesis explored the influence of domain discretisation detailing and complex geometric substitution on the representative nature of model output data, in relation to the foundational parametric solvers applied to the software. Demonstrating the importance in understanding the balance between the level of detail required for analysis and the computational time required for simulation.

The Fire Dynamics Simulations constructed, showed reasonable correlation to the ISO 13785-1 experimental data developed within this thesis, with the understanding of errors sourcing back to the interaction of inputs and solvers. The data demonstrated a variable influence of ventilation conditions within the 50mm testing sample dependent on the position of interest. For instance, the region near to the lateral obstruction demonstrated a confined chimney space with regard to the adjacent U-type flashings. Hence, more adverse conditions were demonstrated higher in the rig due to delay in oxidation and combustion of fuel. Whilst locations farther from the obstruction depicted open ventilation conditions as more critical in the upper regions of the cavity. The text further highlights, that perforated sheeting is unrepresentative of reduced oxygenated conditions in near-field analysis and hence should only be used to analyse portions of façade rigs far from the obstruction. Thus, perforated sheeting seems to be an impractical solution for representation of reduced oxygen conditions in intermediate-scale façade testing methodologies.

Discrepancies between experimental components and FDS inputs applied within this thesis, have accentuated the present problem of inexact implementation or substitution of façade components, from approved design to as-built construction. Slight variation in oxygenation through vertical joint arrangements, disparity in conductivity of panels and substitution of perforated sheet representative inputs, result in potential variations of fire performance of a

façade, outside that which it has been designed and anticipated. This affirms the need to ensure all façade construction, whether research based or industrial, is undertaken in the manner outlined by the compliant design. Certification of as-built construction would act to safeguard future ventilated façade constructions from unanticipated fire propagation and maintain consistency of fire science research adding to the body of knowledge.

Finally, the extension of studies performed in FDS software, considered the potential influence of cavity widths and barriers for later validation. The information indicated the importance in selection of performance metrics, as data indicated more critical conditions within the 50mm sample, however simulations demonstrated greater flame heights in the 25mm case. Further, the influence of lateral ventilation was considered minor in comparison to the influence of cavity widths. While the cavity barrier was seen to function appropriately, in stopping flow above the barrier and limiting the strength of the chimney effect in the region below. The focus of studies to be performed herein, should be centred around the completion of the experimental proceedings in order to provide continued validation of the simulated data presented. Performed in parallel to additional iterations of the FDS modelling, with a focus on the applied conductivity of calcium silicate boards, as well as the extension of simulation times for the investigation of the heat flux experienced in the simulated sample.

8. References

Agarwal, G., 2017. *Evaluation of the Fire Performance of Aluminium Composite Material (ACM) Assemblies using ANSI/FM 4880,* Norwood: FM Global.

Akadiri, P. O., Chinyio, E. A. & Olomolaiye, P. O., 2012. Design of a Sustainable Building: A Conceptual Framework for Implementing Sustainability in the Building Sector. *Buildings,* Volume 2, pp. 126-152.

Anderson, B. & Kosmina, L., 2019. *Conventions for U-value calculations,* Watford: BRE Global Ltd..

Bikas, D. et al., 2017. Ventilated Facades: Requirements and Specifications Across Europe. *Procedia Environmental Sciences,* Volume 38, pp. 148-154.

Boström, L. et al., 2018. *Development of a European approach to assess the fire performance of facades,* Brussels: European Commission.

BRE Global Ltd., 2017. *BRE Global Client Report: BS8414-1:2015 + A1:2017 test referred to as DCLG test 1,* London: Department for Communities and Local Government, UK Government.

Building Code Commission, 1994. *BCC Ruling No. 94-19-397,* Toronto: Ontario Ministry of Municipal Affairs and Housing .

Canadian Commission on Building and Fire Codes, 2015. *National Building Code of Canada.* 14th ed. Ottawa: National Research Council of Canada.

Carvel, R., 2018. *Fire Science & Fire Dynamics,* Edinburgh: The University of Edinburgh.

Chen, T. B. Y. et al., 2019. Fire Risk Assessment of Combustible Exterior Cladding Using a Collective Numerical Database. *Fire ,* 2(1), pp. 1-14.

Choi, K. K. & Taylor, W., 1984. Combustibility of Insulation in Cavity Walls. *Fire Sciences,* Volume 2, pp. 179-188.

Čolić, A. & Pečur, I. B., 2020. *Influence of Horizontal and Vertical Barriers on Fire Development for Vertical Facades,* Zagreb: University of Zagreb.

Colwell, S. & Baker, T., 2013. *Fire Performance of External Thermal Insulation for Walls of Multistorey Buildings,* Watford: BRE Trust.

Drysdale, D., 2011. *An Introduction to Fire Dynamics.* 3rd ed. Chichester : John Wiley & Sons, Ltd..

Efectis UK/Ireland Ltd., 2018. *Reaction to Fire Test Report No EUI - 18 - 000030,* Newtownabbey: Efectis UK/Ireland Ltd.

Foley, M. & Drysdale, D., 1995. Heat Transfer from Flames Between Vertical Parallel Walls. *Fire Safety Journal,* Volume 24, pp. 53-73.

Genco, G., 2015. *Lacrosse Building Fire ,* Melbourne : City of Melbourne .

Grove, J. R., 1968. *The Measurement of Quenching Diameters and their Relation to the Flameproof Grouping of Gases and Vapours.* London, The Institution of Chemical Engineers.

Guillaume, E. et al., 2018. Study of fire behaviour of facade mock-ups equipped with aluminium composite material-based cladding, using intermediate-scale test method. *Fire and Materials,* 42(5), pp. 561-577.

HM Government, 2019. *Fire Safety Approved Document B.* 2019 Edition ed. London: Her Majesty's Government.

Hu, L., Liu, S. & Zhang, X., 2017. Flame heights of line-source buoyant turbulent non-premixed jets with air entrainment constraint by two parallel side walls. *Fuel,* Volume 200, pp. 583-589.

Hurley, M. & Rosenbaum, E., 2015. *Performance-Based Fire Safety Design.* 1st ed. Boca Raton: CRC Press.

Ingason, H., 1994. *Two Dimensional Rack Storage Fires.* Ottawa, International Association for Fire Safety Science.

Innowood, 2016. *An Introduction to: Ventilated Facade Systems in Modern Design,* Pyrmont: Innowood.

International Organization for Standardization, 2002. *ISO 13785-1:2002 Reaction-to-fire tests for facades,* Geneva: ISO.

Karlsson, B. & Quintiere, J. G., 1999. *Enclosure Fire Dynamics.* 1st ed. Boca Raton: CRC Press.

Karlsson, B., Thomas, P. & Holmstedt, G., 1995. *Flame Sizes in a Small Scale Stack: Pilot Experiments,* Lund: Lunds Universiteit, Department of Fire Safety Engineering.

Kinspan Group, 2019. *ACM/MCM Facade System.* [Online]
Available at: https://www.kingspan.com/us/en-us/product-groups/architectural-panel-facade-systems/benchmark-facade-systems/acm-mcm-facade-system
[Accessed 25th March 2020].

Knaack, U., Klein, T., Bilow, M. & Auer, T., 2014. *Facades: Prinicples of Construction.* 2 ed. Basel: Birkhäuser Verlag GmbH.

Kolaitis, D. I., Asimakopoulou, E. K. & Founti, M. A., 2016. *A Full-Scale Fire Test to Investigate the Fire Behaviour of the "Ventilated Facade" System ,* Athens: National Technical University Athens.

Lee, Y. P. et al., 2007. *Flame Heights and Heat FLuxes on a Building Facade and an Opposite Building Wall by Flames Emerging from an Opening,* Berkeley: International Association for Fire Safety Science.

Livkiss, K., 2018. Flame Heights and Heat Transfer in Facade System Ventilation Cavities. *Fire Technology,* Volume 54, pp. 689-713.

Mahdavinejad, M. & Mohammadi, S., 2018. Ecological analysis of natural ventilated facade system and its performance in Tehran's climate. *Ukranian Journal of Ecology,* 8(1), pp. 273-281.

Martinsson, E., 2018. *To evaluate fire properties of a facade - a study on semi natural test methods,* Luleå: Luleå Tekniska Universitet.

McCaffrey, B. & Heskestad, G., 1976. A Robust Bidirectional Low-Velocity Probe for Flame and Fire Application. *Combustion and Flame,* Volume 26, pp. 125-127.

McGrattan, K. et al., 2019. *Fire Dynamics Simulator User's Guide.* 6th ed. Gaithersburg: National Institute of Standards and Technology.

McGrattan, K. et al., 2020. *Fire Dynamics Simulator Technical Reference Guide Volume 3: Validation.* 6th ed. Gaithersburg: National Institute of Standards and Technology.

McKenna, S. et al., 2019. Fire behaviour of modern facade materials - Understanding the Grenfell Tower fire. *Hazardous Materials,* Volume 368, pp. 115-123.

Merci, B., 2019. *Modelling of Turbulence and Combustion* , Gent: Gent University.

Merci, B. & Beji, T., 2016. *Fluid Mechanics Aspects of Fire and Smoke Dynamics in Enclosures.* 1st ed. Leiden: CRC Press/Balkema.

National Housing Federation Ltd., 2018. *Consultation on proposed changes to use of desktop studies in building regulations,* London: National Housing Federation Ltd..

OMEGA Engineering, 2019. *Thermocouple Types.* [Online]
Available at: https://www.omega.com/en-us/resources/thermocouple-types
[Accessed 23 April 2020].

Promat International N.V., 2015. *Calcium Silicat Insulation.* [Online]
Available at: https://www.promat-hpi.com/downloads/get/en/8D778F21B04244AEA2A141C9F5E3DD46
[Accessed 10th February 2020].

Rasbash, D. J., 1977. *Fire Safety Objectives for Buildings.* Morecambe: The University of Edinburgh.

RCM Roofing and Cladding Materials Ltd., 2014. *Structural Timber Association.* [Online]
Available at: https://www.structuraltimber.co.uk/users/attachment/?id=65
[Accessed 13 5 2020].

Rockwool International A/S, 2017. *High quality fire-resistant materials make the difference between a fire in a building and a building on fire,* Copenhagen : Rockwool International A/S.

Siderise Group, 2019. *RH & RV Cavity Barriers,* Maesteg: Siderise Group.

Spearpoint, M., Fu, I. & Frank, K., 2019. Tall building facade fire incident database. *CTBUH Journal,* Issue 2, pp. 34-39.

Taylor, W., 1983. *Fire Spread in Concealed Foamed Plastic Insulation,* Ottawa: National Research Council of Canada .

The Engineering ToolBox, 2005. *Metals and Alloys - Melting Temperatures.* [Online]
Available at: https://www.engineeringtoolbox.com/melting-temperature-metals-d_860.html
[Accessed 15 January 2019].

TLJ Engineering Consultants Ltd., 2016. *Stack Effect or Chimney Effect,* Calgary: TLJ Engineering Consultants Ltd..

Torero, J., 2018. *Grenfell Tower: Phase 1 Report,* Edinburgh: Torero, Abecassis Empis and Cowlard Ltd..

Appendix

A1. 100mm Closed Edge Preliminary FDS input file, Model Iteration ‘iso’

```
&HEAD CHID='iso100c2'/
&MESH ID='mesh1', IJK=40,30,320, XB=0.4,0.8,0,0.3,0,3.2/
&MESH ID='mesh2', IJK=40,30,320, XB=0.8,1.2,0,0.3,0,3.2/
&MESH ID='mesh3', IJK=40,30,320, XB=1.2,1.6,0,0.3,0,3.2/
&MESH ID='mesh4', IJK=40,30,320, XB=1.6,2.0,0,0.3,0,3.2/
&MESH ID='mesh5', IJK=40,30,320, XB=1.6,2.0,0.3,0.6,0,3.2/
&MESH ID='mesh6', IJK=40,30,320, XB=1.6,2.0,0.6,0.9,0,3.2/
&MESH ID='mesh7', IJK=4,24,32, XB=0,0.4,0,2.4,0,3.2/
&MESH ID='mesh8', IJK=4,24,32, XB=2.0,2.4,0,2.4,0,3.2/
&MESH ID='mesh9', IJK=12,6,32, XB=0.4,1.6,0.3,0.9,0,3.2/
&MESH ID='mesh10', IJK=16,15,32, XB=0.4,2.0,0.9,2.4,0,3.2/
&TIME T_END=60/
&MISC SURF_DEFAULT='CALCIUM_SILICATE', TMPA=20/
&DUMP NFRAMES=1000/
&SURF ID='CALCIUM_SILICATE',
MATL_ID='STONE',
THICKNESS=0.02,
DEFAULT=.TRUE.
RGB=128,128,128/
&MATL ID='STONE',
CONDUCTIVITY=0.17
SPECIFIC_HEAT=0.96
DENSITY=870/

&REAC FUEL='PROPANE',
FYI='propane',
C=3,
H=8,
SOOT_YIELD=0.01,
CO_YIELD=0.02,
HEAT_OF_COMBUSTION=46460/

&SURF ID='GAS_BURNING', HRRPUA=833.33/
&OBST XB=0.6,1.8,0.0,0.1,0,0.15/
&VENT XB=0.6,1.8,0.0,0.1,0.15,0.15, SURF_ID='GAS_BURNING', RGB=249,129,70/

Facade Testing Panels
&OBST XB=0.6,1.92,0,0.01,0.4,2.8, RGB=252,15,192, TRANSPARENCY=0.6/
&OBST XB=1.91,1.92,0.01,0.72,0.4,2.8, RGB=252,15,192, TRANSPARENCY=0.6/
&OBST XB=0.66,1.16,0.11,0.12,0.42,1.18, RGB=252,15,192, TRANSPARENCY=0.6/
&OBST XB=0.66,1.16,0.11,0.12,1.22,1.98, RGB=252,15,192, TRANSPARENCY=0.6/
&OBST XB=0.66,1.16,0.11,0.12,2.02,2.78, RGB=252,15,192, TRANSPARENCY=0.6/
&OBST XB=1.26,1.76,0.11,0.12,0.42,1.18, RGB=252,15,192, TRANSPARENCY=0.6/
&OBST XB=1.26,1.76,0.11,0.12,1.22,1.98, RGB=252,15,192, TRANSPARENCY=0.6/
&OBST XB=1.26,1.76,0.11,0.12,2.02,2.78, RGB=252,15,192, TRANSPARENCY=0.6/
&OBST XB=1.8,1.81,0.17,0.67,0.42,1.18, RGB=252,15,192, TRANSPARENCY=0.6/
&OBST XB=1.8,1.81,0.17,0.67,1.22,1.98, RGB=252,15,192, TRANSPARENCY=0.6/
&OBST XB=1.8,1.81,0.17,0.67,2.02,2.78, RGB=252,15,192, TRANSPARENCY=0.6/

Side Obstructions
&OBST XB=0.59,0.6,0,0.12,0.4,2.8, RGB=128,0,128, TRANSPARENCY=0.6/
&OBST XB=1.8,1.92,0.72,0.73,0.4,2.8, RGB=128,0,128, TRANSPARENCY=0.6/

Top Obstructions
Permanent Obstructions
&OBST XB=0.6,1.91,0.01,0.085,2.77,2.78, RGB=128,0,128, TRANSPARENCY=0.6/
&OBST XB=1.835,1.91,0.085,0.72,2.77,2.78, RGB=128,0,128, TRANSPARENCY=0.6/
Intumescent Obstructions
&OBST XB=0.6,0.8,0.085,0.11,2.77,2.78, RGB=128,0,128, TRANSPARENCY=0.6, DEVC_ID='thermal1'/
&OBST XB=0.8,1.2,0.085,0.11,2.77,2.78, RGB=128,0,128, TRANSPARENCY=0.6, DEVC_ID='thermal2'/
&OBST XB=1.2,1.6,0.085,0.11,2.77,2.78, RGB=128,0,128, TRANSPARENCY=0.6, DEVC_ID='thermal3'/
&OBST XB=1.6,1.835,0.085,0.11,2.77,2.78, RGB=128,0,128, TRANSPARENCY=0.6, DEVC_ID='thermal4'/
```

```
&OBST XB=1.81,1.835,0.11,0.3,2.77,2.78, RGB=128,0,128, TRANSPARENCY=0.6, DEVC_ID='thermal5'/
&OBST XB=1.81,1.835,0.3,0.72,2.77,2.78, RGB=128,0,128, TRANSPARENCY=0.6, DEVC_ID='thermal6'/

Ventilation Openings
&VENT XB=0,2.4,2.4,2.4,0,3.2, SURF_ID='OPEN'/
&VENT XB=0,2.4,0,0,2.8,3.2, SURF_ID='OPEN'/
&VENT XB=0,2.4,0,2.4,3.2,3.2, SURF_ID='OPEN'/
&VENT XB=0,0,0,2.4,2.8,3.2, SURF_ID='OPEN'/
&VENT XB=2.4,2.4,0,2.4,2.8,3.2, SURF_ID='OPEN'/

&PROP ID='Thermal Detection', QUANTITY='THERMOCOUPLE'/
&DEVC ID='V1H1', PROP_ID='Thermal Detection', XYZ=0.9,0.06,0.8/
&DEVC ID='V1H2', PROP_ID='Thermal Detection', XYZ=1.2,0.06,0.8/
&DEVC ID='V1H3', PROP_ID='Thermal Detection', XYZ=1.5,0.06,0.8/
&DEVC ID='V1H4', PROP_ID='Thermal Detection', XYZ=1.86,0.06,0.8/
&DEVC ID='V1H5', PROP_ID='Thermal Detection', XYZ=1.86,0.42,0.8/
&DEVC ID='V2H1', PROP_ID='Thermal Detection', XYZ=0.9,0.06,1.2/
&DEVC ID='V2H2', PROP_ID='Thermal Detection', XYZ=1.2,0.06,1.2/
&DEVC ID='V2H3', PROP_ID='Thermal Detection', XYZ=1.5,0.06,1.2/
&DEVC ID='V2H4', PROP_ID='Thermal Detection', XYZ=1.86,0.06,1.2/
&DEVC ID='V2H5', PROP_ID='Thermal Detection', XYZ=1.86,0.42,1.2/
&DEVC ID='V3H1', PROP_ID='Thermal Detection', XYZ=0.9,0.06,1.6/
&DEVC ID='V3H2', PROP_ID='Thermal Detection', XYZ=1.2,0.06,1.6/
&DEVC ID='V3H3', PROP_ID='Thermal Detection', XYZ=1.5,0.06,1.6/
&DEVC ID='V3H4', PROP_ID='Thermal Detection', XYZ=1.86,0.06,1.6/
&DEVC ID='V3H5', PROP_ID='Thermal Detection', XYZ=1.86,0.42,1.6/
&DEVC ID='V4H1', PROP_ID='Thermal Detection', XYZ=0.9,0.06,2/
&DEVC ID='V4H2', PROP_ID='Thermal Detection', XYZ=1.2,0.06,2/
&DEVC ID='V4H3', PROP_ID='Thermal Detection', XYZ=1.5,0.06,2/
&DEVC ID='V4H4', PROP_ID='Thermal Detection', XYZ=1.86,0.06,2/
&DEVC ID='V4H5', PROP_ID='Thermal Detection', XYZ=1.86,0.42,2/
&DEVC ID='V5H1', PROP_ID='Thermal Detection', XYZ=0.9,0.06,2.4/
&DEVC ID='V5H2', PROP_ID='Thermal Detection', XYZ=1.2,0.06,2.4/
&DEVC ID='V5H3', PROP_ID='Thermal Detection', XYZ=1.5,0.06,2.4/
&DEVC ID='V5H4', PROP_ID='Thermal Detection', XYZ=1.86,0.06,2.4/
&DEVC ID='V5H5', PROP_ID='Thermal Detection', XYZ=1.86,0.42,2.4/
&DEVC ID='V6H1', PROP_ID='Thermal Detection', XYZ=0.9,0.06,2.8/
&DEVC ID='V6H2', PROP_ID='Thermal Detection', XYZ=1.2,0.06,2.8/
&DEVC ID='V6H3', PROP_ID='Thermal Detection', XYZ=1.5,0.06,2.8/
&DEVC ID='V6H4', PROP_ID='Thermal Detection', XYZ=1.86,0.06,2.8/
&DEVC ID='V6H5', PROP_ID='Thermal Detection', XYZ=1.86,0.42,2.8/
&PROP ID='Thermal Activation', QUANTITY='LINK TEMPERATURE', RTI=132.0,
ACTIVATION_TEMPERATURE=180.0/
&DEVC ID='thermal1', PROP_ID='Thermal Activation', XYZ=0.7,0.0975,2.77/
&DEVC ID='thermal2', PROP_ID='Thermal Activation', XYZ=1.0,0.0975,2.77/
&DEVC ID='thermal3', PROP_ID='Thermal Activation', XYZ=1.4,0.0975,2.77/
&DEVC ID='thermal4', PROP_ID='Thermal Activation', XYZ=1.7,0.0975,2.77/
&DEVC ID='thermal5', PROP_ID='Thermal Activation', XYZ=1.8225,0.15,2.77/
&DEVC ID='thermal6', PROP_ID='Thermal Activation', XYZ=1.8225,0.45,2.77/

&SLCF PBX=1.86, QUANTITY='TEMPERATURE', VECTOR=.TRUE./
&SLCF PBX=1.86, QUANTITY='VELOCITY', VECTOR=.TRUE., CELL_CENTERED=.TRUE./
&SLCF PBX=1.86, QUANTITY='VOLUME FRACTION', SPEC_ID='OXYGEN'/
&SLCF PBY=0.06, QUANTITY='TEMPERATURE', VECTOR=.TRUE./ oxygen
&SLCF PBY=0.06, QUANTITY='VELOCITY', VECTOR=.TRUE., CELL_CENTERED=.TRUE./
&SLCF PBY=0.06, QUANTITY='VOLUME FRACTION', SPEC_ID='OXYGEN'/

&TAIL/
```

A2. SMV Rendering of 100mm Closed Edge Preliminary design

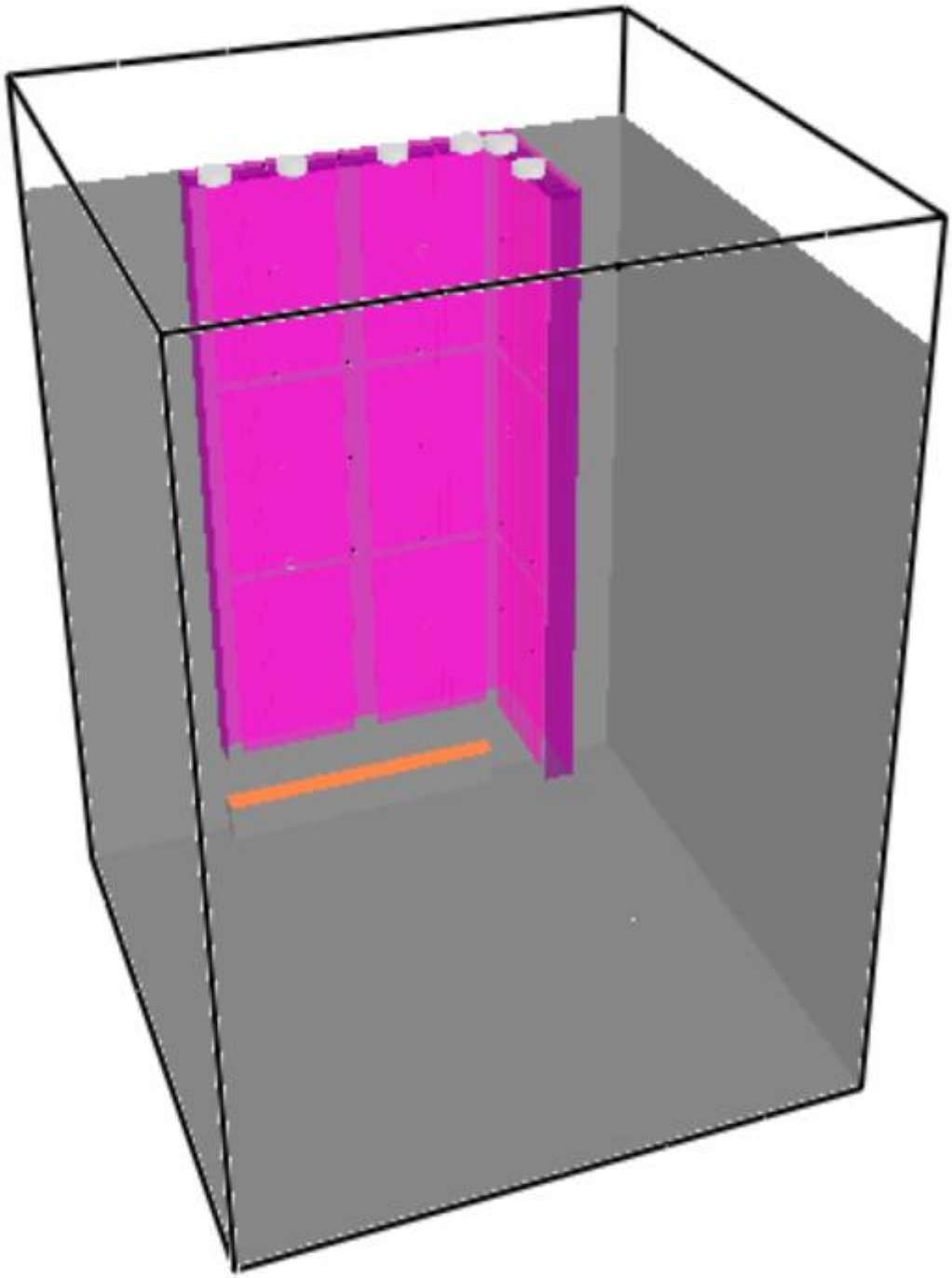

A3. FDS input file for 50mm Cavity Closed Edge, Model Iteration ‘r’

```
&HEAD CHID='r50c2'/
&MESH ID='mesh1', IJK=40,30,320, XB=0.4,0.8,0,0.3,0,3.2/
&MESH ID='mesh2', IJK=40,30,320, XB=0.8,1.2,0,0.3,0,3.2/
&MESH ID='mesh3', IJK=40,30,320, XB=1.2,1.6,0,0.3,0,3.2/
&MESH ID='mesh4', IJK=40,30,320, XB=1.6,2.0,0,0.3,0,3.2/
&MESH ID='mesh5', IJK=40,30,320, XB=1.6,2.0,0.3,0.6,0,3.2/
&MESH ID='mesh6', IJK=40,30,320, XB=1.6,2.0,0.6,0.9,0,3.2/
&MESH ID='mesh7', IJK=4,24,32, XB=0,0.4,0,2.4,0,3.2/
&MESH ID='mesh8', IJK=4,24,32, XB=2.0,2.4,0,2.4,0,3.2/
&MESH ID='mesh9', IJK=12,6,32, XB=0.4,1.6,0.3,0.9,0,3.2/
&MESH ID='mesh10', IJK=16,15,32, XB=0.4,2.0,0.9,2.4,0,3.2/
&TIME T_END=120/
&MISC SURF_DEFAULT='CALCIUM_SILICATE', TMPA=20/
&DUMP NFRAMES=1000/
&SURF ID='CALCIUM_SILICATE',
MATL_ID='STONE',
THICKNESS=0.02,
DEFAULT=.TRUE.
RGB=128,128,128/
&MATL ID='STONE',
CONDUCTIVITY=0.17
SPECIFIC_HEAT=0.96
DENSITY=870/

&REAC FUEL='PROPANE',
FYI='propane',
C=3,
H=8,
SOOT_YIELD=0.01,
CO_YIELD=0.02,
HEAT_OF_COMBUSTION=46460/

&SURF ID='GAS_BURNING', HRRPUA=833.33/
&OBST XB=0.6,1.8,0.0,0.1,0,0.15/
&VENT XB=0.6,1.8,0.0,0.1,0.15,0.15, SURF_ID='GAS_BURNING', RGB=249,129,70/

Facade Testing Panels
&OBST XB=0.6,1.81,0.0,0.01,0.4,2.8, RGB=252,15,192, TRANSPARENCY=0.6/
&OBST XB=1.8,1.81,0.01,0.61,0.4,2.8, RGB=252,15,192, TRANSPARENCY=0.6/
&OBST XB=0.6,1.15,0.06,0.07,0.4,1.19, RGB=252,15,192, TRANSPARENCY=0.6/
&OBST XB=0.6,1.15,0.06,0.07,1.21,2.00, RGB=252,15,192, TRANSPARENCY=0.6/
&OBST XB=0.6,1.15,0.06,0.07,2.02,2.8, RGB=252,15,192, TRANSPARENCY=0.6/
&OBST XB=1.17,1.72,0.06,0.07,0.4,1.19, RGB=252,15,192, TRANSPARENCY=0.6/
&OBST XB=1.17,1.72,0.06,0.07,1.21,2.00, RGB=252,15,192, TRANSPARENCY=0.6/
&OBST XB=1.17,1.72,0.06,0.07,2.02,2.8, RGB=252,15,192, TRANSPARENCY=0.6/
&OBST XB=1.74,1.75,0.09,0.61,0.4,1.19, RGB=252,15,192, TRANSPARENCY=0.6
&OBST XB=1.74,1.75,0.09,0.61,1.21,2.00, RGB=252,15,192, TRANSPARENCY=0.6/
&OBST XB=1.74,1.75,0.09,0.61,2.02,2.8, RGB=252,15,192, TRANSPARENCY=0.6/

U Type Flashing
&OBST XB=1.11,1.21,0.055,0.06,0.41,1.18, RGB=128,0,128, TRANSPARENCY=0.6/ Central head
&OBST XB=1.11,1.21,0.055,0.06,1.22,1.99, RGB=128,0,128, TRANSPARENCY=0.6/ Central head
&OBST XB=1.11,1.21,0.055,0.06,2.03,2.79, RGB=128,0,128, TRANSPARENCY=0.6/ Central head
&OBST XB=1.11,1.115,0.01,0.055,0.41,1.18, RGB=128,0,128, TRANSPARENCY=0.6/ Body 1
&OBST XB=1.11,1.115,0.01,0.055,1.22,1.99, RGB=128,0,128, TRANSPARENCY=0.6/ Body 1
&OBST XB=1.11,1.115,0.01,0.055,2.03,2.79, RGB=128,0,128, TRANSPARENCY=0.6/ Body 1
&OBST XB=1.205,1.21,0.01,0.055,0.41,1.18, RGB=128,0,128, TRANSPARENCY=0.6/ Body 2
&OBST XB=1.205,1.21,0.01,0.055,1.22,1.99, RGB=128,0,128, TRANSPARENCY=0.6/ Body 2
&OBST XB=1.205,1.21,0.01,0.055,2.03,2.79, RGB=128,0,128, TRANSPARENCY=0.6/ Body 2

Z Type Flashing
&OBST XB=0.655,0.66,0.01,0.06,0.41,0.51, RGB=128,0,128, TRANSPARENCY=0.6/ Left Profile
&OBST XB=0.655,0.66,0.01,0.06,0.745,0.845, RGB=128,0,128, TRANSPARENCY=0.6/ Left Profile
&OBST XB=0.655,0.66,0.01,0.06,1.08,1.18, RGB=128,0,128, TRANSPARENCY=0.6/ Left Profile
&OBST XB=0.655,0.66,0.01,0.06,1.22,1.32, RGB=128,0,128, TRANSPARENCY=0.6/ Left Profile
```

```
&OBST XB=0.655,0.66,0.01,0.06,1.555,1.655, RGB=128,0,128, TRANSPARENCY=0.6/ Left Profile
&OBST XB=0.655,0.66,0.01,0.06,1.89,1.99, RGB=128,0,128, TRANSPARENCY=0.6/ Left Profile
&OBST XB=0.655,0.66,0.01,0.06,2.03,2.13, RGB=128,0,128, TRANSPARENCY=0.6/ Left Profile
&OBST XB=0.655,0.66,0.01,0.06,2.36,2.46, RGB=128,0,128, TRANSPARENCY=0.6/ Left Profile
&OBST XB=0.655,0.66,0.01,0.06,2.69,2.79, RGB=128,0,128, TRANSPARENCY=0.6/ Left Profile
&OBST XB=1.66,1.665,0.01,0.06,0.41,0.51, RGB=128,0,128, TRANSPARENCY=0.6/ Right Profile
&OBST XB=1.66,1.665,0.01,0.06,0.745,0.845, RGB=128,0,128, TRANSPARENCY=0.6/ Right Profile
&OBST XB=1.66,1.665,0.01,0.06,1.08,1.18, RGB=128,0,128, TRANSPARENCY=0.6/ Right Profile
&OBST XB=1.66,1.665,0.01,0.06,1.22,1.32, RGB=128,0,128, TRANSPARENCY=0.6/ Right Profile
&OBST XB=1.66,1.665,0.01,0.06,1.555,1.655, RGB=128,0,128, TRANSPARENCY=0.6/ Right Profile
&OBST XB=1.66,1.665,0.01,0.06,1.89,1.99, RGB=128,0,128, TRANSPARENCY=0.6/ Right Profile
&OBST XB=1.66,1.665,0.01,0.06,2.03,2.13, RGB=128,0,128, TRANSPARENCY=0.6/ Right Profile
&OBST XB=1.66,1.665,0.01,0.06,2.36,2.46, RGB=128,0,128, TRANSPARENCY=0.6/ Right Profile
&OBST XB=1.66,1.665,0.01,0.06,2.69,2.79, RGB=128,0,128, TRANSPARENCY=0.6/ Right Profile
&OBST XB=1.75,1.80,0.145,0.15,0.41,0.51, RGB=128,0,128, TRANSPARENCY=0.6/ Wing Left Profile
&OBST XB=1.75,1.80,0.145,0.15,0.745,0.845, RGB=128,0,128, TRANSPARENCY=0.6/ Wing Left Profile
&OBST XB=1.75,1.80,0.145,0.15,1.08,1.18, RGB=128,0,128, TRANSPARENCY=0.6/ Wing Left Profile
&OBST XB=1.75,1.80,0.145,0.15,1.22,1.32, RGB=128,0,128, TRANSPARENCY=0.6/ Wing Left Profile
&OBST XB=1.75,1.80,0.145,0.15,1.555,1.655, RGB=128,0,128, TRANSPARENCY=0.6/ Wing Left Profile
&OBST XB=1.75,1.80,0.145,0.15,1.89,1.99, RGB=128,0,128, TRANSPARENCY=0.6/ Wing Left Profile
&OBST XB=1.75,1.80,0.145,0.15,2.03,2.13, RGB=128,0,128, TRANSPARENCY=0.6/ Wing Left Profile
&OBST XB=1.75,1.80,0.145,0.15,2.36,2.46, RGB=128,0,128, TRANSPARENCY=0.6/ Wing Left Profile
&OBST XB=1.75,1.80,0.145,0.15,2.69,2.79, RGB=128,0,128, TRANSPARENCY=0.6/ Wing Left Profile
&OBST XB=1.75,1.80,0.55,0.555,0.41,0.51, RGB=128,0,128, TRANSPARENCY=0.6/ Wing Right Profile
&OBST XB=1.75,1.80,0.55,0.555,0.745,0.845, RGB=128,0,128, TRANSPARENCY=0.6/ Wing Right Profile
&OBST XB=1.75,1.80,0.55,0.555,1.08,1.18, RGB=128,0,128, TRANSPARENCY=0.6/ Wing Right Profile
&OBST XB=1.75,1.80,0.55,0.555,1.22,1.32, RGB=128,0,128, TRANSPARENCY=0.6/ Wing Right Profile
&OBST XB=1.75,1.80,0.55,0.555,1.555,1.655, RGB=128,0,128, TRANSPARENCY=0.6/ Wing Right Profile
&OBST XB=1.75,1.80,0.55,0.555,1.89,1.99, RGB=128,0,128, TRANSPARENCY=0.6/ Wing Right Profile
&OBST XB=1.75,1.80,0.55,0.555,2.03,2.13, RGB=128,0,128, TRANSPARENCY=0.6/ Wing Right Profile
&OBST XB=1.75,1.80,0.55,0.555,2.36,2.46, RGB=128,0,128, TRANSPARENCY=0.6/ Wing Right Profile
&OBST XB=1.75,1.80,0.55,0.555,2.69,2.79, RGB=128,0,128, TRANSPARENCY=0.6/ Wing Right Profile

Side Obstructions
&OBST XB=0.59,0.6,0.0,0.07,0.4,2.8, RGB=128,0,128, TRANSPARENCY=0.6/
&OBST XB=1.74,1.81,0.61,0.62,0.4,2.8, RGB=128,0,128, TRANSPARENCY=0.6/

Ventilation Openings
&VENT XB=0,2.4,2.4,2.4,0,3.2, SURF_ID='OPEN'/
&VENT XB=0,2.4,0,0,2.8,3.2, SURF_ID='OPEN'/
&VENT XB=0,2.4,0,2.4,3.2,3.2, SURF_ID='OPEN'/
&VENT XB=0,0,0,2.4,2.8,3.2, SURF_ID='OPEN'/
&VENT XB=2.4,2.4,0,2.4,2.8,3.2, SURF_ID='OPEN'/

&PROP ID='Thermal Detection', QUANTITY='THERMOCOUPLE'/
&DEVC ID='V1H1', PROP_ID='Thermal Detection', XYZ=0.9,0.035,0.8/
&DEVC ID='V1H2', PROP_ID='Thermal Detection', XYZ=1.16,0.035,0.8/
&DEVC ID='V1H3', PROP_ID='Thermal Detection', XYZ=1.5,0.035,0.8/
&DEVC ID='V1H4', PROP_ID='Thermal Detection', XYZ=1.775,0.035,0.8/
&DEVC ID='V1H5', PROP_ID='Thermal Detection', XYZ=1.775,0.31,0.8/
&DEVC ID='V2H1', PROP_ID='Thermal Detection', XYZ=0.9,0.035,1.2/
&DEVC ID='V2H2', PROP_ID='Thermal Detection', XYZ=1.16,0.035,1.2/
&DEVC ID='V2H3', PROP_ID='Thermal Detection', XYZ=1.5,0.035,1.2/
&DEVC ID='V2H4', PROP_ID='Thermal Detection', XYZ=1.775,0.035,1.2/
&DEVC ID='V2H5', PROP_ID='Thermal Detection', XYZ=1.775,0.31,1.2/
&DEVC ID='V3H1', PROP_ID='Thermal Detection', XYZ=0.9,0.035,1.6/
&DEVC ID='V3H2', PROP_ID='Thermal Detection', XYZ=1.16,0.035,1.6/
&DEVC ID='V3H3', PROP_ID='Thermal Detection', XYZ=1.5,0.035,1.6/
&DEVC ID='V3H4', PROP_ID='Thermal Detection', XYZ=1.775,0.035,1.6/
&DEVC ID='V3H5', PROP_ID='Thermal Detection', XYZ=1.775,0.31,1.6/
&DEVC ID='V4H1', PROP_ID='Thermal Detection', XYZ=0.9,0.035,2/
&DEVC ID='V4H2', PROP_ID='Thermal Detection', XYZ=1.16,0.035,2/
&DEVC ID='V4H3', PROP_ID='Thermal Detection', XYZ=1.5,0.035,2/
&DEVC ID='V4H4', PROP_ID='Thermal Detection', XYZ=1.775,0.035,2/
&DEVC ID='V4H5', PROP_ID='Thermal Detection', XYZ=1.775,0.31,2/
&DEVC ID='V5H1', PROP_ID='Thermal Detection', XYZ=0.9,0.035,2.4/
&DEVC ID='V5H2', PROP_ID='Thermal Detection', XYZ=1.16,0.035,2.4/
```

```
&DEVC ID='V5H3', PROP_ID='Thermal Detection', XYZ=1.5,0.035,2.4/
&DEVC ID='V5H4', PROP_ID='Thermal Detection', XYZ=1.775,0.035,2.4/
&DEVC ID='V5H5', PROP_ID='Thermal Detection', XYZ=1.775,0.31,2.4/
&DEVC ID='V6H1', PROP_ID='Thermal Detection', XYZ=0.9,0.035,2.8/
&DEVC ID='V6H2', PROP_ID='Thermal Detection', XYZ=1.16,0.035,2.8/
&DEVC ID='V6H3', PROP_ID='Thermal Detection', XYZ=1.5,0.035,2.8/
&DEVC ID='V6H4', PROP_ID='Thermal Detection', XYZ=1.775,0.035,2.8/
&DEVC ID='V6H5', PROP_ID='Thermal Detection', XYZ=1.775,0.31,2.8/
&DEVC ID='hf', QUANTITY='RADIATIVE HEAT FLUX GAS', XYZ=1.2,0.01,2.9, ORIENTATION=0,1,0/

&SLCF PBX=1.775, QUANTITY='TEMPERATURE', VECTOR=.TRUE./
&SLCF PBX=1.775, QUANTITY='VELOCITY', VECTOR=.TRUE., CELL_CENTERED=.TRUE./
&SLCF PBX=1.775, QUANTITY='VOLUME FRACTION', SPEC_ID='OXYGEN'/
&SLCF PBY=0.035, QUANTITY='TEMPERATURE', VECTOR=.TRUE./ oxygen
&SLCF PBY=0.035, QUANTITY='VELOCITY', VECTOR=.TRUE., CELL_CENTERED=.TRUE./
&SLCF PBY=0.035, QUANTITY='VOLUME FRACTION', SPEC_ID='OXYGEN'/

&TAIL/
```

A4. Simplified Perforated Sheet FDS input file, Model Iteration ‘iso’

```
&HEAD CHID='iso025pre2'/
&MESH ID='mesh1', IJK=40,30,320, XB=0.4,0.8,0,0.3,0,3.2/
&MESH ID='mesh2', IJK=40,30,320, XB=0.8,1.2,0,0.3,0,3.2/
&MESH ID='mesh3', IJK=40,30,320, XB=1.2,1.6,0,0.3,0,3.2/
&MESH ID='mesh4', IJK=40,30,320, XB=1.6,2.0,0,0.3,0,3.2/
&MESH ID='mesh5', IJK=40,30,320, XB=1.6,2.0,0.3,0.6,0,3.2/
&MESH ID='mesh6', IJK=40,30,320, XB=1.6,2.0,0.6,0.9,0,3.2/
&MESH ID='mesh7', IJK=4,24,32, XB=0,0.4,0,2.4,0,3.2/
&MESH ID='mesh8', IJK=4,24,32, XB=2.0,2.4,0,2.4,0,3.2/
&MESH ID='mesh9', IJK=12,6,32, XB=0.4,1.6,0.3,0.9,0,3.2/
&MESH ID='mesh10', IJK=16,15,32, XB=0.4,2.0,0.9,2.4,0,3.2/
&TIME T_END=60/
&MISC SURF_DEFAULT='CALCIUM_SILICATE', TMPA=20/
&DUMP NFRAMES=1000/
&SURF ID='CALCIUM_SILICATE',
MATL_ID='STONE',
THICKNESS=0.02,
DEFAULT=.TRUE.
RGB=128,128,128/
&MATL ID='STONE',
CONDUCTIVITY=0.17
SPECIFIC_HEAT=0.96
DENSITY=870/

&REAC FUEL='PROPANE',
FYI='propane',
C=3,
H=8,
SOOT_YIELD=0.01,
CO_YIELD=0.02,
HEAT_OF_COMBUSTION=46460/

&SURF ID='GAS_BURNING', HRRPUA=833.33/
&OBST XB=0.6,1.8,0.0,0.1,0,0.15/
&VENT XB=0.6,1.8,0.0,0.1,0.15,0.15, SURF_ID='GAS_BURNING', RGB=249,129,70/

Facade Testing Panels
&OBST XB=0.6,1.845,0.0,0.01,0.4,2.8, RGB=252,15,192, TRANSPARENCY=0.6/
&OBST XB=1.835,1.845,0.01,0.645,0.4,2.8, RGB=252,15,192, TRANSPARENCY=0.6/
&OBST XB=0.66,1.16,0.035,0.045,0.42,1.18, RGB=252,15,192, TRANSPARENCY=0.6/
&OBST XB=0.66,1.16,0.035,0.045,1.22,1.98, RGB=252,15,192, TRANSPARENCY=0.6/
&OBST XB=0.66,1.16,0.035,0.045,2.02,2.78, RGB=252,15,192, TRANSPARENCY=0.6/
&OBST XB=1.26,1.76,0.035,0.045,0.42,1.18, RGB=252,15,192, TRANSPARENCY=0.6/
&OBST XB=1.26,1.76,0.035,0.045,1.22,1.98, RGB=252,15,192, TRANSPARENCY=0.6/
&OBST XB=1.26,1.76,0.035,0.045,2.02,2.78, RGB=252,15,192, TRANSPARENCY=0.6/
&OBST XB=1.8,1.81,0.095,0.595,0.42,1.18, RGB=252,15,192, TRANSPARENCY=0.6/
&OBST XB=1.8,1.81,0.095,0.595,1.22,1.98, RGB=252,15,192, TRANSPARENCY=0.6/
&OBST XB=1.8,1.81,0.095,0.595,2.02,2.78, RGB=252,15,192, TRANSPARENCY=0.6/

Side Obstructions
&OBST XB=0.59,0.6,0.0,0.015,0.4,0.6, RGB=128,0,128, TRANSPARENCY=0.6/
&OBST XB=0.59,0.6,0.03,0.045,0.4,0.6, RGB=128,0,128, TRANSPARENCY=0.6/
&OBST XB=0.59,0.6,0.015,0.03,0.6,0.8, RGB=128,0,128, TRANSPARENCY=0.6/
&OBST XB=0.59,0.6,0.0,0.015,0.8,1.0, RGB=128,0,128, TRANSPARENCY=0.6/
&OBST XB=0.59,0.6,0.03,0.045,0.8,1.0, RGB=128,0,128, TRANSPARENCY=0.6/
&OBST XB=0.59,0.6,0.015,0.03,1.0,1.2, RGB=128,0,128, TRANSPARENCY=0.6/
&OBST XB=0.59,0.6,0.0,0.015,1.2,1.4, RGB=128,0,128, TRANSPARENCY=0.6/
&OBST XB=0.59,0.6,0.03,0.045,1.2,1.4, RGB=128,0,128, TRANSPARENCY=0.6/
&OBST XB=0.59,0.6,0.015,0.03,1.4,1.6, RGB=128,0,128, TRANSPARENCY=0.6/
&OBST XB=0.59,0.6,0.0,0.015,1.6,1.8, RGB=128,0,128, TRANSPARENCY=0.6/
&OBST XB=0.59,0.6,0.03,0.045,1.6,1.8, RGB=128,0,128, TRANSPARENCY=0.6/
&OBST XB=0.59,0.6,0.015,0.03,1.8,2.0, RGB=128,0,128, TRANSPARENCY=0.6/
&OBST XB=0.59,0.6,0.0,0.015,2.0,2.2, RGB=128,0,128, TRANSPARENCY=0.6/
&OBST XB=0.59,0.6,0.03,0.045,2.0,2.2, RGB=128,0,128, TRANSPARENCY=0.6/
&OBST XB=0.59,0.6,0.015,0.03,2.2,2.4, RGB=128,0,128, TRANSPARENCY=0.6/
```

```
&OBST XB=0.59,0.6,0.0,0.015,2.4,2.6, RGB=128,0,128, TRANSPARENCY=0.6/
&OBST XB=0.59,0.6,0.03,0.045,2.4,2.6, RGB=128,0,128, TRANSPARENCY=0.6/
&OBST XB=0.59,0.6,0.015,0.03,2.6,2.8, RGB=128,0,128, TRANSPARENCY=0.6/

&OBST XB=1.8,1.815,0.645,0.655,0.4,0.6, RGB=128,0,128, TRANSPARENCY=0.6/
&OBST XB=1.83,1.845,0.645,0.655,0.4,0.6, RGB=128,0,128, TRANSPARENCY=0.6/
&OBST XB=1.815,1.83,0.645,0.655,0.6,0.8, RGB=128,0,128, TRANSPARENCY=0.6/
&OBST XB=1.8,1.815,0.645,0.655,0.8,1.0, RGB=128,0,128, TRANSPARENCY=0.6/
&OBST XB=1.83,1.845,0.645,0.655,0.8,1.0, RGB=128,0,128, TRANSPARENCY=0.6/
&OBST XB=1.815,1.83,0.645,0.655,1.0,1.2, RGB=128,0,128, TRANSPARENCY=0.6/
&OBST XB=1.8,1.815,0.645,0.655,1.2,1.4, RGB=128,0,128, TRANSPARENCY=0.6/
&OBST XB=1.83,1.845,0.645,0.655,1.2,1.4, RGB=128,0,128, TRANSPARENCY=0.6/
&OBST XB=1.815,1.83,0.645,0.655,1.4,1.6, RGB=128,0,128, TRANSPARENCY=0.6/
&OBST XB=1.8,1.815,0.645,0.655,1.6,1.8, RGB=128,0,128, TRANSPARENCY=0.6/
&OBST XB=1.83,1.845,0.645,0.655,1.6,1.8, RGB=128,0,128, TRANSPARENCY=0.6/
&OBST XB=1.815,1.83,0.645,0.655,1.8,2.0, RGB=128,0,128, TRANSPARENCY=0.6/
&OBST XB=1.8,1.815,0.645,0.655,2.0,2.2, RGB=128,0,128, TRANSPARENCY=0.6/
&OBST XB=1.83,1.845,0.645,0.655,2.0,2.2, RGB=128,0,128, TRANSPARENCY=0.6/
&OBST XB=1.815,1.83,0.645,0.655,2.2,2.4, RGB=128,0,128, TRANSPARENCY=0.6/
&OBST XB=1.8,1.815,0.645,0.655,2.4,2.6, RGB=128,0,128, TRANSPARENCY=0.6/
&OBST XB=1.83,1.845,0.645,0.655,2.4,2.6, RGB=128,0,128, TRANSPARENCY=0.6/
&OBST XB=1.815,1.83,0.645,0.655,2.6,2.8, RGB=128,0,128, TRANSPARENCY=0.6/

Top Obstructions
&OBST XB=0.6,0.8,0.01,0.035,2.77,2.78, RGB=128,0,128, TRANSPARENCY=0.6, DEVC_ID='thermal1'/
&OBST XB=0.8,1.2,0.01,0.035,2.77,2.78, RGB=128,0,128, TRANSPARENCY=0.6, DEVC_ID='thermal2'/
&OBST XB=1.2,1.6,0.01,0.035,2.77,2.78, RGB=128,0,128, TRANSPARENCY=0.6, DEVC_ID='thermal3'/
&OBST XB=1.6,1.835,0.01,0.035,2.77,2.78, RGB=128,0,128, TRANSPARENCY=0.6, DEVC_ID='thermal4'/
&OBST XB=1.81,1.835,0.035,0.3,2.77,2.78, RGB=128,0,128, TRANSPARENCY=0.6, DEVC_ID='thermal5'/
&OBST XB=1.81,1.835,0.3,0.645,2.77,2.78, RGB=128,0,128, TRANSPARENCY=0.6, DEVC_ID='thermal6'/

Ventilation Openings
&VENT XB=0,2.4,2.4,2.4,0,3.2, SURF_ID='OPEN'/
&VENT XB=0,2.4,0,0,2.8,3.2, SURF_ID='OPEN'/
&VENT XB=0,2.4,0,2.4,3.2,3.2, SURF_ID='OPEN'/
&VENT XB=0,0,0,2.4,2.8,3.2, SURF_ID='OPEN'/
&VENT XB=2.4,2.4,0,2.4,2.8,3.2, SURF_ID='OPEN'/

&PROP ID='Thermal Detection', QUANTITY='THERMOCOUPLE'/
&DEVC ID='V1H1', PROP_ID='Thermal Detection', XYZ=0.9,0.0225,0.8/
&DEVC ID='V1H2', PROP_ID='Thermal Detection', XYZ=1.2,0.0225,0.8/
&DEVC ID='V1H3', PROP_ID='Thermal Detection', XYZ=1.5,0.0225,0.8/
&DEVC ID='V1H4', PROP_ID='Thermal Detection', XYZ=1.8225,0.0225,0.8/
&DEVC ID='V1H5', PROP_ID='Thermal Detection', XYZ=1.8225,0.345,0.8/
&DEVC ID='V2H1', PROP_ID='Thermal Detection', XYZ=0.9,0.0225,1.2/
&DEVC ID='V2H2', PROP_ID='Thermal Detection', XYZ=1.2,0.0225,1.2/
&DEVC ID='V2H3', PROP_ID='Thermal Detection', XYZ=1.5,0.0225,1.2/
&DEVC ID='V2H4', PROP_ID='Thermal Detection', XYZ=1.8225,0.0225,1.2/
&DEVC ID='V2H5', PROP_ID='Thermal Detection', XYZ=1.8225,0.345,1.2/
&DEVC ID='V3H1', PROP_ID='Thermal Detection', XYZ=0.9,0.0225,1.6/
&DEVC ID='V3H2', PROP_ID='Thermal Detection', XYZ=1.2,0.0225,1.6/
&DEVC ID='V3H3', PROP_ID='Thermal Detection', XYZ=1.5,0.0225,1.6/
&DEVC ID='V3H4', PROP_ID='Thermal Detection', XYZ=1.8225,0.0225,1.6/
&DEVC ID='V3H5', PROP_ID='Thermal Detection', XYZ=1.8225,0.345,1.6/
&DEVC ID='V4H1', PROP_ID='Thermal Detection', XYZ=0.9,0.0225,2/
&DEVC ID='V4H2', PROP_ID='Thermal Detection', XYZ=1.2,0.0225,2/
&DEVC ID='V4H3', PROP_ID='Thermal Detection', XYZ=1.5,0.0225,2/
&DEVC ID='V4H4', PROP_ID='Thermal Detection', XYZ=1.8225,0.0225,2/
&DEVC ID='V4H5', PROP_ID='Thermal Detection', XYZ=1.8225,0.345,2/
&DEVC ID='V5H1', PROP_ID='Thermal Detection', XYZ=0.9,0.0225,2.4/
&DEVC ID='V5H2', PROP_ID='Thermal Detection', XYZ=1.2,0.0225,2.4/
&DEVC ID='V5H3', PROP_ID='Thermal Detection', XYZ=1.5,0.0225,2.4/
&DEVC ID='V5H4', PROP_ID='Thermal Detection', XYZ=1.8225,0.0225,2.4/
&DEVC ID='V5H5', PROP_ID='Thermal Detection', XYZ=1.8225,0.345,2.4/
&DEVC ID='V6H1', PROP_ID='Thermal Detection', XYZ=0.9,0.0225,2.8/
&DEVC ID='V6H2', PROP_ID='Thermal Detection', XYZ=1.2,0.0225,2.8/
&DEVC ID='V6H3', PROP_ID='Thermal Detection', XYZ=1.5,0.0225,2.8/
```

```
&DEVC ID='V6H4', PROP_ID='Thermal Detection', XYZ=1.8225,0.0225,2.8/
&DEVC ID='V6H5', PROP_ID='Thermal Detection', XYZ=1.8225,0.345,2.8/
&PROP ID='Thermal Activation', QUANTITY='LINK TEMPERATURE', RTI=132.,
ACTIVATION_TEMPERATURE=180./
&DEVC ID='thermal1', PROP_ID='Thermal Activation', XYZ=0.7,0.0225,2.77/
&DEVC ID='thermal2', PROP_ID='Thermal Activation', XYZ=1.0,0.0225,2.77/
&DEVC ID='thermal3', PROP_ID='Thermal Activation', XYZ=1.4,0.0225,2.77/
&DEVC ID='thermal4', PROP_ID='Thermal Activation', XYZ=1.7,0.0225,2.77/
&DEVC ID='thermal5', PROP_ID='Thermal Activation', XYZ=1.8225,0.15,2.77/
&DEVC ID='thermal6', PROP_ID='Thermal Activation', XYZ=1.8225,0.45,2.77/

&SLCF PBX=1.8225, QUANTITY='TEMPERATURE', VECTOR=.TRUE./
&SLCF PBX=1.8225, QUANTITY='VELOCITY', VECTOR=.TRUE., CELL_CENTERED=.TRUE./
&SLCF PBX=1.8225, QUANTITY='VOLUME FRACTION', SPEC_ID='OXYGEN'/
&SLCF PBY=0.0225, QUANTITY='TEMPERATURE', VECTOR=.TRUE./ oxygen
&SLCF PBY=0.0225, QUANTITY='VELOCITY', VECTOR=.TRUE., CELL_CENTERED=.TRUE./
&SLCF PBY=0.0225, QUANTITY='VOLUME FRACTION', SPEC_ID='OXYGEN'/

&TAIL/
```

A5. a) Error Analysis plot for thermal detectors in Vertical Elevations V4 between the 6-mesh, 10mm and 20mm cell length cases

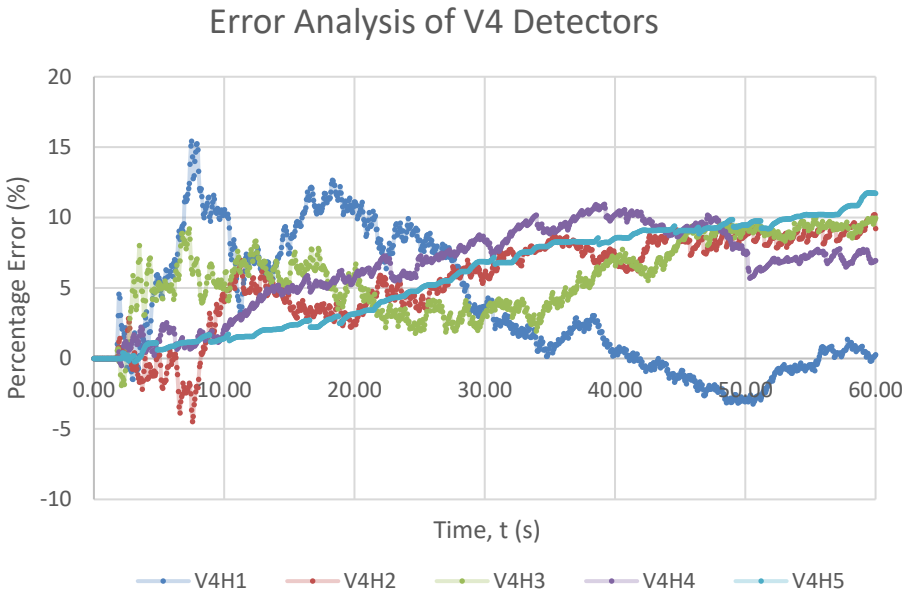

A5. b) Error Analysis plot for thermal detectors in Vertical Elevation V5 between the 6-mesh, 10mm and 20mm cell length cases

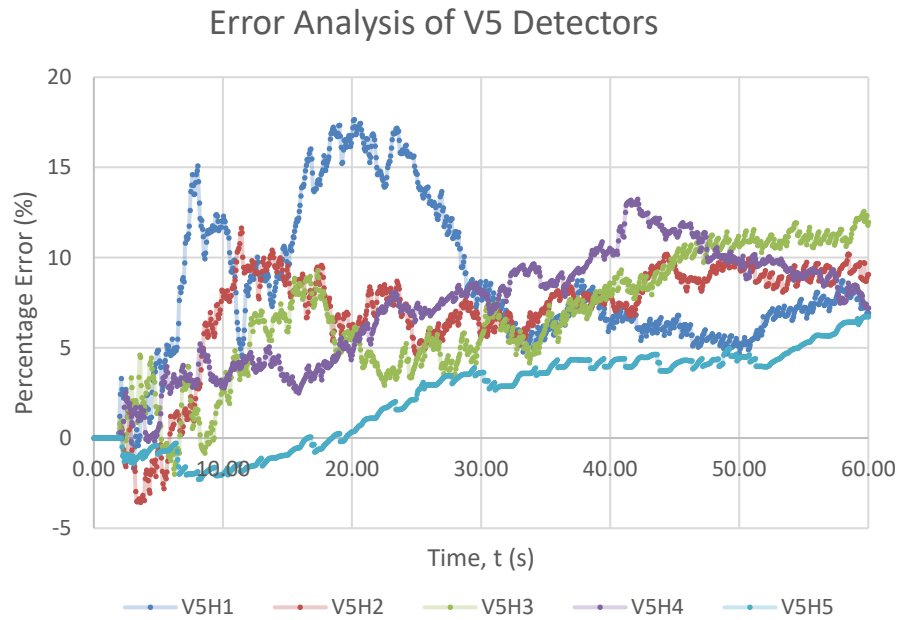

A6. 10-mesh 10mm cell size FDS input file, Model Iteration ‘open75’

```
&HEAD CHID='iso_13785-1_open75_10'/
&MESH ID='mesh1', IJK=40,30,320, XB=0.4,0.8,0,0.3,0,3.2/
&MESH ID='mesh2', IJK=40,30,320, XB=0.8,1.2,0,0.3,0,3.2/
&MESH ID='mesh3', IJK=40,30,320, XB=1.2,1.6,0,0.3,0,3.2/
&MESH ID='mesh4', IJK=40,30,320, XB=1.6,2.0,0,0.3,0,3.2/
&MESH ID='mesh5', IJK=40,30,320, XB=1.6,2.0,0.3,0.6,0,3.2/
&MESH ID='mesh6', IJK=40,30,320, XB=1.6,2.0,0.6,0.9,0,3.2/
&MESH ID='mesh7', IJK=4,24,32, XB=0,0.4,0,2.4,0,3.2/
&MESH ID='mesh8', IJK=4,24,32, XB=2.0,2.4,0,2.4,0,3.2/
&MESH ID='mesh9', IJK=12,6,32, XB=0.4,1.6,0.3,0.9,0,3.2/
&MESH ID='mesh10', IJK=16,15,32, XB=0.4,2.0,0.9,2.4,0,3.2/

&TIME T_END=60/
&MISC SURF_DEFAULT='CALCIUM_SILICATE', TMPA=20/
&DUMP NFRAMES=1000/
&SURF ID='CALCIUM_SILICATE',
MATL_ID='STONE',
THICKNESS=0.02,
DEFAULT=.TRUE.
RGB=128,128,128/
&MATL ID='STONE',
CONDUCTIVITY=0.01
SPECIFIC_HEAT=0.96
DENSITY=450/

&REAC FUEL='PROPANE',
FYI='propane',
C=3,
H=8,
SOOT_YIELD=0.01,
CO_YIELD=0.02,
HEAT_OF_COMBUSTION=46460/

&SURF ID='GAS_BURNING', HRRPUA=833.33/
&OBST XB=0.6,1.8,0.0975,0.1975,0,0.15/
&VENT XB=0.6,1.8,0.0975,0.1975,0.15,0.15, SURF_ID='GAS_BURNING', RGB=249,129,70/

Facade Testing Panels
&OBST XB=0.6,1.895,0.1,0.11,0.4,2.8, RGB=252,15,192, TRANSPARENCY=0.6/
&OBST XB=1.885,1.895,0.11,0.795,0.4,2.8, RGB=252,15,192, TRANSPARENCY=0.6/
&OBST XB=0.66,1.16,0.185,0.195,0.42,1.18, RGB=252,15,192, TRANSPARENCY=0.6/
&OBST XB=0.66,1.16,0.185,0.195,1.22,1.98, RGB=252,15,192, TRANSPARENCY=0.6/
&OBST XB=0.66,1.16,0.185,0.195,2.02,2.78, RGB=252,15,192, TRANSPARENCY=0.6/
&OBST XB=1.26,1.76,0.185,0.195,0.42,1.18, RGB=252,15,192, TRANSPARENCY=0.6/
&OBST XB=1.26,1.76,0.185,0.195,1.22,1.98, RGB=252,15,192, TRANSPARENCY=0.6/
&OBST XB=1.26,1.76,0.185,0.195,2.02,2.78, RGB=252,15,192, TRANSPARENCY=0.6/
&OBST XB=1.8,1.81,0.245,0.745,0.42,1.18, RGB=252,15,192, TRANSPARENCY=0.6/
&OBST XB=1.8,1.81,0.245,0.745,1.22,1.98, RGB=252,15,192, TRANSPARENCY=0.6/
&OBST XB=1.8,1.81,0.245,0.745,2.02,2.78, RGB=252,15,192, TRANSPARENCY=0.6/

Additional Obstruction
&OBST XB=0.59,1.895,0,0.1,0.4,2.8, RGB=240,255,255, TRANSPARENCY=0.6/

Ventilation Openings
&VENT XB=0,2.4,2.4,2.4,0,3.2, SURF_ID='OPEN'/
&VENT XB=0,2.4,0,0,2.8,3.2, SURF_ID='OPEN'/
&VENT XB=0,2.4,0,2.4,3.2,3.2, SURF_ID='OPEN'/
&VENT XB=0,0,0,2.4,2.8,3.2, SURF_ID='OPEN'/
&VENT XB=2.4,2.4,0,2.4,2.8,3.2, SURF_ID='OPEN'/

&PROP ID='Thermal Detection', QUANTITY='LINK TEMPERATURE',  RTI=132.0,
ACTIVATION_TEMPERATURE=74.0/
&DEVC ID='V1H1', PROP_ID='Thermal Detection', XYZ=0.9,0.1475,0.8/
&DEVC ID='V1H2', PROP_ID='Thermal Detection', XYZ=1.2,0.1475,0.8/
&DEVC ID='V1H3', PROP_ID='Thermal Detection', XYZ=1.5,0.1475,0.8/
```

```
&DEVC ID='V1H4', PROP_ID='Thermal Detection', XYZ=1.8475,0.1475,0.8/
&DEVC ID='V1H5', PROP_ID='Thermal Detection', XYZ=1.8475,0.495,0.8/
&DEVC ID='V2H1', PROP_ID='Thermal Detection', XYZ=0.9,0.1475,1.2/
&DEVC ID='V2H2', PROP_ID='Thermal Detection', XYZ=1.2,0.1475,1.2/
&DEVC ID='V2H3', PROP_ID='Thermal Detection', XYZ=1.5,0.1475,1.2/
&DEVC ID='V2H4', PROP_ID='Thermal Detection', XYZ=1.8475,0.1475,1.2/
&DEVC ID='V2H5', PROP_ID='Thermal Detection', XYZ=1.8475,0.495,1.2/
&DEVC ID='V3H1', PROP_ID='Thermal Detection', XYZ=0.9,0.1475,1.6/
&DEVC ID='V3H2', PROP_ID='Thermal Detection', XYZ=1.2,0.1475,1.6/
&DEVC ID='V3H3', PROP_ID='Thermal Detection', XYZ=1.5,0.1475,1.6/
&DEVC ID='V3H4', PROP_ID='Thermal Detection', XYZ=1.8475,0.1475,1.6/
&DEVC ID='V3H5', PROP_ID='Thermal Detection', XYZ=1.8475,0.495,1.6/
&DEVC ID='V4H1', PROP_ID='Thermal Detection', XYZ=0.9,0.1475,2/
&DEVC ID='V4H2', PROP_ID='Thermal Detection', XYZ=1.2,0.1475,2/
&DEVC ID='V4H3', PROP_ID='Thermal Detection', XYZ=1.5,0.1475,2/
&DEVC ID='V4H4', PROP_ID='Thermal Detection', XYZ=1.8475,0.1475,2/
&DEVC ID='V4H5', PROP_ID='Thermal Detection', XYZ=1.8475,0.495,2/
&DEVC ID='V4H1', PROP_ID='Thermal Detection', XYZ=0.9,0.1475,2.4/
&DEVC ID='V4H2', PROP_ID='Thermal Detection', XYZ=1.2,0.1475,2.4/
&DEVC ID='V4H3', PROP_ID='Thermal Detection', XYZ=1.5,0.1475,2.4/
&DEVC ID='V4H4', PROP_ID='Thermal Detection', XYZ=1.8475,0.1475,2.4/
&DEVC ID='V4H5', PROP_ID='Thermal Detection', XYZ=1.8475,0.495,2.4/


&SLCF PBX=1.8475, QUANTITY='TEMPERATURE', VECTOR=.TRUE./
&SLCF PBX=1.8475, QUANTITY='VELOCITY', VECTOR=.TRUE., CELL_CENTERED=.TRUE./
&SLCF PBX=1.8475, QUANTITY='VOLUME FRACTION', SPEC_ID='OXYGEN'/
&SLCF PBY=0.1475, QUANTITY='TEMPERATURE', VECTOR=.TRUE./
&SLCF PBY=0.1475, QUANTITY='VELOCITY', VECTOR=.TRUE., CELL_CENTERED=.TRUE./
&SLCF PBY=0.1475, QUANTITY='VOLUME FRACTION', SPEC_ID='OXYGEN'/

&TAIL/
```

A7. a) SMV velocity slice files depicting cavity barrier influence on the chimney effect for the 50mm Open Sample, screen-capture recorded at 10s (top) and 30s (bottom)

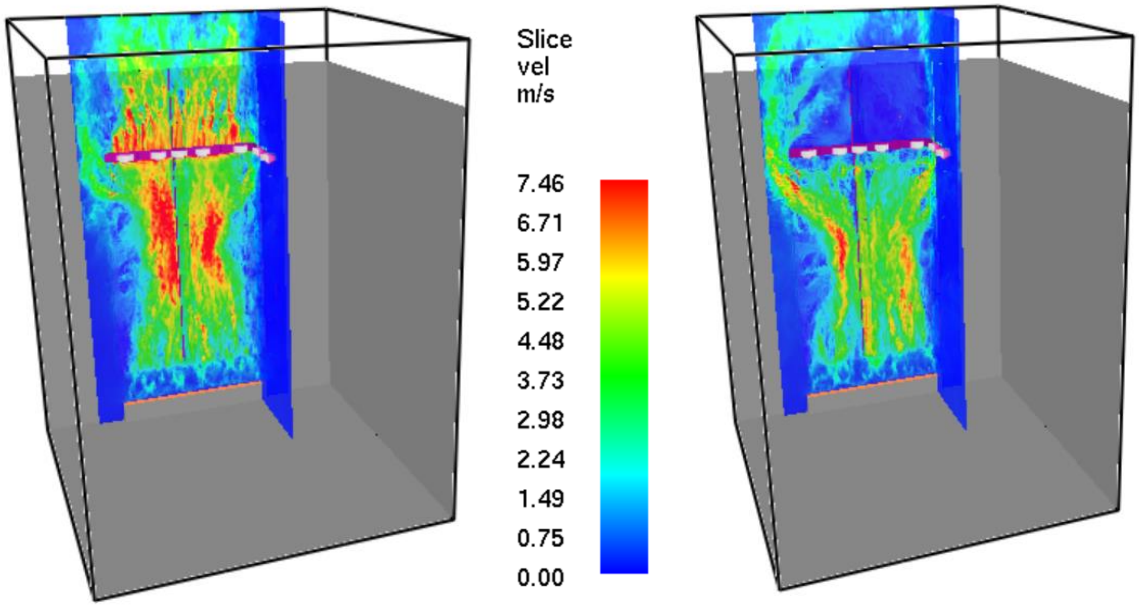

A7. b) SMV velocity slice files depicting cavity barrier influence on the chimney effect for the 25mm Closed Sample, screen-capture recorded at 10s (top) and 45s (bottom)

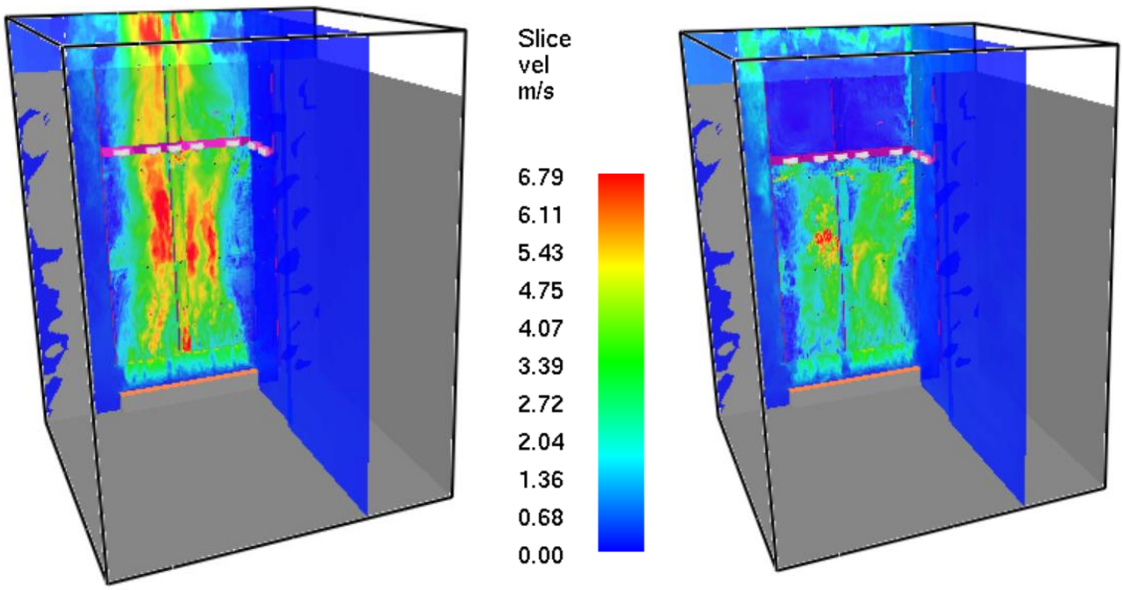

A7. c) SMV velocity slice files depicting cavity barrier influence on the chimney effect for the 25mm Open Sample, screen-capture recorded at 10s (top) and 45s (bottom)

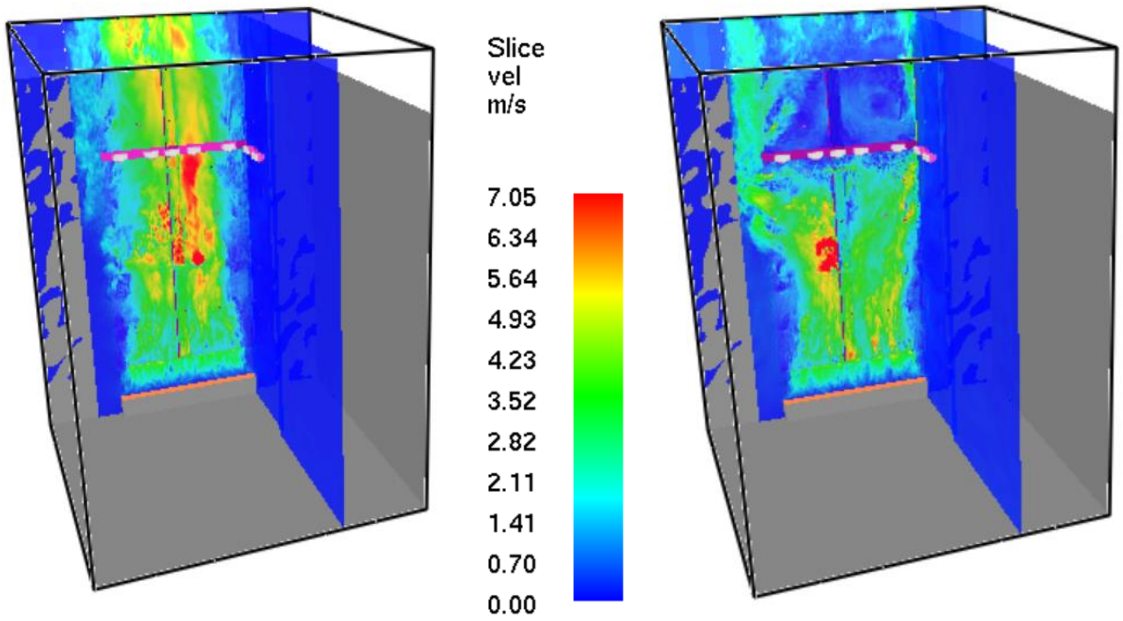

A7. d) SMV velocity slice files depicting cavity barrier influence on the chimney effect for the 100mm Closed Sample, screen-capture recorded at 10s (top) and 55s (bottom)

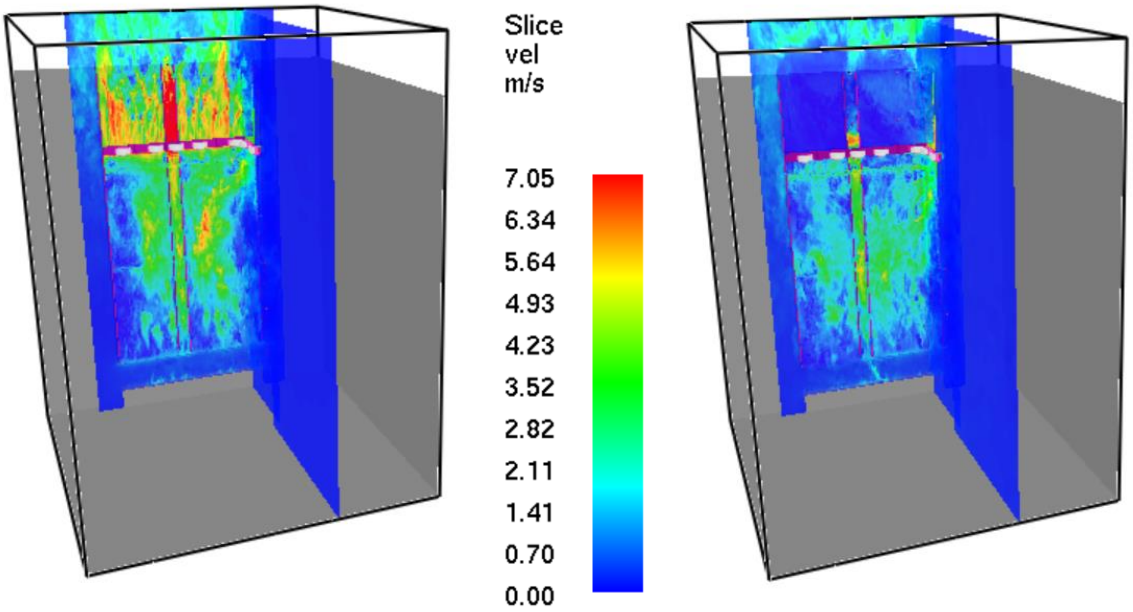

A7. e) SMV velocity slice files depicting cavity barrier influence on the chimney effect for the 100mm Open Sample, screen-capture recorded at 10s (top) and 55s (bottom)

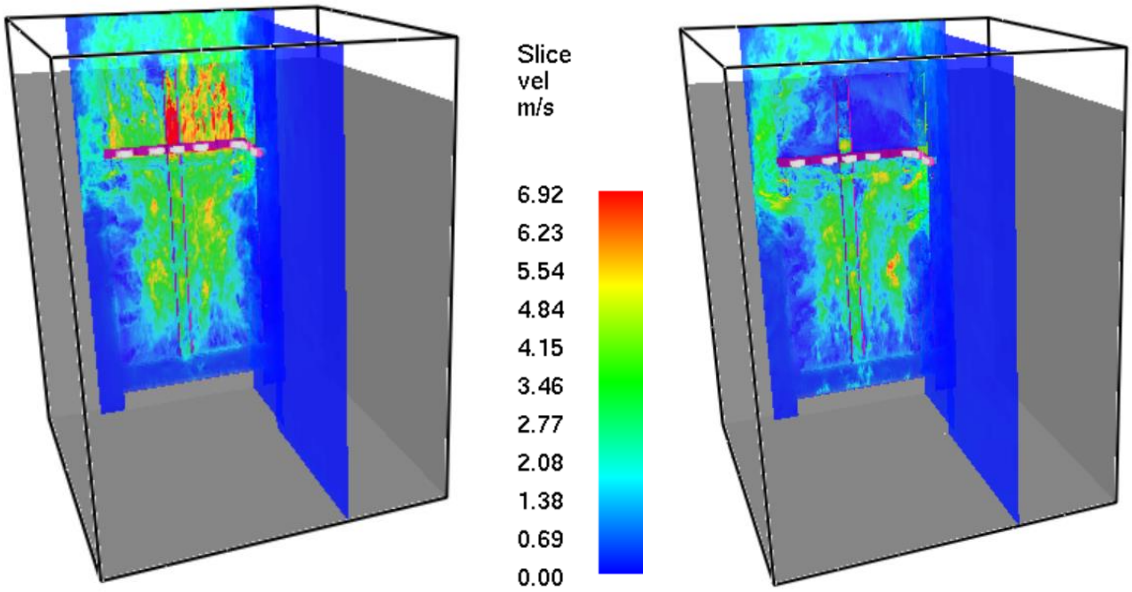

A8. a) V5H3 Thermocouple validation plot for 50mm samples

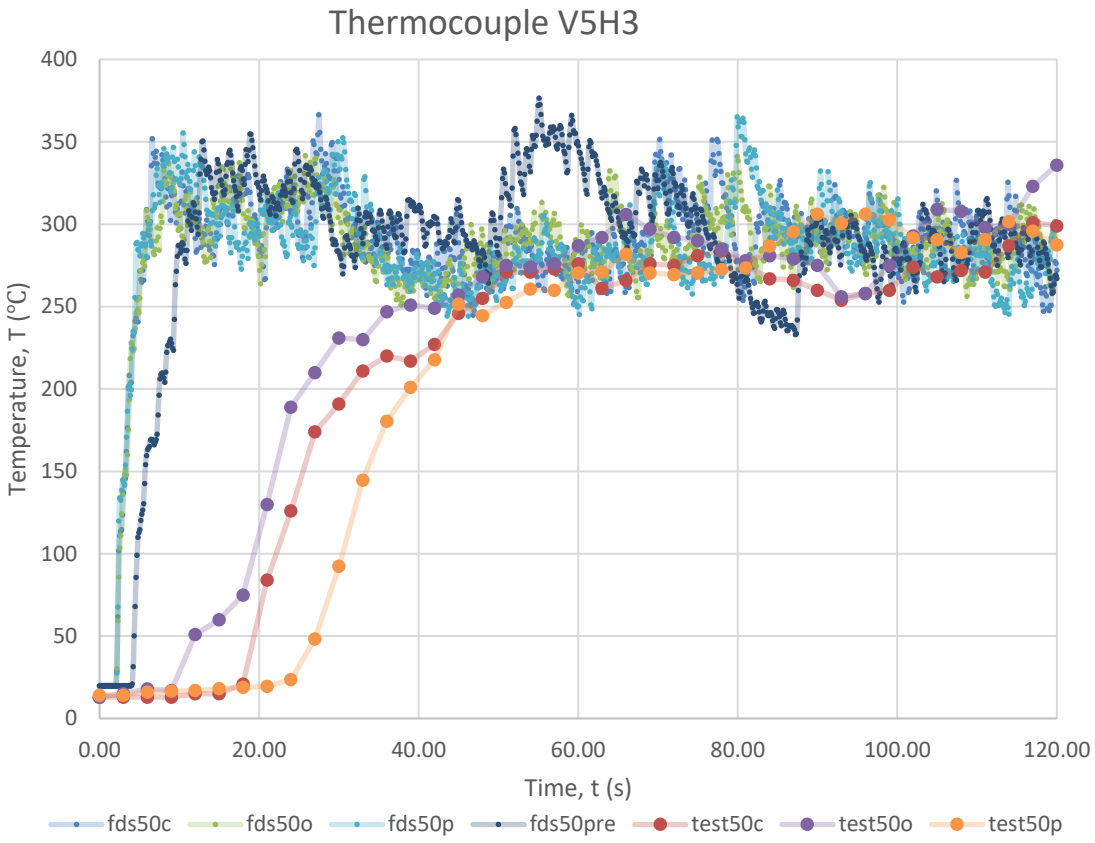

A8. b) V5H3 Thermocouple full experimental data set for 50mm samples

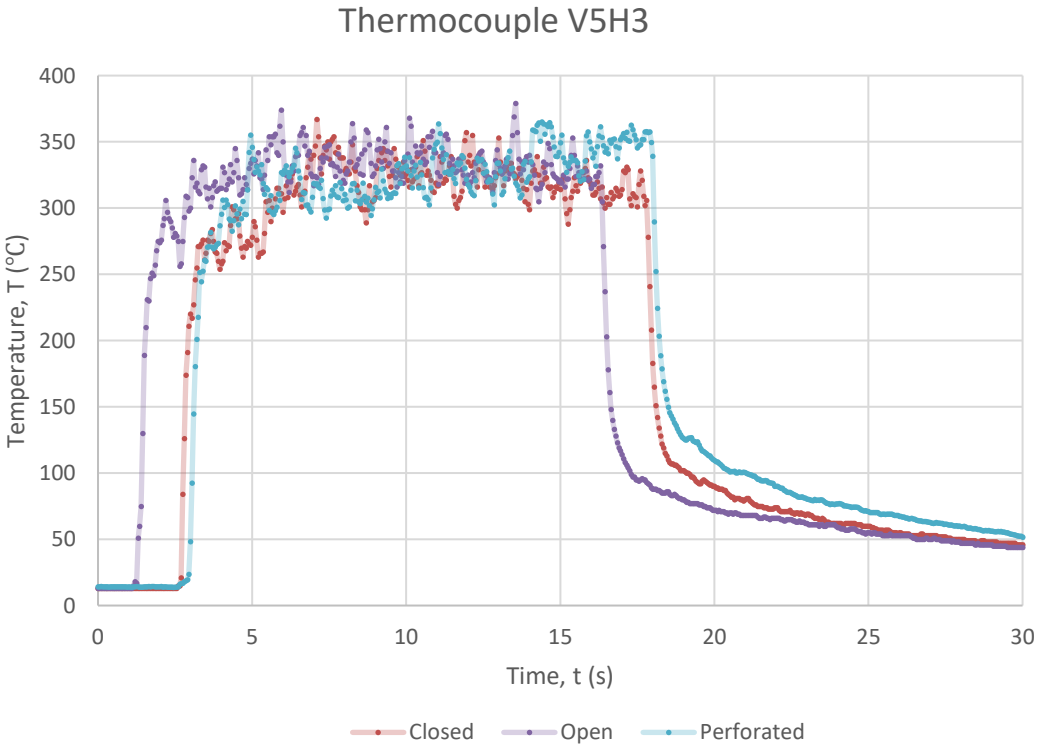

A9. SMV Temperature output for flame height of 100mm open cavity

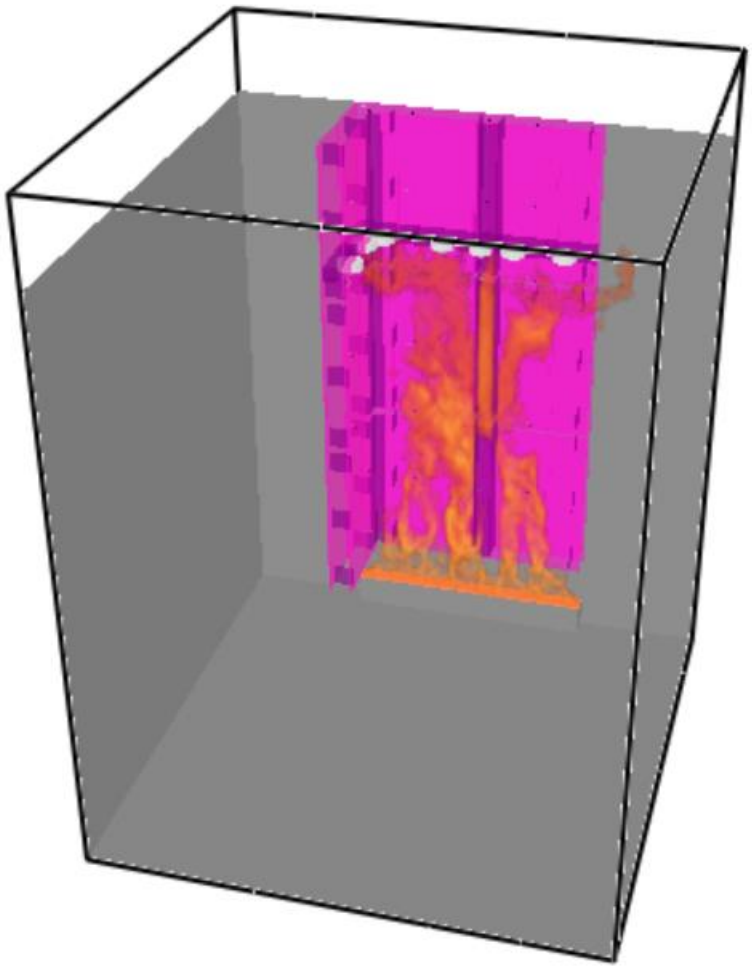

A10. SMV Temperature output files for comparison of flame heights of the 25 (top), 50 (middle) & 100mm (bottom) closed cavities

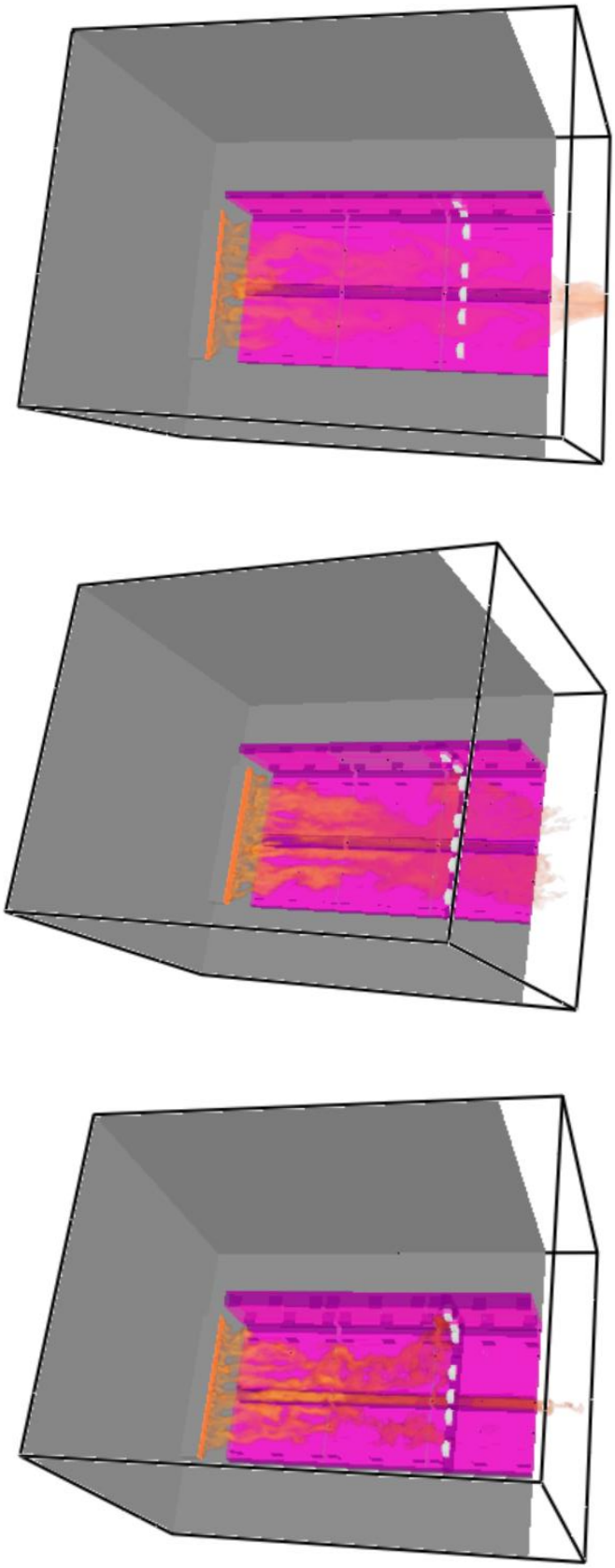

A11. a) Live Fire Test Open Cavity Set-up

A11. b) Live Fire Test Closed Cavity Set-up

A11. c) Live Fire Test Perforated Cavity Lateral Obstruction

A11. d) Live Fire Test Open Cavity

A11. e) Live Fire Test Closed Cavity under Fire

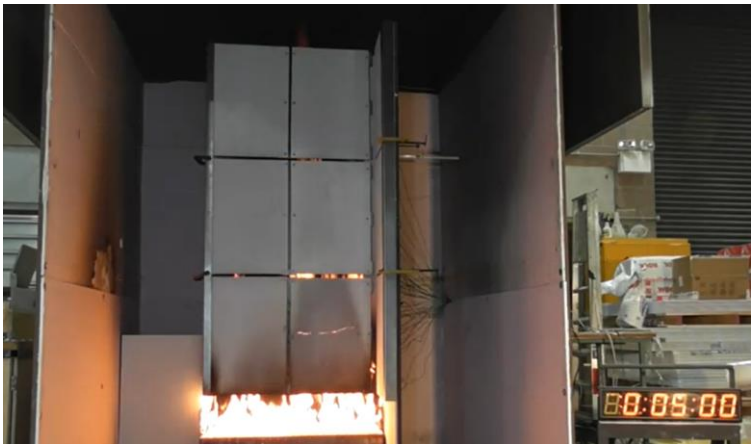

A11. f) Live Fire Test Perforated Cavity Obstruction under Fire

A12. Open vent. 25mm Cavity Width with cavity barrier, Model Iteration ‘a’

```
&HEAD CHID='a25o'/
&MESH ID='mesh1', IJK=40,30,320, XB=0.4,0.8,0,0.3,0,3.2/
&MESH ID='mesh2', IJK=40,30,320, XB=0.8,1.2,0,0.3,0,3.2/
&MESH ID='mesh3', IJK=40,30,320, XB=1.2,1.6,0,0.3,0,3.2/
&MESH ID='mesh4', IJK=40,30,320, XB=1.6,2.0,0,0.3,0,3.2/
&MESH ID='mesh5', IJK=40,30,320, XB=1.6,2.0,0.3,0.6,0,3.2/
&MESH ID='mesh6', IJK=40,30,320, XB=1.6,2.0,0.6,0.9,0,3.2/
&MESH ID='mesh7', IJK=4,24,32, XB=0,0.4,0,2.4,0,3.2/
&MESH ID='mesh8', IJK=4,24,32, XB=2.0,2.4,0,2.4,0,3.2/
&MESH ID='mesh9', IJK=12,6,32, XB=0.4,1.6,0.3,0.9,0,3.2/
&MESH ID='mesh10', IJK=16,15,32, XB=0.4,2.0,0.9,2.4,0,3.2/
&TIME T_END=60/
&MISC SURF_DEFAULT='CALCIUM_SILICATE', TMPA=20/
&DUMP NFRAMES=1000/
&SURF ID='CALCIUM_SILICATE',
MATL_ID='STONE',
THICKNESS=0.02,
DEFAULT=.TRUE.
RGB=128,128,128/
&MATL ID='STONE',
CONDUCTIVITY=0.17
SPECIFIC_HEAT=0.96
DENSITY=870/

&REAC FUEL='PROPANE',
FYI='propane',
C=3,
H=8,
SOOT_YIELD=0.01,
CO_YIELD=0.02,
HEAT_OF_COMBUSTION=46460/

&SURF ID='GAS_BURNING', HRRPUA=833.33/
&OBST XB=0.6,1.8,0.0,0.1,0,0.15/
&VENT XB=0.6,1.8,0.0,0.1,0.15,0.15, SURF_ID='GAS_BURNING', RGB=249,129,70/

Facade Testing Panels
&OBST XB=0.6,1.81,0.0,0.01,0.4,2.8, RGB=252,15,192, TRANSPARENCY=0.6/
&OBST XB=1.8,1.81,0.01,0.61,0.4,2.8, RGB=252,15,192, TRANSPARENCY=0.6/
&OBST XB=0.6,1.16,0.035,0.045,0.4,1.19, RGB=252,15,192, TRANSPARENCY=0.6/
&OBST XB=0.6,1.16,0.035,0.045,1.21,2.00, RGB=252,15,192, TRANSPARENCY=0.6/
&OBST XB=0.6,1.16,0.035,0.045,2.02,2.8, RGB=252,15,192, TRANSPARENCY=0.6/
&OBST XB=1.18,1.74,0.035,0.045,0.4,1.19, RGB=252,15,192, TRANSPARENCY=0.6/
&OBST XB=1.18,1.74,0.035,0.045,1.21,2.00, RGB=252,15,192, TRANSPARENCY=0.6/
&OBST XB=1.18,1.74,0.035,0.045,2.02,2.8, RGB=252,15,192, TRANSPARENCY=0.6/
&OBST XB=1.765,1.775,0.06,0.61,0.4,1.19, RGB=252,15,192, TRANSPARENCY=0.6/
&OBST XB=1.765,1.775,0.06,0.61,1.21,2.00, RGB=252,15,192, TRANSPARENCY=0.6/
&OBST XB=1.765,1.775,0.06,0.61,2.02,2.8, RGB=252,15,192, TRANSPARENCY=0.6/

U Type Flashing
&OBST XB=1.12,1.22,0.03,0.035,0.41,1.18, RGB=128,0,128, TRANSPARENCY=0.6/ Central head
&OBST XB=1.12,1.22,0.03,0.035,1.22,1.99, RGB=128,0,128, TRANSPARENCY=0.6/ Central head
&OBST XB=1.12,1.22,0.03,0.035,2.03,2.79, RGB=128,0,128, TRANSPARENCY=0.6/ Central head
&OBST XB=1.12,1.125,0.01,0.03,0.41,1.18, RGB=128,0,128, TRANSPARENCY=0.6/ Body 1
&OBST XB=1.12,1.125,0.01,0.03,1.22,1.99, RGB=128,0,128, TRANSPARENCY=0.6/ Body 1
&OBST XB=1.12,1.125,0.01,0.03,2.03,2.79, RGB=128,0,128, TRANSPARENCY=0.6/ Body 1
&OBST XB=1.215,1.22,0.01,0.03,0.41,1.18, RGB=128,0,128, TRANSPARENCY=0.6/ Body 2
&OBST XB=1.215,1.22,0.01,0.03,1.22,1.99, RGB=128,0,128, TRANSPARENCY=0.6/ Body 2
&OBST XB=1.215,1.22,0.01,0.03,2.03,2.79, RGB=128,0,128, TRANSPARENCY=0.6/ Body 2

Z Type Flashing
&OBST XB=0.655,0.66,0.01,0.035,0.41,0.51, RGB=128,0,128, TRANSPARENCY=0.6/ Left Profile
&OBST XB=0.655,0.66,0.01,0.035,0.745,0.845, RGB=128,0,128, TRANSPARENCY=0.6/ Left Profile
&OBST XB=0.655,0.66,0.01,0.035,1.08,1.18, RGB=128,0,128, TRANSPARENCY=0.6/ Left Profile
&OBST XB=0.655,0.66,0.01,0.035,1.22,1.32, RGB=128,0,128, TRANSPARENCY=0.6/ Left Profile
```

```
&OBST XB=0.655,0.66,0.01,0.035,1.555,1.655, RGB=128,0,128, TRANSPARENCY=0.6/ Left Profile
&OBST XB=0.655,0.66,0.01,0.035,1.89,1.99, RGB=128,0,128, TRANSPARENCY=0.6/ Left Profile
&OBST XB=0.655,0.66,0.01,0.035,2.03,2.13, RGB=128,0,128, TRANSPARENCY=0.6/ Left Profile
&OBST XB=0.655,0.66,0.01,0.035,2.36,2.46, RGB=128,0,128, TRANSPARENCY=0.6/ Left Profile
&OBST XB=0.655,0.66,0.01,0.035,2.69,2.79, RGB=128,0,128, TRANSPARENCY=0.6/ Left Profile
&OBST XB=1.68,1.685,0.01,0.035,0.41,0.51, RGB=128,0,128, TRANSPARENCY=0.6/ Right Profile
&OBST XB=1.68,1.685,0.01,0.035,0.745,0.845, RGB=128,0,128, TRANSPARENCY=0.6/ Right Profile
&OBST XB=1.68,1.685,0.01,0.035,1.08,1.18, RGB=128,0,128, TRANSPARENCY=0.6/ Right Profile
&OBST XB=1.68,1.685,0.01,0.035,1.22,1.32, RGB=128,0,128, TRANSPARENCY=0.6/ Right Profile
&OBST XB=1.68,1.685,0.01,0.035,1.555,1.655, RGB=128,0,128, TRANSPARENCY=0.6/ Right Profile
&OBST XB=1.68,1.685,0.01,0.035,1.89,1.99, RGB=128,0,128, TRANSPARENCY=0.6/ Right Profile
&OBST XB=1.68,1.685,0.01,0.035,2.03,2.13, RGB=128,0,128, TRANSPARENCY=0.6/ Right Profile
&OBST XB=1.68,1.685,0.01,0.035,2.36,2.46, RGB=128,0,128, TRANSPARENCY=0.6/ Right Profile
&OBST XB=1.68,1.685,0.01,0.035,2.69,2.79, RGB=128,0,128, TRANSPARENCY=0.6/ Right Profile
&OBST XB=1.775,1.80,0.115,0.12,0.41,0.51, RGB=128,0,128, TRANSPARENCY=0.6/ Wing Left Profile
&OBST XB=1.775,1.80,0.115,0.12,0.745,0.845, RGB=128,0,128, TRANSPARENCY=0.6/ Wing Left Profile
&OBST XB=1.775,1.80,0.115,0.12,1.08,1.18, RGB=128,0,128, TRANSPARENCY=0.6/ Wing Left Profile
&OBST XB=1.775,1.80,0.115,0.12,1.22,1.32, RGB=128,0,128, TRANSPARENCY=0.6/ Wing Left Profile
&OBST XB=1.775,1.80,0.115,0.12,1.555,1.655, RGB=128,0,128, TRANSPARENCY=0.6/ Wing Left Profile
&OBST XB=1.775,1.80,0.115,0.12,1.89,1.99, RGB=128,0,128, TRANSPARENCY=0.6/ Wing Left Profile
&OBST XB=1.775,1.80,0.115,0.12,2.03,2.13, RGB=128,0,128, TRANSPARENCY=0.6/ Wing Left Profile
&OBST XB=1.775,1.80,0.115,0.12,2.36,2.46, RGB=128,0,128, TRANSPARENCY=0.6/ Wing Left Profile
&OBST XB=1.775,1.80,0.115,0.12,2.69,2.79, RGB=128,0,128, TRANSPARENCY=0.6/ Wing Left Profile
&OBST XB=1.775,1.80,0.55,0.555,0.41,0.51, RGB=128,0,128, TRANSPARENCY=0.6/ Wing Right Profile
&OBST XB=1.775,1.80,0.55,0.555,0.745,0.845, RGB=128,0,128, TRANSPARENCY=0.6/ Wing Right Profile
&OBST XB=1.775,1.80,0.55,0.555,1.08,1.18, RGB=128,0,128, TRANSPARENCY=0.6/ Wing Right Profile
&OBST XB=1.775,1.80,0.55,0.555,1.22,1.32, RGB=128,0,128, TRANSPARENCY=0.6/ Wing Right Profile
&OBST XB=1.775,1.80,0.55,0.555,1.555,1.655, RGB=128,0,128, TRANSPARENCY=0.6/ Wing Right Profile
&OBST XB=1.775,1.80,0.55,0.555,1.89,1.99, RGB=128,0,128, TRANSPARENCY=0.6/ Wing Right Profile
&OBST XB=1.775,1.80,0.55,0.555,2.03,2.13, RGB=128,0,128, TRANSPARENCY=0.6/ Wing Right Profile
&OBST XB=1.775,1.80,0.55,0.555,2.36,2.46, RGB=128,0,128, TRANSPARENCY=0.6/ Wing Right Profile
&OBST XB=1.775,1.80,0.55,0.555,2.69,2.79, RGB=128,0,128, TRANSPARENCY=0.6/ Wing Right Profile

Corner Seal
&OBST XB=1.72,1.775,0.03,0.035,0.41,1.18, RGB=128,0,128, TRANSPARENCY=0.6/ Corner L rail
&OBST XB=1.72,1.775,0.03,0.035,1.22,1.99, RGB=128,0,128, TRANSPARENCY=0.6/ Corner L rail
&OBST XB=1.72,1.775,0.03,0.035,2.03,2.79, RGB=128,0,128, TRANSPARENCY=0.6/ Corner L rail
&OBST XB=1.77,1.775,0.035,0.09,0.41,1.18, RGB=128,0,128, TRANSPARENCY=0.6/ W T rail head
&OBST XB=1.77,1.775,0.035,0.09,1.22,1.99, RGB=128,0,128, TRANSPARENCY=0.6/ W T rail head
&OBST XB=1.77,1.775,0.035,0.09,2.03,2.79, RGB=128,0,128, TRANSPARENCY=0.6/ W T rail head

Cavity Barrier
&OBST XB=0.6,0.85,0.01,0.035,2.13,2.20, RGB=128,0,128, TRANSPARENCY=0.6, DEVC_ID='thermal1'/
&OBST XB=0.85,1.12,0.01,0.035,2.13,2.20, RGB=128,0,128, TRANSPARENCY=0.6, DEVC_ID='thermal2'/
&OBST XB=1.125,1.215,0.01,0.03,2.13,2.20, RGB=128,0,128, TRANSPARENCY=0.6, DEVC_ID='thermal3'/
&OBST XB=1.22,1.5,0.01,0.035,2.13,2.20, RGB=128,0,128, TRANSPARENCY=0.6, DEVC_ID='thermal4'/
&OBST XB=1.5,1.8,0.01,0.035,2.13,2.20, RGB=128,0,128, TRANSPARENCY=0.6, DEVC_ID='thermal5'/
&OBST XB=1.775,1.8,0.035,0.35,2.13,2.20, RGB=128,0,128, TRANSPARENCY=0.6, DEVC_ID='thermal6'/
&OBST XB=1.775,1.8,0.35,0.61,2.13,2.20, RGB=128,0,128, TRANSPARENCY=0.6, DEVC_ID='thermal7'/

Ventilation Openings
&VENT XB=0,2.4,2.4,2.4,0,3.2, SURF_ID='OPEN'/
&VENT XB=0,2.4,0,0,2.8,3.2, SURF_ID='OPEN'/
&VENT XB=0,2.4,0,2.4,3.2,3.2, SURF_ID='OPEN'/
&VENT XB=0,0,0,2.4,2.8,3.2, SURF_ID='OPEN'/
&VENT XB=2.4,2.4,0,2.4,2.8,3.2, SURF_ID='OPEN'/

&PROP ID='Thermal Detection', QUANTITY='THERMOCOUPLE'/
&DEVC ID='V1H1', PROP_ID='Thermal Detection', XYZ=0.9,0.0225,0.8/
&DEVC ID='V1H2', PROP_ID='Thermal Detection', XYZ=1.17,0.0225,0.8/
&DEVC ID='V1H3', PROP_ID='Thermal Detection', XYZ=1.5,0.0225,0.8/
&DEVC ID='V1H4', PROP_ID='Thermal Detection', XYZ=1.7875,0.0225,0.8/
&DEVC ID='V1H5', PROP_ID='Thermal Detection', XYZ=1.7875,0.31,0.8/
&DEVC ID='V2H1', PROP_ID='Thermal Detection', XYZ=0.9,0.0225,1.2/
&DEVC ID='V2H2', PROP_ID='Thermal Detection', XYZ=1.17,0.0225,1.2/
&DEVC ID='V2H3', PROP_ID='Thermal Detection', XYZ=1.5,0.0225,1.2/
&DEVC ID='V2H4', PROP_ID='Thermal Detection', XYZ=1.7875,0.0225,1.2/
```

```
&DEVC ID='V2H5', PROP_ID='Thermal Detection', XYZ=1.7875,0.31,1.2/
&DEVC ID='V3H1', PROP_ID='Thermal Detection', XYZ=0.9,0.0225,1.6/
&DEVC ID='V3H2', PROP_ID='Thermal Detection', XYZ=1.17,0.0225,1.6/
&DEVC ID='V3H3', PROP_ID='Thermal Detection', XYZ=1.5,0.0225,1.6/
&DEVC ID='V3H4', PROP_ID='Thermal Detection', XYZ=1.7875,0.0225,1.6/
&DEVC ID='V3H5', PROP_ID='Thermal Detection', XYZ=1.7875,0.31,1.6/
&DEVC ID='V4H1', PROP_ID='Thermal Detection', XYZ=0.9,0.0225,2/
&DEVC ID='V4H2', PROP_ID='Thermal Detection', XYZ=1.17,0.0225,2/
&DEVC ID='V4H3', PROP_ID='Thermal Detection', XYZ=1.5,0.0225,2/
&DEVC ID='V4H4', PROP_ID='Thermal Detection', XYZ=1.7875,0.0225,2/
&DEVC ID='V4H5', PROP_ID='Thermal Detection', XYZ=1.7875,0.31,2/
&DEVC ID='V5H1', PROP_ID='Thermal Detection', XYZ=0.9,0.0225,2.4/
&DEVC ID='V5H2', PROP_ID='Thermal Detection', XYZ=1.17,0.0225,2.4/
&DEVC ID='V5H3', PROP_ID='Thermal Detection', XYZ=1.5,0.0225,2.4/
&DEVC ID='V5H4', PROP_ID='Thermal Detection', XYZ=1.7875,0.0225,2.4/
&DEVC ID='V5H5', PROP_ID='Thermal Detection', XYZ=1.7875,0.31,2.4/
&DEVC ID='V6H1', PROP_ID='Thermal Detection', XYZ=0.9,0.0225,2.8/
&DEVC ID='V6H2', PROP_ID='Thermal Detection', XYZ=1.17,0.0225,2.8/
&DEVC ID='V6H3', PROP_ID='Thermal Detection', XYZ=1.5,0.0225,2.8/
&DEVC ID='V6H4', PROP_ID='Thermal Detection', XYZ=1.7875,0.0225,2.8/
&DEVC ID='V6H5', PROP_ID='Thermal Detection', XYZ=1.7875,0.31,2.8/
&PROP ID='Thermal Activation', QUANTITY='LINK TEMPERATURE', RTI=132.0,
ACTIVATION_TEMPERATURE=180.0/
&DEVC ID='thermal1', PROP_ID='Thermal Activation', XYZ=0.75,0.0225,2.13/
&DEVC ID='thermal2', PROP_ID='Thermal Activation', XYZ=1.00,0.0225,2.13/
&DEVC ID='thermal3', PROP_ID='Thermal Activation', XYZ=1.17,0.0225,2.13/
&DEVC ID='thermal4', PROP_ID='Thermal Activation', XYZ=1.35,0.0225,2.13/
&DEVC ID='thermal5', PROP_ID='Thermal Activation', XYZ=1.65,0.0225,2.13/
&DEVC ID='thermal6', PROP_ID='Thermal Activation', XYZ=1.7875,0.20,2.13/
&DEVC ID='thermal7', PROP_ID='Thermal Activation', XYZ=1.7875,0.45,2.13/

&SLCF PBX=1.7875, QUANTITY='TEMPERATURE', VECTOR=.TRUE./
&SLCF PBX=1.7875, QUANTITY='VELOCITY', VECTOR=.TRUE., CELL_CENTERED=.TRUE./
&SLCF PBX=1.7875, QUANTITY='VOLUME FRACTION', SPEC_ID='OXYGEN'/
&SLCF PBY=0.0225, QUANTITY='TEMPERATURE', VECTOR=.TRUE./ oxygen
&SLCF PBY=0.0225, QUANTITY='VELOCITY', VECTOR=.TRUE., CELL_CENTERED=.TRUE./
&SLCF PBY=0.0225, QUANTITY='VOLUME FRACTION', SPEC_ID='OXYGEN'/

&TAIL/
```

A13. Closed vent. 100mm Cavity Width with cavity barrier, Model Iteration ‘a’

```
&HEAD CHID='a100c'/
&MESH ID='mesh1', IJK=40,30,320, XB=0.4,0.8,0,0.3,0,3.2/
&MESH ID='mesh2', IJK=40,30,320, XB=0.8,1.2,0,0.3,0,3.2/
&MESH ID='mesh3', IJK=40,30,320, XB=1.2,1.6,0,0.3,0,3.2/
&MESH ID='mesh4', IJK=40,30,320, XB=1.6,2.0,0,0.3,0,3.2/
&MESH ID='mesh5', IJK=40,30,320, XB=1.6,2.0,0.3,0.6,0,3.2/
&MESH ID='mesh6', IJK=40,30,320, XB=1.6,2.0,0.6,0.9,0,3.2/
&MESH ID='mesh7', IJK=4,24,32, XB=0,0.4,0,2.4,0,3.2/
&MESH ID='mesh8', IJK=4,24,32, XB=2.0,2.4,0,2.4,0,3.2/
&MESH ID='mesh9', IJK=12,6,32, XB=0.4,1.6,0.3,0.9,0,3.2/
&MESH ID='mesh10', IJK=16,15,32, XB=0.4,2.0,0.9,2.4,0,3.2/
&TIME T_END=60/
&MISC SURF_DEFAULT='CALCIUM_SILICATE', TMPA=20/
&DUMP NFRAMES=1000/
&SURF ID='CALCIUM_SILICATE',
MATL_ID='STONE',
THICKNESS=0.02,
DEFAULT=.TRUE.
RGB=128,128,128/
&MATL ID='STONE',
CONDUCTIVITY=0.17
SPECIFIC_HEAT=0.96
DENSITY=870/

&REAC FUEL='PROPANE',
FYI='propane',
C=3,
H=8,
SOOT_YIELD=0.01,
CO_YIELD=0.02,
HEAT_OF_COMBUSTION=46460/

&SURF ID='GAS_BURNING', HRRPUA=833.33/
&OBST XB=0.6,1.8,0.0,0.1,0,0.15/
&VENT XB=0.6,1.8,0.0,0.1,0.15,0.15, SURF_ID='GAS_BURNING', RGB=249,129,70/

Facade Testing Panels
&OBST XB=0.6,1.81,0.0,0.01,0.4,2.8, RGB=252,15,192, TRANSPARENCY=0.6/
&OBST XB=1.8,1.81,0.01,0.61,0.4,2.8, RGB=252,15,192, TRANSPARENCY=0.6/
&OBST XB=0.6,1.125,0.11,0.12,0.4,1.19, RGB=252,15,192, TRANSPARENCY=0.6/
&OBST XB=0.6,1.125,0.11,0.12,1.21,2.00, RGB=252,15,192, TRANSPARENCY=0.6/
&OBST XB=0.6,1.125,0.11,0.12,2.02,2.8, RGB=252,15,192, TRANSPARENCY=0.6/
&OBST XB=1.145,1.67,0.11,0.12,0.4,1.19, RGB=252,15,192, TRANSPARENCY=0.6/
&OBST XB=1.145,1.67,0.11,0.12,1.21,2.00, RGB=252,15,192, TRANSPARENCY=0.6/
&OBST XB=1.145,1.67,0.11,0.12,2.02,2.8, RGB=252,15,192, TRANSPARENCY=0.6/
&OBST XB=1.69,1.7,0.14,0.61,0.4,1.19, RGB=252,15,192, TRANSPARENCY=0.6/
&OBST XB=1.69,1.7,0.14,0.61,1.21,2.00, RGB=252,15,192, TRANSPARENCY=0.6/
&OBST XB=1.69,1.7,0.14,0.61,2.02,2.8, RGB=252,15,192, TRANSPARENCY=0.6/

U Type Flashing
&OBST XB=1.085,1.185,0.105,0.11,0.41,1.18, RGB=128,0,128, TRANSPARENCY=0.6/ Central head
&OBST XB=1.085,1.185,0.105,0.11,1.22,1.99, RGB=128,0,128, TRANSPARENCY=0.6/ Central head
&OBST XB=1.085,1.185,0.105,0.11,2.03,2.79, RGB=128,0,128, TRANSPARENCY=0.6/ Central head
&OBST XB=1.085,1.09,0.01,0.105,0.41,1.18, RGB=128,0,128, TRANSPARENCY=0.6/ Body 1
&OBST XB=1.085,1.09,0.01,0.105,1.22,1.99, RGB=128,0,128, TRANSPARENCY=0.6/ Body 1
&OBST XB=1.085,1.09,0.01,0.105,2.03,2.79, RGB=128,0,128, TRANSPARENCY=0.6/ Body 1
&OBST XB=1.18,1.185,0.01,0.105,0.41,1.18, RGB=128,0,128, TRANSPARENCY=0.6/ Body 2
&OBST XB=1.18,1.185,0.01,0.105,1.22,1.99, RGB=128,0,128, TRANSPARENCY=0.6/ Body 2
&OBST XB=1.18,1.185,0.01,0.105,2.03,2.79, RGB=128,0,128, TRANSPARENCY=0.6/ Body 2

Z Type Flashing
&OBST XB=0.655,0.66,0.01,0.11,0.41,0.51, RGB=128,0,128, TRANSPARENCY=0.6/ Left Profile
&OBST XB=0.655,0.66,0.01,0.11,0.745,0.845, RGB=128,0,128, TRANSPARENCY=0.6/ Left Profile
&OBST XB=0.655,0.66,0.01,0.11,1.08,1.18, RGB=128,0,128, TRANSPARENCY=0.6/ Left Profile
&OBST XB=0.655,0.66,0.01,0.11,1.22,1.32, RGB=128,0,128, TRANSPARENCY=0.6/ Left Profile
```

&OBST XB=0.655,0.66,0.01,0.11,1.555,1.655, RGB=128,0,128, TRANSPARENCY=0.6/ Left Profile
&OBST XB=0.655,0.66,0.01,0.11,1.89,1.99, RGB=128,0,128, TRANSPARENCY=0.6/ Left Profile
&OBST XB=0.655,0.66,0.01,0.11,2.03,2.13, RGB=128,0,128, TRANSPARENCY=0.6/ Left Profile
&OBST XB=0.655,0.66,0.01,0.11,2.36,2.46, RGB=128,0,128, TRANSPARENCY=0.6/ Left Profile
&OBST XB=0.655,0.66,0.01,0.11,2.69,2.79, RGB=128,0,128, TRANSPARENCY=0.6/ Left Profile
&OBST XB=1.61,1.615,0.01,0.11,0.41,0.51, RGB=128,0,128, TRANSPARENCY=0.6/ Right Profile
&OBST XB=1.61,1.615,0.01,0.11,0.745,0.845, RGB=128,0,128, TRANSPARENCY=0.6/ Right Profile
&OBST XB=1.61,1.615,0.01,0.11,1.08,1.18, RGB=128,0,128, TRANSPARENCY=0.6/ Right Profile
&OBST XB=1.61,1.615,0.01,0.11,1.22,1.32, RGB=128,0,128, TRANSPARENCY=0.6/ Right Profile
&OBST XB=1.61,1.615,0.01,0.11,1.555,1.655, RGB=128,0,128, TRANSPARENCY=0.6/ Right Profile
&OBST XB=1.61,1.615,0.01,0.11,1.89,1.99, RGB=128,0,128, TRANSPARENCY=0.6/ Right Profile
&OBST XB=1.61,1.615,0.01,0.11,2.03,2.13, RGB=128,0,128, TRANSPARENCY=0.6/ Right Profile
&OBST XB=1.61,1.615,0.01,0.11,2.36,2.46, RGB=128,0,128, TRANSPARENCY=0.6/ Right Profile
&OBST XB=1.61,1.615,0.01,0.11,2.69,2.79, RGB=128,0,128, TRANSPARENCY=0.6/ Right Profile
&OBST XB=1.70,1.80,0.195,0.20,0.41,0.51, RGB=128,0,128, TRANSPARENCY=0.6/ Wing Left Profile
&OBST XB=1.70,1.80,0.195,0.20,0.745,0.845, RGB=128,0,128, TRANSPARENCY=0.6/ Wing Left Profile
&OBST XB=1.70,1.80,0.195,0.20,1.08,1.18, RGB=128,0,128, TRANSPARENCY=0.6/ Wing Left Profile
&OBST XB=1.70,1.80,0.195,0.20,1.22,1.32, RGB=128,0,128, TRANSPARENCY=0.6/ Wing Left Profile
&OBST XB=1.70,1.80,0.195,0.20,1.555,1.655, RGB=128,0,128, TRANSPARENCY=0.6/ Wing Left Profile
&OBST XB=1.70,1.80,0.195,0.20,1.89,1.99, RGB=128,0,128, TRANSPARENCY=0.6/ Wing Left Profile
&OBST XB=1.70,1.80,0.195,0.20,2.03,2.13, RGB=128,0,128, TRANSPARENCY=0.6/ Wing Left Profile
&OBST XB=1.70,1.80,0.195,0.20,2.36,2.46, RGB=128,0,128, TRANSPARENCY=0.6/ Wing Left Profile
&OBST XB=1.70,1.80,0.195,0.20,2.69,2.79, RGB=128,0,128, TRANSPARENCY=0.6/ Wing Left Profile
&OBST XB=1.70,1.80,0.55,0.555,0.41,0.51, RGB=128,0,128, TRANSPARENCY=0.6/ Wing Right Profile
&OBST XB=1.70,1.80,0.55,0.555,0.745,0.845, RGB=128,0,128, TRANSPARENCY=0.6/ Wing Right Profile
&OBST XB=1.70,1.80,0.55,0.555,1.08,1.18, RGB=128,0,128, TRANSPARENCY=0.6/ Wing Right Profile
&OBST XB=1.70,1.80,0.55,0.555,1.22,1.32, RGB=128,0,128, TRANSPARENCY=0.6/ Wing Right Profile
&OBST XB=1.70,1.80,0.55,0.555,1.555,1.655, RGB=128,0,128, TRANSPARENCY=0.6/ Wing Right Profile
&OBST XB=1.70,1.80,0.55,0.555,1.89,1.99, RGB=128,0,128, TRANSPARENCY=0.6/ Wing Right Profile
&OBST XB=1.70,1.80,0.55,0.555,2.03,2.13, RGB=128,0,128, TRANSPARENCY=0.6/ Wing Right Profile
&OBST XB=1.70,1.80,0.55,0.555,2.36,2.46, RGB=128,0,128, TRANSPARENCY=0.6/ Wing Right Profile
&OBST XB=1.70,1.80,0.55,0.555,2.69,2.79, RGB=128,0,128, TRANSPARENCY=0.6/ Wing Right Profile

Corner Seal
&OBST XB=1.65,1.705,0.105,0.11,0.41,1.18, RGB=128,0,128, TRANSPARENCY=0.6/ Corner L rail
&OBST XB=1.65,1.705,0.105,0.11,1.22,1.99, RGB=128,0,128, TRANSPARENCY=0.6/ Corner L rail
&OBST XB=1.65,1.705,0.105,0.11,2.03,2.79, RGB=128,0,128, TRANSPARENCY=0.6/ Corner L rail
&OBST XB=1.7,1.705,0.11,0.17,0.41,1.18, RGB=128,0,128, TRANSPARENCY=0.6/ W T rail head
&OBST XB=1.7,1.705,0.11,0.17,1.22,1.99, RGB=128,0,128, TRANSPARENCY=0.6/ W T rail head
&OBST XB=1.7,1.705,0.11,0.17,2.03,2.79, RGB=128,0,128, TRANSPARENCY=0.6/ W T rail head

Side Obstructions
&OBST XB=0.59,0.6,0,0.12,0.4,2.8, RGB=128,0,128, TRANSPARENCY=0.6/
&OBST XB=1.69,1.81,0.61,0.62,0.4,2.8, RGB=128,0,128, TRANSPARENCY=0.6/

Top Obstructions
Permanent Obstructions
&OBST XB=0.60,0.85,0.01,0.085,2.13,2.20, RGB=128,0,128, TRANSPARENCY=0.6/
&OBST XB=0.85,1.085,0.01,0.085,2.13,2.20, RGB=128,0,128, TRANSPARENCY=0.6/
&OBST XB=1.09,1.18,0.01,0.08,2.13,2.20, RGB=128,0,128, TRANSPARENCY=0.6/
&OBST XB=1.185,1.5,0.01,0.085,2.13,2.20, RGB=128,0,128, TRANSPARENCY=0.6/
&OBST XB=1.5,1.8,0.01,0.085,2.13,2.20, RGB=128,0,128, TRANSPARENCY=0.6/
&OBST XB=1.725,1.8,0.085,0.35,2.13,2.20, RGB=128,0,128, TRANSPARENCY=0.6/
&OBST XB=1.725,1.8,0.35,0.61,2.13,2.20, RGB=128,0,128, TRANSPARENCY=0.6/

Intumescent Obstructions
&OBST XB=0.60,0.85,0.085,0.11,2.13,2.20, RGB=128,0,128, TRANSPARENCY=0.6, DEVC_ID='thermal1'/
&OBST XB=0.85,1.085,0.085,0.11,2.13,2.20, RGB=128,0,128, TRANSPARENCY=0.6, DEVC_ID='thermal2'/
&OBST XB=1.09,1.18,0.085,0.105,2.13,2.20, RGB=128,0,128, TRANSPARENCY=0.6, DEVC_ID='thermal3'/
&OBST XB=1.185,1.5,0.085,0.11,2.13,2.20, RGB=128,0,128, TRANSPARENCY=0.6, DEVC_ID='thermal4'/
&OBST XB=1.5,1.725,0.085,0.11,2.13,2.20, RGB=128,0,128, TRANSPARENCY=0.6, DEVC_ID='thermal5'/
&OBST XB=1.7,1.725,0.11,0.35,2.13,2.20, RGB=128,0,128, TRANSPARENCY=0.6, DEVC_ID='thermal6'/
&OBST XB=1.7,1.725,0.35,0.61,2.13,2.20, RGB=128,0,128, TRANSPARENCY=0.6, DEVC_ID='thermal7'/

Ventilation Openings
&VENT XB=0,2.4,2.4,2.4,0,3.2, SURF_ID='OPEN'/
&VENT XB=0,2.4,0,0,2.8,3.2, SURF_ID='OPEN'/

```
&VENT XB=0,2.4,0,2.4,3.2,3.2, SURF_ID='OPEN'/
&VENT XB=0,0,0,2.4,2.8,3.2, SURF_ID='OPEN'/
&VENT XB=2.4,2.4,0,2.4,2.8,3.2, SURF_ID='OPEN'/

&PROP ID='Thermal Detection', QUANTITY='THERMOCOUPLE'/
&DEVC ID='V1H1', PROP_ID='Thermal Detection', XYZ=0.9,0.06,0.8/
&DEVC ID='V1H2', PROP_ID='Thermal Detection', XYZ=1.135,0.06,0.8/
&DEVC ID='V1H3', PROP_ID='Thermal Detection', XYZ=1.5,0.06,0.8/
&DEVC ID='V1H4', PROP_ID='Thermal Detection', XYZ=1.75,0.06,0.8/
&DEVC ID='V1H5', PROP_ID='Thermal Detection', XYZ=1.75,0.31,0.8/
&DEVC ID='V2H1', PROP_ID='Thermal Detection', XYZ=0.9,0.06,1.2/
&DEVC ID='V2H2', PROP_ID='Thermal Detection', XYZ=1.135,0.06,1.2/
&DEVC ID='V2H3', PROP_ID='Thermal Detection', XYZ=1.5,0.06,1.2/
&DEVC ID='V2H4', PROP_ID='Thermal Detection', XYZ=1.75,0.06,1.2/
&DEVC ID='V2H5', PROP_ID='Thermal Detection', XYZ=1.75,0.31,1.2/
&DEVC ID='V3H1', PROP_ID='Thermal Detection', XYZ=0.9,0.06,1.6/
&DEVC ID='V3H2', PROP_ID='Thermal Detection', XYZ=1.135,0.06,1.6/
&DEVC ID='V3H3', PROP_ID='Thermal Detection', XYZ=1.5,0.06,1.6/
&DEVC ID='V3H4', PROP_ID='Thermal Detection', XYZ=1.75,0.06,1.6/
&DEVC ID='V3H5', PROP_ID='Thermal Detection', XYZ=1.75,0.31,1.6/
&DEVC ID='V4H1', PROP_ID='Thermal Detection', XYZ=0.9,0.06,2/
&DEVC ID='V4H2', PROP_ID='Thermal Detection', XYZ=1.135,0.06,2/
&DEVC ID='V4H3', PROP_ID='Thermal Detection', XYZ=1.5,0.06,2/
&DEVC ID='V4H4', PROP_ID='Thermal Detection', XYZ=1.75,0.06,2/
&DEVC ID='V4H5', PROP_ID='Thermal Detection', XYZ=1.75,0.31,2/
&DEVC ID='V5H1', PROP_ID='Thermal Detection', XYZ=0.9,0.0975,2.4/
&DEVC ID='V5H2', PROP_ID='Thermal Detection', XYZ=1.135,0.0975,2.4/
&DEVC ID='V5H3', PROP_ID='Thermal Detection', XYZ=1.5,0.0975,2.4/
&DEVC ID='V5H4', PROP_ID='Thermal Detection', XYZ=1.7125,0.0975,2.4/
&DEVC ID='V5H5', PROP_ID='Thermal Detection', XYZ=1.7125,0.31,2.4/
&DEVC ID='V6H1', PROP_ID='Thermal Detection', XYZ=0.9,0.0975,2.8/
&DEVC ID='V6H2', PROP_ID='Thermal Detection', XYZ=1.135,0.0975,2.8/
&DEVC ID='V6H3', PROP_ID='Thermal Detection', XYZ=1.5,0.0975,2.8/
&DEVC ID='V6H4', PROP_ID='Thermal Detection', XYZ=1.7125,0.0975,2.8/
&DEVC ID='V6H5', PROP_ID='Thermal Detection', XYZ=1.7125,0.31,2.8/
&PROP ID='Thermal Activation', QUANTITY='LINK TEMPERATURE', RTI=132.0,
ACTIVATION_TEMPERATURE=180.0/
&DEVC ID='thermal1', PROP_ID='Thermal Activation', XYZ=0.75,0.0975,2.13/
&DEVC ID='thermal2', PROP_ID='Thermal Activation', XYZ=1.00,0.0975,2.13/
&DEVC ID='thermal3', PROP_ID='Thermal Activation', XYZ=1.16,0.0975,2.13/
&DEVC ID='thermal4', PROP_ID='Thermal Activation', XYZ=1.35,0.0975,2.13/
&DEVC ID='thermal5', PROP_ID='Thermal Activation', XYZ=1.65,0.0975,2.13/
&DEVC ID='thermal6', PROP_ID='Thermal Activation', XYZ=1.7125,0.20,2.13/
&DEVC ID='thermal7', PROP_ID='Thermal Activation', XYZ=1.7125,0.45,2.13/

&SLCF PBX=1.75, QUANTITY='TEMPERATURE', VECTOR=.TRUE./
&SLCF PBX=1.75, QUANTITY='VELOCITY', VECTOR=.TRUE., CELL_CENTERED=.TRUE./
&SLCF PBX=1.75, QUANTITY='VOLUME FRACTION', SPEC_ID='OXYGEN'/
&SLCF PBX=1.7125, QUANTITY='TEMPERATURE', VECTOR=.TRUE./
&SLCF PBX=1.7125, QUANTITY='VELOCITY', VECTOR=.TRUE., CELL_CENTERED=.TRUE./
&SLCF PBX=1.7125, QUANTITY='VOLUME FRACTION', SPEC_ID='OXYGEN'/
&SLCF PBY=0.06, QUANTITY='TEMPERATURE', VECTOR=.TRUE./ oxygen
&SLCF PBY=0.06, QUANTITY='VELOCITY', VECTOR=.TRUE., CELL_CENTERED=.TRUE./
&SLCF PBY=0.06, QUANTITY='VOLUME FRACTION', SPEC_ID='OXYGEN'/
&SLCF PBY=0.0975, QUANTITY='TEMPERATURE', VECTOR=.TRUE./ oxygen
&SLCF PBY=0.0975, QUANTITY='VELOCITY', VECTOR=.TRUE., CELL_CENTERED=.TRUE./
&SLCF PBY=0.0975, QUANTITY='VOLUME FRACTION', SPEC_ID='OXYGEN'/

&TAIL/
```